0931

PB 206 939

Sponsor Contract No. CPA 70-62
CEM Contract No. 4082

Prediction by Numerical Models of Transport and Diffusion in an Urban Boundary Layer

by

Joseph P. Pandolfo
Marshall A. Atwater
and
Gerald E. Anderson

July 1971

Final Report

Volume I

to

Division of Meteorology
Bureau of Air Pollution Sciences
Office of Research and Monitoring
Environmental Protection Agency
Raleigh, North Carolina 27609

Reproduced by
NATIONAL TECHNICAL
INFORMATION SERVICE
Springfield, Va. 22151

THE CENTER FOR THE ENVIRONMENT AND MAN, INC.
275 Windsor Street Hartford, Connecticut
06103

BIBLIOGRAPHIC DATA SHEET	1. Report No. APTD-0931	2.	3. Recipient's Accession No.
4. Title and Subtitle Prediction by Numerical Models of Transport and Diffusion in an Urban Boundary Layer			5. Report Date July 1971 6.
7. Author(s) Joseph P. Pandolfo, Marshall A. Atwater and Gerald Anderson			8. Performing Organization Rept. No. Volume I
9. Performing Organization Name and Address The Center for the Environment and Man, Inc. 275 Windsor Street Hartford, Connecticut 06103			10. Project/Task/Work Unit No. 11. Contract/Grant No. CPA 70-62
12. Sponsoring Organization Name and Address Environmental Protection Agency Office of Research and Monitoring Division of Meteorology Raleigh, North Carolina 27609			13. Type of Report & Period Covered Final 14.

15. Supplementary Notes

16. Abstracts A three-dimensional numerical model based on the Eulerian conservation equations for momentum, heat, water vapor, salinity, and air pollutants was used to examine the transport and diffusion processes in the planetary boundary layer. Horizontal diffusion was incorporated through a strongly and implicitly diffusive finite-difference scheme for the horizontal advection terms, viz, upwind differencing. However, terms representing other transport and diffusion processes were explicitly included in the differential equations. It is feasible to simulate the temporal variation of meteorological and pollutant variables, on a three-dimensional array containing several thousand grid points, within practical limits on a computer. Simulated urban-rural low level temperature differences in winter are qualitatively realistic. The depth of the mixing level and the strength and height of the mixing level are dependent on the simulated interface temperature as should be expected. The simulated daytime vertical profile of pollutants show a well-mixed surface layer with quasi-constant concentrations. The nighttime profiles show definite peaks of concentration near the source height. The presence of reasonable (hypothetical) concentrations of nontransparent pollutants reduces the amplitude of the diurnal temperature wave at the interface by 2 K and may alter the air temperature within the polluted layer about 2 K. Differences in low level pollutant concentration of about 25 percent are noted between simulations with transparent and nontransparent pollutants. Three-dimensional fields of meteorological and pollutant variables were simulated using Connecticut source inventory data and typical (hypothetical) winter meteorological conditions. These simulations show systematic patterns of higher temperatures and deeper polluted layers over the urban areas than over rural areas. They also show systematic patterns of low level convergence of the horizontal flow over urban areas.

17. Key Words and Document Analysis 17a. Descriptors

Air pollution
Atmospheric diffusion
Mathematical models
Urban areas
Atmospheric physics
Temperature
Diurnal variations
Seasonal variations
Altitude
Rural areas

17b. Identifiers/Open-Ended Terms

17c. COSATI Field/Group 13B

18. Availability Statement Unlimited	19. Security Class (This Report) UNCLASSIFIED	21. No. of Pages 148
	20. Security Class (This Page) UNCLASSIFIED	22. Price

Sponsor Contract No. CPA 70-62
CEM Contract No. 4082

Prediction by Numerical Models of Transport and Diffusion in an Urban Boundary Layer

by

Joseph P. Pandolfo
Marshall A. Atwater
and
Gerald E. Anderson

July 1971

Final Report

Volume I

to

Division of Meteorology
Bureau of Air Pollution Sciences
Office of Research and Monitoring
Environmental Protection Agency
Raleigh, North Carolina 27609

THE CENTER FOR THE ENVIRONMENT AND MAN, INC.
275 Windsor Street Hartford, Connecticut
06103

ABSTRACT

A three-dimensional numerical model based on the Eulerian conservation equations for momentum, heat, water vapor, salinity, and air pollutants was used to examine the transport and diffusion processes in the planetary boundary layer. Horizontal diffusion was incorporated through a strongly and implicitly diffusive finite-difference scheme for the horizontal advection terms, viz. upwind differencing. However, terms representing other transport and diffusion processes were explicitly included in the differential equations.

The results demonstrate that it is feasible to simulate the temporal variation of meteorological and pollutant variables, on a three-dimensional array containing several thousand grid points, within practical limits on a computer.

Simulated urban-rural low level temperature differences in winter are qualitatively realistic. The depth of the mixing level and the strength and height of the mixing level are dependent on the simulated interface temperature as should be expected. The simulated daytime vertical profile of pollutants show a well-mixed surface layer with quasi-constant concentrations. The nighttime profiles show definite peaks of concentration near the source height. The presence of reasonable (hypothetical) concentrations of nontransparent pollutants reduces the amplitude of the diurnal temperature wave at the interface by 2°K and may alter the air temperature within the polluted layer by about 2°K. Differences in low level pollutant concentration of about 25 percent are noted between simulations with transparent and nontransparent pollutants.

Three-dimensional fields of meteorological and pollutant variables were simulated using Connecticut source inventory data and typical (hypothetical)

winter meteorological conditions. These simulations show systematic patterns of higher temperatures and deeper polluted layers over the urban areas than over rural areas. They also show systematic patterns of low level convergence of the horizontal flow over urban areas.

TABLE OF CONTENTS

Section	Title	Page
1.0	INTRODUCTION	1
2.0	THE PLANETARY BOUNDARY LAYER MODEL	6
2.1	General Description	6
2.1.1	The interrelationships	6
2.1.2	Symbols	8
2.1.3	The general conservation equation	12
2.2	Special Forms of the Conservation Equation and Auxiliary Equations	12
2.2.1	The atmospheric layer	12
2.2.2	The water layer	14
2.2.3	Dependent variables in the soil	15
2.2.4	The air-water-soil interface	15
2.3	Vertical Diffusion Coefficient	18
2.4	Source Terms	21
2.4.1	Solar radiation	21
2.4.1.1	Solar radiation in the atmospheric layer	23
2.4.1.2	Solar source term in water	24
2.4.2	Infrared radiation	26
2.4.3	Pollutant sources	28
2.5	The Horizontal Advection Calculations	
2.5.1	Second-order error as effective diffusion	29
2.5.2	The stability criterion for the two-dimensional upwind differencing scheme	36
2.6	Some Details of Practical Interest	38
3.0	EXPERIMENTAL RESULTS WITH THE SINGLE STATION (z-t) MODEL	40
3.1	The Single Station Model	40
3.2	An Experiment Illustrating the Effects of Variation of Surface Physical Parameters	41
3.2.1	The data	41
3.2.2	The interface temperature	44
3.2.3	Vertical stability and mixing depth	47

TABLE OF CONTENTS (Continued)

Section	Title	Page
3.3	The Sensitivity to the Effective Height of Pollution Sources	48
3.3.1	The data	48
3.3.2	The simulated profiles of pollution concentration	50
3.3.3	Implications of experimental results for the design of simpler models	53
3.4	Experiment for Radiatively Non-transparent Pollutants	55
3.4.1	The data	55
3.4.2	An experiment with constant and specified pollutant concentration profiles	56
3.4.3	An experiment with the simulated pollution concentration profiles being affected by mixing	64
4.0	EXPERIMENTS USING THE THREE-DIMENSIONAL BOUNDARY LAYER	67
4.1	The Connecticut Experiment	67
4.2	Simulated Temperatures and Winds	69
4.3	Experimental Pollution Concentration	72
5.0	SUMMARY AND RECOMMENDATIONS FOR FUTURE WORK	80
6.0	ACKNOWLEDGEMENTS	83
7.0	REFERENCES	84
APPENDICES:		87
A	Specification for a Program of the Atmosphere-Ocean-Land Planetary Boundary Layer with Pollutants	89
B	Specifications for Analysis of the Boundary Layer Model Results	131
C	Related Studies	135
D	Properties of the Modified Gamma Distribution	137

LIST OF ILLUSTRATIONS

Number	Description	Page
3.2-1	The interface temperature as a function of time and rural-urban parameters.	46
3.3-1	Concentration profiles for night and day with various effective source heights.	51
3.3-2	Simulated pollutant concentration ($\mu gm/m^3$) as a function of height and time.	53
3.4-1	The simulated surface temperature as a function of time.	57
3.4-2	The simulated vertical profile of temperature at 0600.	59
3.4-3	The temperature change induced by pollutants for the rural simulation.	60
3.4-4	The temperature change induced by pollutants for the urban simulation.	61
3.4-5	The eddy diffusivity coefficients (cm^2/sec) for the non-polluted urban simulation.	62
3.4-6	The eddy diffusivity coefficients (cm^2/sec) for the polluted urban simulation.	63
3.4-7	The change in temperature and concentration with the pollutant is changed from a transparent pollutant to an opaque pollutant.	66
4.1-1	The grid squares used for the Connecticut experiment	68
4.2-1	The simulated temperature (°K) at the indicated horizontal grid points for the Connecticut experiment at 0 m and 1000 m at 0300 LST.	70
4.2-2	The simulated temperature (°K) at 0300 LST for a north-south cross section through Hartford ("Station 4") to Long Island Sound ("Station 22").	71
4.2-3	The simulated horizontal wind components (cm/sec) at 0300 LST at a height of 6 m for the Connecticut experiment.	73
4.2-4	The simulated horizontal wind components (cm/sec) at 0300 LST at a height of 500 m for the Connecticut experiment.	74
4.2-5	The simulated vertical velocity (cm/sec) at 0300 LST at heights of 150 and 500 m for the Connecticut experiment.	75

LIST OF ILLUSTRATIONS (Continued)

Number	Description	Page
4.3-1	The simulated pollutant concentrations ($\mu gm/m^3$) at 0300 LST at heights of 6 and 25 m for the Connecticut experiment.	76
4.3-2	The simulated pollutant concentrations ($\mu gm/m^3$) at 0300 LST at heights of 300 and 500 m for the Connecticut experiment.	77
4.3-3	The simulated pollutant concentrations ($\mu gm/m^3$) at 0300 LST for a north-south cross section through Hartford ("Station 4") to Long Island Sound ("Station 22").	79

LIST OF TABLES

Number	Description	Page
1	Extinction coefficients in the ocean.	25
2	Interface parameters for urban, rural, and land simulations.	42
3	Rural/urban surface values used in each of the simulations.	42
4	Data for the winter simulations.	43
5	Data for the summer simulations.	44
6	Summary of maximum and minimum temperatures for various simulations.	45
7	Depth (m) of the mixing layer and strength of the nocturnal inversion (°K).	47
8	Initial atmospheric data and physical surface values.	48
9	Source emissions of sulfur dioxide [lbs/day/$(1524)^2 m^2$] and particulates [lbs/day/$(1524)^2 m^2$] for January.	49
10	Turbulence scale (σ_z) in m.	54
11	Source emissions of SO_2 ($\mu gm/m^3$/sec) urban, rural, or water characteristics of the underlying surface from Table 2 and roughness heights in cm.	69

1.0 INTRODUCTION

The models that are to be described in this report differ in one essential feature from other recently developed air pollution transport and diffusion models (e.g., see Calder [1969], Randerson [1970], and Sklarew [1970]). These other models are also based on numerical integration of the K-theory form of the mass conservation equation for pollutant; however, they require that wind and diffusivity fields be given *a priori*, and independently of the pollutant fields. Our models, on the other hand, numerically integrate K-theory forms of the conservation equations for momentum, heat, and atmospheric water content, in addition to the pollutant conservation equations. They incorporate formulas relating the coefficients of turbulent transfer in the vertical to wind and temperature fields. Therefore, they are capable of generating wind and diffusivity fields that are physically derived and consistent in spatial and temporal scale with the pollutant fields obtained. Furthermore, they provide a procedure for the generation of wind and diffusivity fields, that is, in principle, generally applicable to any geographic location, season of the year or hour of the day, or type of underlying surface. Finally there can be effects of the pollutant field, through the temperature fields, on the wind and diffusivity fields. These effects may, in many practical cases, be insignificant or negligible. However, they may, in other situations, be quite significant. In the latter case, it would be highly desirable to have models available that can generate meteorological and pollutant fields simultaneously.

Over the past several years, a base of work on such models has been developed at The Travelers Research Center (TRC), and its successor organization, The Center for the Environment and Man (CEM). The models developed in that work consider the effects of boundary layer turbulence in stratified flow, of mixing in the presence of various types of surface roughness, and of cloud-

dependent radiative heating at the surface, and throughout the boundary layer. They were based on the Eulerian conservation equations for momentum, heat, water vapor, and suspended liquid water. In this framework, the models were peculiarly suited to the explicit quantitative consideration of internal sources, sinks, and transformations of the dependent variables.

In the early stages of that work, the research concentrated on the description of these processes, and on the simulation of their simultaneous action, in greater vertical detail than was usual in meteorological models. The effects of horizontal transport were assumed to be given in the early models. Fuller consideration of this process was postponed until two model versions applicable at a single horizontal grid point were developed. In one of these versions, the surface had prespecified roughness, terrain slope, albedo, thermal conductivity, and degree of moistness; and was allowed to contain artificial thermal sources, in addition to receiving natural radiation. This version was applied to the vertically detailed simulation of the planetary boundary layer at a location with an underlying land surface, or arbitrarily specifiable physical properties (see e.g., Cooley, et al. [1968]). In its final form, this version was ideally suited for the study or simulation of urban-rural contrasts due to differences in these properties and to the presence of concentrated artificial urban heat sources. A second version contained oceanic roughness as a parameter to be determined by the model solutions, and coupled the atmospheric boundary layer to a simultaneously modelled underlying turbulent oceanic layer (see Pandolfo [1969]).

With the achievement of this simulative capability for a single location, attention was then directed to the treatment of horizontal variations and transports in the boundary layer.

There was then developed a more complete model which applied the air-sea single grid point model, on a square array of grid points in the horizontal, in order to analyze data obtained from an extensive observational study of a tropical ocean region (BOMEX). This more recent line of study resulted in a series of simulation experiments with the complete model, which continues to the present under NSF sponsorship.

Work had also proceeded on the development of a radiation model to include the effects of pollutants on the temperature profile. It was shown (Atwater [1970, 1971]) that particulates and nitrogen dioxide can have a significant effect on urban temperature profiles.

Thus, there were available at this stage of development, models capable of generating physically consistent simulations of boundary layer meteorology and vertical diffusion, with the dependent (meteorological) variables presently considered. Addition of pollution constituents to the list of dependent variables, then allowed not only the pollutant effect on meteorology to be simulated, but the feedback effect of atmospheric processes (transport, diffusion, and radiation) on the pollutants. This addition was made within the conceptual and logical framework of our already developed computer programs for the models. To consider just one example, computer modelling of photochemical transformations should be closely analogous to the modelling of atmospheric condensation-evaporation effects on the water vapor, liquid water, and heat content of the boundary layer.

There was one atmospheric process not yet explicitly considered in the models, viz., horizontal diffusion. The air-sea model used a strongly and implicitly diffusive finite difference scheme for the advection terms, viz. upwind differencing. The theory underlying the diffusive effects of this and other schemes is discussed by Mollenkamp [1968]. The theory allows some

manipulation of the computational scheme to control the effective horizontal diffusion coefficient.

It was then proposed (CEM P69-009, November 1969) that components from these models be incorporated into a third three(space)-dimensional model which was to be used to demonstrate the feasibility of development of what is eventually to be an urban air pollution prediction model. First, the feasibility was to be demonstrated with a detailed physical-numerical meteorological model of the urban boundary layer, capable, at least, of grossly simulating urban-rural weather differences. Secondly, the inclusion of pollutant concentration as a dependent variable of the model was to be undertaken. The results obtained in the program resulting from that proposal are summarized in Section 5.0.

The physical equations forming the basis of the models developed under this contract are discussed in detail in Section 2.0. The calculation formulas are given in detail in the specifications presented in Appendices A and B to this report. The computer programs used for numerical solution of these models are to be described in Volume II. Section 3.0 describes some experiments with a specialized version of the model, which appear to have successfully simulated, in general, some well known urban-rural meteorological differences, to have generated results that can provide guidance in the design of simpler pollution transport diffusion models (e.g., see Section 3.3.2) and to have identified potentially significant coupled effects of the pollutants and the meteorology. Section 4.0 describes the first results obtained using an inventory that includes all major sources of pollutants in the modelled region.

Other work has been conducted at CEM over the past year in studies that are relevant to this project. This work is described in Appendix C to this report.

The summary in Section 5.0 shows that the purpose of this contract, viz. to demonstrate the feasibility of urban air pollution prediction models including meteorological and pollutant variables, has been achieved. This feasibility is to be understood as referring to the practical computer capabilities at this stage. The verisimilitude and value of the simulation results remain to be demonstrated in the next few years.

Reports on the work as it progressed were presented at an information meeting on Atmospheric Diffusion Modelling Studies by NAPCA contractors (Nov. 16-17, 1970, Raleigh), and at the AMS/APCA Conference on Air Pollution Meteorology (April 5-9, 1971, Raleigh).

2.0 THE PLANETARY BOUNDARY LAYER MODEL

2.1 General Description

2.1.1 The interrelationships

The planetary boundary layer model that is described here is an expanded form of the three-dimensional models developed in previous projects. The model now includes pollutants as dependent variables and the subsurface may be either land or water at each of the grid points in the horizontal array. The model is based on the general conservation equation, given in Section 2.1.3, which is integrated in time. One of the basic factors in that equation is the vertical diffusion coefficient , which is computed according to the formulas described in Section 2.3. Special forms of the conservation equations for the atmosphere, water, and soil and the interface between the atmosphere and subsurface are given in Section 2.2. The computation of the source terms is described in Section 2.4, and a description of the horizontal advection computation and stability criteria are given in Section 2.5. A discussion of the complex interrelationships between the dependent variables in an urban region follows.

If we start with the conservation equation for the pollutant, we see that the local time changes of pollutant are related directly to the air velocity in the advection term. They are related indirectly to the vertical shear of the horizontal velocity, and the vertical gradients of temperature and humidity, through the eddy diffusivity factor appearing in the vertical diffusion term.

The humidity changes are also directly related to the velocity and indirectly related to the vertical gradients of horizontal velocity, temperature, and humidity through the dependence of the diffusivity on the Richardson number.

The temperature changes are also dependent on this set of quantities, and in addition, are determined, in part, by the adiabatic warming (or cooling)

undergone by the air due to vertical motions, and, in part, by the absorption and emission of solar and infrared radiation represented by the source terms S_1 and S_2. These last terms indirectly relate temperature changes to the vertical temperature, humidity, and (in some cases) pollutant profiles of the entire atmospheric column, at the location considered, and to the temperature of the underlying surface. The relationships between these properties and the strength of the radiative heat source form, perhaps, the most complex portion of the model, and are described at length in Sections 2.4.1 and 2.4.2.

The changes in horizontal velocity are, again, directly related to the velocity and the Richardson number, through the advection and diffusion terms in the momentum equation, and are, in addition, dependent on the Coriolis parameter and the horizontal pressure gradient at the height considered (i.e. the geostrophic wind). The last term in the momentum equations also indirectly relates the horizontal velocity change to the horizontal temperature gradients, through the thermal wind equation.

Finally, the vertical velocity is directly related to the horizontal velocity gradients, and indirectly, through them, to all the other parameters listed above.

One variable that appears to be most actively involved in affecting all the others is the interface temperature. It is an important determinant of the Richardson number, particularly in the lowest levels of the boundary layer; and it determines the telluric radiative flux as seen by the entire vertical column of air above the interface. In its horizontal variations, it plays an important role in determining the vertical variation of the horizontal pressure gradient, and indirectly affects not only the magnitude and direction of the horizontal wind, but also its vertical structure. The special form of the thermodynamic equation used to calculate the interface temperature is

given below in Section 2.2.4.

Inspection of this equation reveals that the interface temperature is highly dependent on the physical nature of the underlying material. The differences in the physical properties of land and water surfaces, can, therefore, under the proper conditions, develop such strong horizontal gradients of low level temperature that significant local circulations result, viz. the well-known land-sea breezes. The weaker contrasts in the physical properties of the urban and rural surface can also lead to the development of local circulations in certain situations. The quantitative description of these underlying layers is, therefore, an important part of the complete model.

In summary, the dynamics of the boundary layer in an urban region, as represented even in this highly idealized set of equations, appear to be governed by numerous and complicated linkages between state variables.

2.1.2 Symbols

The symbols used in this section are defined below with their units (n.d. is nondimensional). Occasionally a symbol, used once, will be defined when used.

a	Surface albedo (n.d.).
a_w	Absorptivity of solar radiation by water vapor (n.d.).
A_i	Internal source (sink) for the dependent variable. Units are determined by the i(th) variable.
A	Atmospheric heat flux (ly/sec)
B_a, B_s	Aerosol absorption and scattering coefficient (cm^{-1})
c	Cloud amount (hundredths of sky cover).
c_a	Specific heat of air (cal/gm/°K).
c_s	Specific heat of subsurface (cal/gm/°K).
c_w	Specific heat of water (cal/gm/°K).

E	Surface evaporation (gm $H_2O/cm^2/sec$).
$E_\lambda(T)$	Planck's function (ly/sec/μ).
f	Coriolis parameter (sec^{-1}).
F	Flux of pollutant at surface (gm poll/gm air/sec).
F_e	Flux of pollutant at elevated level (gm poll/gm air/sec).
$F\downarrow(z)$	Downward infrared flux at height z (ly/sec).
$F\uparrow(z)$	Upward infrared flux (ly/sec).
$(F_n)_{ir}$	Net infrared flux (ly/sec)
g	Gravitational acceleration (cm/sec^2).
h	Priestley constant (n.d.).
H	Height at top of boundary layer (cm).
$I(z)$	Incident solar radiation at height z (ly/sec).
I_0	Incident solar radiation at top of the atmosphere (ly/sec).
I_1	Incident solar flux at top of boundary layer (ly/sec).
I_1'	Incident solar flux at top of boundary layer in absence of cloud (ly/sec).
I_a	Absorbed solar flux (ly/sec).
I_s	Scattered solar flux (ly/sec).
k	von Karman constant (n.d.).
k_a	Absorption coefficient (cm^2/gm).
k_s	Scattering coefficient (cm^2/gm).
K_e	Vertical diffusion coefficient for conductivity-diffusivity (cm^2/sec).
K_i	Generalized vertical diffusion coefficient (cm^2/sec).
K_m	Vertical diffusion coefficient for momentum (cm^2/sec).
L	Latent heat (cal/gm).
m	Complex refractive index (n.d.).
M	Halstead moisture parameter, $0 \leq M \leq 1$ (n.d.).
$n(r)$	Number density of particles of radius r (cm^{-3}).

p	Pressure (mb).
P_1	Concentration of pollutant 1 ($\mu gm/m^3$).
P_2	Concentration of pollutant 2 ($\mu gm/m^3$).
P_r	Precipitation rate (cm/sec).
q	Specific humidity (gm/kgm).
q_s	Specific humidity at saturation (gm/kgm).
$Q_\lambda(m,r)$	Mie efficiency factor (n.d.).
r	Radius (cm).
R_s	Incident solar flux at the interface (ly/sec).
R_x	Artificial heat source due to combustion (ly/sec).
Ri	Richardson number (n.d.).
s	Salinity (gm/kgm).
S	Heat flux into subsurface layer (ly/sec).
S_1	Solar radiation source term (°K/sec).
S_2	Infrared radiation source term (°K/sec).
S_p	Pollutant source term (gm poll/gm air/sec).
S_w	Vertical gradient of the scalar value of the average orbital velocity in a turbulent wave (sec^{-1}).
t	Time (sec).
T	Temperature (°K).
T_r	Temperature of rain (°K).
u	Eastward component of velocity (cm/sec); or path length of water vapor (cm).
u_g	Eastward component of geostrophic velocity (cm/sec).
u_T	Path length of water vapor above top of boundary layer (cm).
v	Northward component of velocity (cm/sec).
v_g	Northward component of geostrophic velocity (cm/sec).
$\vec{V}$	Three-dimensional velocity vector (cm/sec).

$\vec{V}_2$	Two-dimensional (horizontal) velocity vector (cm/sec).
w	Upward component of velocity (cm/sec).
$W_{19.5}$	Wind speed at 19.5 m (cm/sec).
X_i	Generalized dependent variable.
z	Height (cm).
z_c	Height of cloud base (cm).
z_0	Roughness height (cm).
Z	Solar zenith angle (deg).
α	Monin-Obukhov constant (n.d.).
Γ	Dry adiabatic lapse rate (°K/cm).
δ	Steepness of characteristic turbulent wave (height to length ratio)(n.d.).
Δt	Time increment (sec).
ΔX_i	Generalized three-dimensional gradient for dependent variable X_i . Units dependent on variable X_i .
λ	Wavelength of turbulent wave (cm); or wavelength of radiation (cm).
ρ	Density (gm/cm^3).
σ	Stefan-Boltzman constant ($\ell y/°K^4/min$).
σ_T	Density parameter of sea water at atmospheric pressure (gm/cm^3).
τ	Transmissivity of radiation (n.d.).
ϕ	Transmissivity of solar radiation through clouds (n.d.).
ψ	Diffusivity factor (n.d.).

The following subscripts are used to further define variables.

a	atmosphere
g	geostrophic
I	interface
s	subsurface (water or soil)
w	water

2.1.3 The general conservation equation

The basic equation for the dependent variables takes the form

$$\frac{\partial X_i}{\partial t} + \vec{V}\cdot\nabla X_i = \frac{\partial}{\partial z}\left(K_i\,(Ri,\,z)\,\frac{\partial X_i}{\partial z}\right) + A_i \qquad (2.1\text{-}1)$$

$$i = 1, \ldots 6 \ .$$

The dependent variables include, at most, eastward and northward component of the wind or water currents (u,v), humidity (g), salinity (s), air and subsurface temperature (T), and air pollutants (P_1,P_2). The following sections will describe the specific equations for the atmosphere and subsurface, and the internal computations of the gradients, exchange coefficients, and source rates.

2.2 Special Forms of the Conservation Equation and Auxiliary Equations

2.2.1 The atmospheric layer

The model will include six dependent variables in the atmosphere simultaneously. The equations for the horizontal wind components are written (Pandolfo [1969]) as

$$\frac{\partial u}{\partial t} = -\vec{V}\cdot\nabla u + \frac{\partial}{\partial z}\left[\left(K_m(Ri,z)\right)\frac{\partial u}{\partial z}\right] + f[v - v_g(z)] \qquad (2.2\text{-}1)$$

$$\frac{\partial v}{\partial t} = -\vec{V}\cdot\nabla v + \frac{\partial}{\partial z}\left[\left(K_m(Ri,z)\right)\frac{\partial v}{\partial z}\right] - f[u - u_g(z)] \qquad (2.2\text{-}2)$$

where all symbols have been defined in Section 2.1.2.

The equation for temperature is written (Pandolfo [1969]) as

$$\frac{\partial T}{\partial t} = -\vec{V}\cdot\nabla T + \frac{\partial}{\partial z}\left[\left(K_e(Ri,z)\,\frac{\partial T}{\partial z}\right] + \Gamma\,\frac{\partial K_e}{\partial z} + S_1 + S_2 + w\Gamma \ . \qquad (2.2\text{-}3)$$

The humidity equation is written

$$\frac{\partial q}{\partial t} = -\vec{V}\cdot\nabla q + \frac{\partial}{\partial z}\left[\left(K_e(Ri,z)\right)\frac{\partial q}{\partial z}\right] . \qquad (2.2\text{-}4)$$

The equations for the prediction of pollutants are written

$$\frac{\partial P_i}{\partial t} = -\vec{V}\cdot\nabla P_i + \frac{\partial}{\partial z}\left[\left(K_e(Ri,z)\right)\frac{\partial P_i}{\partial z}\right] + (S_p)_i ; \quad i = 1,2 . \qquad (2.2\text{-}5)$$

The formula for the vertical diffusion coefficient and the Richardson numbers are given in Section 2.3.

Geostrophic winds at any height in the layer are computed from the upper boundary value and from the horizontal temperature gradients by use of the integrated form of the thermal wind equation (see e.g. Hess [1959], eq. 12.11)

$$u_g(z) = u_g(H) \cdot \frac{T(z)}{T(H)} + \frac{g\cdot T(z)}{f}\int_z^H \frac{1}{T^2}\frac{\partial T}{\partial y}\,dz , \qquad (2.2\text{-}6)$$

and

$$v_g(z) = v_g(H)\,\frac{T(z)}{T(H)} - \frac{g\cdot T(z)}{f}\int_z^H \frac{1}{T^2}\frac{\partial T}{\partial x}\,dz . \qquad (2.2\text{-}7)$$

Vertical velocities at any height are computed from the horizontal velocity gradients by use of the continuity equation for an incompressible fluid,

$$w(z) = -\int_0^z \left(\frac{\partial u}{\partial x} + \frac{\partial v}{\partial y}\right) dz . \qquad (2.2\text{-}8)$$

The vertical velocity is, therefore, assumed to be zero at the interface. Note that it is not necessary to specify w at either the upper or lower boundaries.

2.2.2 The water layer

The time dependent equations for the u and v components of the current are written (Pandolfo [1969]) as

$$\frac{\partial u}{\partial t} = -\vec{V}\cdot\nabla u + \frac{\partial}{\partial z}\left[\left(K_m(Ri,z)\right)\frac{\partial u}{\partial z}\right] + f[v - v_g(z)] \qquad (2.2\text{-}9)$$

and

$$\frac{\partial v}{\partial t} = -\vec{V}\cdot\nabla v + \frac{\partial}{\partial z}\left[\left(K_m(Ri,z)\right)\frac{\partial v}{\partial z}\right] - f[u - u_g(z)] \; . \qquad (2.2\text{-}10)$$

The temperature in the water layer is computed from Pandolfo [1969]

$$\frac{\partial T}{\partial t} = -\vec{V}\cdot\nabla T + \frac{\partial}{\partial z}\left[\left(K_e(Ri,z)\right)\frac{\partial T}{\partial z}\right] + S_1 \; . \qquad (2.2\text{-}11)$$

The salinity is computed from

$$\frac{\partial s}{\partial t} = -\vec{V}\cdot\nabla s + \frac{\partial}{\partial z}\left[\left(K_e(Ri,z)\right)\frac{\partial s}{\partial z}\right] \; , \qquad (2.2\text{-}12)$$

with the diffusion coefficient and Richardson numbers defined in Section 2.3.

The geostrophic currents at any depth are computed from the analogue to the thermal wind equation for the atmosphere, viz.

$$u_g(z) = u_g(z=0) + \frac{g}{f}\int_{z=0}^{z}\frac{1}{\rho}\frac{\partial \rho}{\partial y}\,dz \qquad (2.2\text{-}13)$$

and

$$v_g(z) = -v_g(z=0) + \frac{g}{f}\int_{z=0}^{z}\frac{1}{\rho}\frac{\partial \rho}{\partial x}\,dz \; . \qquad (2.2\text{-}14)$$

The horizontal density gradients are computed from the horizontal temperature and salinity gradients based on the relationships presented by Cox et al. [1970].

Vertical velocities at any depth are computed from the continuity equation

$$w(z) = \int_0^z \left(\frac{\partial u}{\partial x} + \frac{\partial v}{\partial y}\right) dz \quad . \tag{2.2-15}$$

2.2.3 Dependent variables in the soil

Temperature is the only time dependent variable in the soil and is given by the equation for the conservation of heat;

$$\frac{\partial T}{\partial t} = \frac{\partial}{\partial z}\left(K_e(z)\,\frac{\partial T}{\partial z}\right) \tag{2.2-16}$$

where $K_e(z)$ is the thermal diffusivity, which is specified as a function of height. No other variables are simulated in the soil.

2.2.4 The air-water-soil interface

Values of the dependent variables are obtained at the interface and are highly dependent on the nature of the subsurface (water or soil). In the case of water, several equation parameters are computed, while for soil, they are specified. These parameters include albedo, a moisture parameter, specific heat of the subsurface material, density of the subsurface material, and the roughness height.

It is assumed that there are no discontinuities in velocity or temperature. This leads to the interface velocity condition over water given by

$$(\vec{V}_I)_a = (\vec{V}_I)_w \quad . \tag{2.2-17}$$

For a soil subsurface, a no slip condition is used, i.e. $\vec{V}_2 = 0$, at $z = z_0$, i.e., the velocity vanishes at some height above the interface. For a water surface, the additional condition imposed is that the horizontal shearing stress is continuous

$$\rho_a \left(K_m \frac{\partial \vec{V}_2}{\partial z}\right)_a = \rho_w \left(K_m \frac{\partial \vec{V}_2}{\partial z}\right)_w \quad . \tag{2.2-18}$$

The interface specific humidity q_I is computed from

$$q_I = M(q_s) + (1 - M)\, q_1 \,. \tag{2.2-19}$$

where q_1 is the humidity at the first atmospheric grid level. The parameter is 1 for water and 0 for dry soil. For moist soil cases, M takes on intermediate fractional values. Halstead et al. [1957] discussed the empirical evaluation of M when it falls into this intermediate range.

The evaporation, E , is computed from

$$E = \rho_a K_{e_a} \frac{\partial q}{\partial z} \,. \tag{2.2-20}$$

The interface salinity, when required, is computed from

$$s = 1 - \frac{E - P_r}{\rho_w K_{e_w} \frac{\partial \ell n s}{\partial z}} \,. \tag{2.2-21}$$

The interface temperature is computed by an iterative solution to the heat balance equation (see e.g., Pandolfo [1969]) by

$$0 = R_s + F\downarrow(0) - LE(T_I) - \sigma T_I^4 - \rho_a c_a K_{e_a} \left[\left(\frac{\partial T}{\partial z}\right)_+ + \Gamma\right](T_I)$$
$$- \rho_s c_s K_{e_s} \left(\frac{\partial T}{\partial z}\right)_- (T_I) + c_w \rho_w P_r (T_r - T_I) + R_x \,. \tag{2.2-22}$$

The assumption that the temperature is continuous at the interface is applied in the calculation of the individual term in the balance equation.

The solar radiation term is computed from

$$R_s = (1 - a)\, I(0) - \tau_s\, I(0) \tag{2.2-23}$$

with τ_s the transmission of solar energy through the water interface (zero for a soil interface) and $I(0)$ is the solar energy at the surface and is examined in greater detail in Section 2.4.1.2. The solar energy reaching the

surface is computed by methods described in more detail in the Section 2.4.1. The albedo is specified when the subsurface is soil and is computed from

$$a = -.0139 + .0467 \tan Z \; ; \quad a \geq .03 \qquad (2.2\text{-}24)$$

when the subsurface is water (Sverdrup et al. [1942]).

The infrared radiative flux received at the interface is calculated by methods described below in Section 2.4.2.

The seventh term includes the effect of rain on the heat balance temperature. The temperature of the rain is assumed to equal the height average of wet bulb temperature in the layer of air near the surface. While the thickness of the layer appears to be realistic for the tropical oceans, the validity of this thickness has not been tested in other regions.

The final term is an artifical heat source (heat added per unit area per unit time) due to the activities of man, by combustion of fossil fuels.

When the subsurface is soil, the albedo, the density, the specific heat, the thermal diffusivity, and the moisture parameters are specified. They are computed for water.

The quartic temperature equation that is the heat balance equation is solved at each time step by an iterative procedure.

The value of pollutant concentration at the interface is calculated from a flux value using the formula

$$P_I = P_1 - \frac{F\Delta z}{\rho K_e(Ri,z)} \qquad (2.2\text{-}25)$$

where F is the surface flux of pollutant, as given in the inventory. Note that $K_e(Ri,z)$ and P_1, the pollutant at the first atmospheric level are calculated by the model.

2.3 Vertical Diffusion Coefficient

The vertical diffusion coefficients are internally computed in the model as a function of the vertical gradients of wind, humidity, and temperature. The method has been previously described by Pandolfo [1969] and Pandolfo and Brown [1970].

When the subsurface is water, as in the BOMEX experiment, the formulas for the Richardson number and vertical diffusion coefficients are modified to include mixing length variations due to the presence of a "mean turbulent wave" at the interface. The formulations used here are based on work by Kitaigorodsky [1961]. The parameters needed include δ the wave steepness (height to length ratio), and λ the wavelength. The wavelength is found using the wind speed at 19.5m (Pierson [1964]) by

$$\lambda = 28.03 \times 10^{-4} \, (w_{19.5})^2 \quad . \tag{2.3-1}$$

Pierson also suggested that a constant steepness is appropriate for many applications in "fully developed" seas. The value 0.055 is used in the model when "fully developed" waves are indicated and is zero when the surface is soil.

Note that the modelling formulas shown are for "fully developed" seas and are applied when over water to bring the parameterized wave state into immediate and complete adjustment with the low level wind. The method needs revision for the simulation of duration-limited or fetch-limited cases. For example, the wavelength could be reduced by a given fraction.

The relevant wave property used in the calculation of the Richardson numbers and exchange coefficients is the vertical gradient of the scalar value of the average orbital velocity in a turbulent wave given by

$$S_w = g^{\frac{1}{2}} \, \delta \left(\frac{\lambda}{2\pi} \right)^{-\frac{1}{2}} e^{-z2\pi/\lambda} \quad . \tag{2.3-2}$$

In essence, this velocity shear, S_w, is added to the shear of the mean velocity when calculating Richardson numbers and vertical diffusion coefficients.

Richardson numbers are not computed at the first grid levels adjacent to the interface in either the atmospheric or water layers for computational convenience. This does not lead to unrealistic results for a shallow enough grid layer. Therefore, the Richardson numbers are assumed to be zero at these grid levels in the following computations for the water case.

Whenever the subsurface is land, the term S_w is zero.

The Richardson numbers in the atmosphere are computed as a function of height from

$$Ri = \frac{g}{\bar{T}} \left(\frac{\partial T}{\partial z} + \Gamma + .61\bar{T} \left(\frac{\partial q}{\partial z}\right)\right)\left(\left|\frac{\partial \vec{V}_2}{\partial z}\right| + S_w \right)^{-2} \qquad Ri \leq \frac{1}{|\alpha|} \qquad (2.3\text{-}3)$$

The Richardson numbers in water are computed from

$$R_i = - \frac{g}{\bar{\rho}_w} \left(\frac{\partial \rho_w}{\partial z}\right)\left(\left|\frac{\partial \vec{V}_2}{\partial z}\right| + S_w \right)^{-2} . \qquad (2.3\text{-}4)$$

The density gradient $(\partial \rho_w / \partial z)$ is computed (e.g., Sverdrup et al. [1942]) from

$$\frac{\partial \rho_w}{\partial z} = 10^{-3} \frac{\partial \sigma_T}{\partial z} = 10^{-3} \left(\frac{\partial \sigma_T}{\partial T} \frac{\partial T}{\partial z} + \frac{\partial \sigma_T}{\partial s} \frac{\partial s}{\partial z} \right) , \qquad (2.3\text{-}5)$$

where the values of $\partial \sigma_T / \partial T$ and $\partial \sigma_T / \partial s$ are obtained by differentiation of an empirically obtained formula for σ_T given by Cox et al. [1970].

The exchange coefficient formulas for the atmospheric layer are consistent with the profile formulas discussed by Pandolfo [1966], except that the shear S_w is added to the shear $|\partial \vec{V}_2 / \partial z|$.

Thus, for stable conditions, the eddy viscosity K_m is given by

$$K_m = k^2 \left(z + \frac{\delta \lambda}{2} \right)^2 \left(\left|\frac{\partial \vec{V}_2}{\partial z}\right| + S_w \right)\left(1 + \alpha Ri \right)^2 , \quad Ri \geq 0 \qquad (2.3\text{-}6)$$

where $k = 0.4$; and the eddy conductivity-diffusivity is assumed to be

$$K_e = K_m . \tag{2.3-7}$$

For lapse forced convection conditions, the formulas are

$$K_m = k^2 \left(z + \frac{\delta\lambda}{2}\right)^2 \left(\left|\frac{\partial \vec{V}_z}{\partial z}\right| + S_w\right)(1 - \alpha Ri)^{-2} \tag{2.3-8}$$

and

$$K_e = K_m (1 - \alpha Ri)^{-2} \quad , \quad -.048 < Ri < 0 . \tag{2.3-9}$$

For lapse free convection conditions, i.e. for $Ri \leq -0.048$, the formulas are

$$K_e = h \left(z + \frac{\delta\lambda}{2}\right)^2 \left|\frac{g}{\bar{T}} \left(\frac{\partial T}{\partial z} + \Gamma + .61\bar{T} \left(\frac{\partial q}{\partial z}\right)\right)\right|^{\frac{1}{2}} \tag{2.3-10}$$

and

$$K_m = K_e \left(\frac{3}{C}\right)^{-1/2} |Ri|^{-1/6} , \tag{2.3-11}$$

where

$$C = 3k^{4/3} h^{-2/3} , \qquad Ri \leq -.048 \tag{2.3-12}$$

and h is the Priestley constant. See Pandolfo [1966] for more detail on the formulas and constants used in lapse conditions.

Computed values for the eddy exchange coefficients for extreme stability are meaningless whenever they fall below estimates for minimum values in the atmospheric boundary layer (Pandolfo [1969]). The minimum values used for the atmosphere are

$$10^4 \leq K \text{ cm}^2/\text{sec} \qquad z \geq 100 \text{ m}$$

$$10^2 \leq K \text{ cm}^2/\text{sec} \qquad z < 100 \text{ m} .$$

The exchange-coefficient formulas used for the oceanic layer are the modified Rossby-Montgomery formulas (after Kitaigorodsky [1961]) for stable stratification:

$$K_m = k_1^2 \left(\left| \frac{\partial \vec{V}_2}{\partial z} \right| + S_w \right) (1 + 10Ri)^{-1/2}, \quad Ri \geq 0 \tag{2.3-13}$$

and

$$K_e = k_1^2 \left(\left| \frac{\partial \vec{V}_2}{\partial z} \right| + S_w \right) \left(1 + \frac{10}{3} Ri \right)^{-3/2} . \tag{2.3-14}$$

For these formulas, Kitaigorodsky assigned an estimated value of $k_1^2 = 0.02$.

For unstable stratification in the oceanic layer, the exchange coefficients are given by

$$K_e = h \left(z + \frac{\delta\lambda}{2} \right)^2 \left| g \frac{\partial \ell n \rho}{\partial z} \right|^{1/2} \tag{2.3-15}$$

and

$$K_m = K_e \left(\frac{3}{C} \right)^{-1/2} |Ri|^{-1/6} \qquad Ri < 0 , \tag{2.3-16}$$

where

$$C = 3k^{4/3} h^{-2/3} . \tag{2.3-17}$$

Limiting values of the water exchange coefficient for stable conditions, based on values that correspond to molecular viscosity, conductivity and diffusivity are

$$K_m \geq 0.14 \text{ cm}^2/\text{sec}$$

$$K_e \geq 0.0014 \text{ cm}^2/\text{sec} .$$

2.4 Source Terms

2.4.1 Solar radiation

The computation of the incoming solar energy at the surface is an important parameter in the heat balance equation in Section 2.2.4 and induces the diurnal variation of the surface temperature. Further, the solar radiation results in additional source terms for both the atmospheric and oceanic temperature equations given in Sections 2.2.1 and 2.2.2.

Initially the incoming solar radiation is computed at the top of the boundary layer by using the integral form of Beer's law for a horizontal surface (e.g. Hess [1959], eq. 8.7)

$$I_{1_\lambda} = I_{0_\lambda} \cos Z \exp\left(-\int_{z_1}^{\infty} k_\lambda \rho(z) \sec Z \, dz\right) = I_{0_\lambda} \tau \cos Z \, . \tag{2.4-1}$$

However, many empirical relations have been developed to account for integration over wavelengths in the solar spectrum. The method used here is based on a method by Kondrat'yev [1969, eq. 5.10] and by McDonald [1960]. The integrated incoming solar radiation is given by

$$I_1' = I_0 \cos Z \, [.5(1 - \tau_s) - a_w] \tag{2.4-2}$$

where τ_s is the transmission through the atmosphere that results from molecular scattering and absorption by ozone and oxygen, the number .5 accounts for forward scattering, and a_w is the absorption of water vapor. The transmission τ_s is given (Kondrat'yev [1969]) by

$$\tau_s = 1.041 - 0.16 \, [(9.49 \times 10^{-4} \, P_B + .051) \sec Z]^{\frac{1}{2}} \tag{2.4-3}$$

where P_B is the pressure at the top of the boundary layer and the absorption for water vapor is given by MacDonald [1960] as

$$a_w = .77 \, (u_T \sec Z)^{.3} \tag{2.4-4}$$

where u_T is the path length of water vapor above the boundary layer given by

$$u_T = \frac{1}{g} \int_{p(z_N)}^{\infty} q \, dp \, . \tag{2.4-5}$$

The differences between the results using this method and the results using a more detailed (38 wave intervals) equation of Atwater [1970] are of the same magnitude as instrumental errors of measurement.

The incoming solar radiation is modified by the presence of clouds above the boundary layer. The transmission through clouds is based on data by Fritz [1951] for transmissivity and is given by Pandolfo et al. [1970] as

$$I_1 = I_1' \prod_{i=1}^{n} [1 - c_i(1 - \phi_i)] \qquad (2.4\text{-}6)$$

for n cloud layers.

2.4.1.1 Solar radiation in the atmospheric layer

The source term for solar radiation in the atmospheric boundary layer is given by (Hess [1959], p. 146)

$$S_1 = \frac{g}{c_p} \frac{dI_a}{dp} \qquad (2.4\text{-}7)$$

where the derivative is computed from the appropriate functions in the previous sections. The computation, therefore accounts for absorption. Scattering is taken into account when the total flux reaching a level is computed, but this part of the depletion does not contribute to the source term. Thus, the derivative of the solar intensity for absorbed radiation is given for water vapor by McDonald [1960]

$$dI_a = -7.55 \times 10^{-4} (u_T \, sec Z)^{-7} \, du \, . \qquad (2.4\text{-}8)$$

The depletion due to scattering, which does not contribute to the source term, is given by

$$dI_s = -I_0 \, 3.796 \times 10^{-5} [(9.49 \, P \times 10^{-4} + .051) \, sec Z]^{-\frac{1}{2}} \, dp \, . \qquad (2.4\text{-}9)$$

The presence of aerosols in an urban boundary layer may contribute to the source term (Atwater [1970]). The transmission for absorbing and scattering particles was given by Atwater [1970] as

$$\tau_\lambda = exp\left(-\int_z^\infty \rho(z)\, k_\lambda\, sec Z\, dz\right) \tag{2.4-10}$$

where

$$\rho(z)\, k_\lambda \equiv B_\lambda(z) = \int_{r_1}^{r_2} \pi\, n(r,z)\, r^2\, Q_\lambda(m,r)\, ds\ . \tag{2.4-11}$$

The number distribution is based on a modified gamma distribution, which is described in detail in Appendix D. The Mie efficiency factor $Q_\lambda(m,r)$ is based on the radius and the complex index of refraction (where the imaginary part of the index refers to absorption) and has been described in detail by Deirmendjian [1969]. The wavelength is assumed to be .485μ.

Thus an added contribution to the source term results from the presence of particles and is given by

$$dI_a = - IB_a\, exp\left(-\int_z^\infty B_a\, sec Z\, dz\right)\ . \tag{2.4-12}$$

The analogous formula for scattering is

$$dI_s = - IB_s\, exp\left(-\int_z^\infty B_s\, sec Z\, dz\right)\ , \tag{2.4-13}$$

which contributes to depletion of the radiation reaching the surface.

2.4.1.2 Solar source term in water

The source term for solar radiation in the water layer is computed, from Hess [1959] as

$$S_1 = \frac{1}{\rho_w\, c_w}\, \frac{\partial I_a}{\partial z}\ . \tag{2.4-14}$$

According to Beer's law, the intensity of solar radiation at any level is given by

$$I(-z) = I(0)\, e^{-k_w \Delta z \, sec Z} , \qquad (2.4\text{-}15)$$

where all radiation and absorption terms have been integrated over the solar spectrum. Because of selective extinction in the water, the value of k_w is computed as an empirical function of depth from observations.

The absorption coefficients are computed or linearly interpolated from data for the oceans, presented by Sverdrup et al. [1942] and Kondrat'yev [1969], and are shown in Table 1. For Lake Ontario, an empirical relation based on data presented by Beeton [1962] is given by

$$k_w = 0.524 - 0.014z + .0034z^2 \qquad (2.4\text{-}16)$$

where z is the depth in meters. This formula may turn out to be more generally representative of inland water than are the oceanic tabular values.

TABLE 1

Extinction Coefficients in the Ocean

Depth	k_w
<2 m	$k = 1.034 - .5698\ \ell nz$
2 m	.6370
5 m	.3510
10 m	.2350
20 m	.1650
50 m	.1160
100 m	.0977

2.4.2 Infrared radiation

Schwarzschild's equation (Hess [1959], eq. 8.9), which is given by

$$dI_\lambda = \rho k_\lambda [E_\lambda(T) - I_\lambda] \tag{2.4-17}$$

is used to compute the absorption and emission of radiation in the infrared spectrum. Numerous authors have integrated Schwarzschild's equation for infrared radiation (Elsasser and Culbertson [1960], Atwater [1966]). An approximate solution for monochromatic radiation using conventional boundary conditions, and the assumption of horizontal homogeneity, yields the downward flux at a given height, $F_\lambda{\downarrow}(z)$, as

$$F_\lambda{\downarrow}(z) = - \int_z^\infty E_\lambda(T_{z'}) \frac{\partial \tau(z,z')}{\partial z'} \, dz' \tag{2.4-18}$$

and the upward flux at the same height, $F_\lambda{\uparrow}(z)$, as

$$F_\lambda{\uparrow}(z) = E_\lambda(T_g) \, \tau_\lambda(z,0) - \int_0^z E_\lambda(T_{z'}) \frac{\partial \tau(z,z')}{\partial z'} \, dz' \tag{2.4-19}$$

where $\tau(z,z')$, the transmission function, is defined by

$$\tau(z,z') = exp\left(- |\psi \int_z^{z'} \left(\sum_{i=1}^{n} \rho(z)_i \, k_{\lambda i} \right) dz| \right) \tag{2.4-20}$$

where ψ is a diffusivity factor independent of λ which accounts for integration over all zenith angles.

Many studies have been performed to establish the values of the diffusivity factor with values near 1.60 to 1.66 (e.g. Elsasser [1942], Goody [1964], and Boudreau [1968]). The value used here is 1.66. The approximation simplifies the solution of the radiative transfer equations but may introduce errors. No attempt at a determination of these errors is made in this report.

The equations (2.4-18) and (2.4-19) may be integrated over wavelength using the Stefan-Boltzmann law

$$\sigma T^4 = \int_0^\infty E_\lambda(T)\, d\lambda \qquad (2.4\text{-}21)$$

and empirical relations between the absorber concentration as a function of height and the transmission function.

The absorbers used for infrared radiation include water vapor, carbon dioxide, and particles (aerosols). Empirical transmission functions were derived for water vapor from data by Kuhn [1963]. The carbon dioxide transmission function was given by Kondrat'yev [1969]. The aerosol functions are computed from Atwater [1970] as

$$\tau = exp\ [-\rho(z)\ k\ \psi\ dz] \qquad (2.4\text{-}22)$$

where $\rho(z)\ k$ is computed from the relationships presented in Section 2.4.1.1 and is a spectrally averaged function over the infrared spectrum.

When clouds are present, the equation for downcoming flux is rewritten

$$F\downarrow(z) = \int_z^{z_c} \sigma T_z^4\ \partial\tau + \int_{z_c}^\infty (1 - c)\ \sigma T_z^4\ \partial\tau + (c - c')\tau\ (|z_c - z|)\ \sigma T_c^4 \qquad (2.4\text{-}23)$$

where c is the cloud amount in hundredths for a cloud base at height z_c with a temperature T_c, and c' is zero. When more than one cloud layer is used, c' refers to the coverage for the lower cloud layers and the appropriate limits are used for the individual terms. Up to four cloud layers are permitted. At present, no clouds are permitted below level z for upward radiation.

The net infrared flux $F_n(z)_{ir}$, at a given level, is given by

$$F_n(z)_{ir} = F\uparrow(z) + F\downarrow(z) . \qquad (2.4\text{-}23)$$

The infrared radiative source term is given by Hess [1959] as

$$S_2 = \frac{1}{\rho c_p} \frac{dF_n(z)}{dz} . \qquad (2.4\text{-}24)$$

2.4.3 Pollutant sources

The flux of pollutant into the atmosphere is not restricted to a source at the ground but occurs at various elevations. Therefore, the model has been developed to include elevated sources. The emission strengths from the source inventory are divided and assigned, according to the nature of the source to points on the vertical grid. The strength at the interface is set by the method outlined in Section 2.2.4. At the higher elevations, the pollutant is assumed to be instantaneously mixed in the layer that is bounded by the midpoints of the layers adjacent to the grid level. This results in a source term

$$S_p = \frac{F_e}{\rho \Delta z} . \qquad (2.4\text{-}25)$$

2.5 The Horizontal Advection Calculations

Detailed quantitative formulations for horizontal diffusion in the planetary boundary layer, which are adequately based on observations, are not available. Our knowledge of this process as it exists in nature does not extend much further than that lateral turbulent exchange coefficients increase generally as the scale of the phenomena considered increases, and that their magnitude is roughly a few orders of magnitude greater than the corre-

sponding coefficients characteristic of vertical turbulent exchange.

In view of these facts, the relative accuracy of various horizontal finite difference schemes, as are discussed in the recent papers of Molenkamp [1968] and Crowley [1968], appears to be a matter of secondary interest, once the diffusive component of this error is defined. Once the magnitude of this error is known, it may be easily made consistent with our vaguely defined state of knowledge of the horizontal diffusive process in nature. This is the justification given by Orville [1968] for the use of the highly diffusive upwind differencing scheme for the horizontal advection terms.

Our first version of the three-dimensional model follows Orville's procedure in omitting explicit consideration of a horizontal diffusion process, and depends on the diffusive computational error of the upwind differencing scheme to implicitly and roughly simulate the action of this natural process in the numerical model.

The choice of the horizontal grid is dependent on the problem to which the model is applied. The vertical velocity is required to remain zero at the interface and is computed at the upper (and lower, in the case of water) boundary of the boundary layer. Peripheral horizontal gradients are prespecified and are presumed to come from coarser or large scale definitions of surrounding fields. These specified gradients are used to compute the advection at inflow lateral boundary points. The actual finite difference approximation formulas used are presented in detail in Appendix A of this report.

2.5.1 Second-order error as effective diffusion

In a two-dimensional Cartesian coordinate system, the partial differential equation governing the process of advection is of the form

$$\frac{\partial A}{\partial t} = - u \frac{\partial A}{\partial x} - v \frac{\partial A}{\partial y} \qquad (2.5\text{-}1)$$

where A denotes the quantity being advected, t the time, x and y the spatial coordinates, and u,v the velocity components in the x,y directions, respectively. We set out to investigate the truncation error present in the numerical solution as a result of applying the "upwind" difference scheme to equation (2.5-1).

If Δx and Δy are the spatial grid increments, and Δt the time increment, then for $x = i\Delta x$, $y = k\Delta y$, and $t = n\Delta t$, the approximation to $A(x,y,t)$ is denoted by $A^n_{j,k}$. Assuming the velocity components u and v to be constant in time, $u(j\Delta x, k\Delta y)$ and $v(j\Delta x, k\Delta v)$ are denoted by $u_{j,k}$ and $v_{j,k}$, the superscript being unnecessary. With this notation the upwind difference approximation for (2.5-1) is of the form

$$\frac{A^{n+1}_{j,k} - A^n_{j,k}}{\Delta t} = - u_{j,k} \frac{\delta_1 A^n_{j,k}}{\Delta x} - v_{j,k} \frac{\delta_2 A^n_{j,k}}{\Delta y} \qquad (2.5\text{-}2)$$

where

$$\delta_1 A^n_{j,k} = \begin{cases} A^n_{j,k} - A^n_{j-1,k} & \text{for } u_{j,k} > 0 \\ A^n_{j+1,k} - A^n_{j,k} & \text{for } u_{j,k} \leq 0 \end{cases} \qquad (2.5\text{-}3)$$

and

$$\delta_2 A^n_{j,k} = \begin{cases} A^n_{j,k} - A^n_{j,k-1} & \text{for } v_{j,k} > 0 \\ A^n_{j,k+1} - A^n_{j,k} & \text{for } v_{j,k} \leq 0 \end{cases} \qquad (2.5\text{-}4)$$

In a paper by Molenkamp [1968], the author investigates the behavior of the truncation error associated with the upwind difference scheme when applied to the one-dimensional advection equation (no y-dependence). Molenkamp found that when second order terms are retained in the difference approximation, the upwind difference equation is consistent with the differential equation

$$\frac{\partial A}{\partial t} = - u \frac{\partial A}{\partial x} + \frac{1}{2} |u| \left(1 - \left|\frac{u\Delta t}{\Delta x}\right|\right) \Delta x \frac{\partial^2 A}{\partial x^2} \quad , \qquad (2.5\text{-}5)$$

provided u is assumed constant in time and space. It is seen that equation (2.5-5) not only contains the terms properly belonging to the one-dimensional advection equation, but in addition contains a term proportional to the second derivative of A with respect to x. This latter term, representing the lowest order error in the upwind difference scheme, may be considered a diffusion-type term provided the coefficient is positive. Such will be the case if and only if

$$\left|\frac{u\Delta t}{\Delta x}\right| < 1 , \tag{2.5-6}$$

this inequality being precisely the von Neumann criterion for stability of the upwind difference scheme (e.g. see Richtmyer [1963]). By taking in expression (2.5-6) parametric values typical for thermal convection, Molenkamp found that the effective diffusion coefficient introduced by the upwind differencing can be comparable in magnitude to estimated turbulent diffusion coefficients. Guided by Molenkamp's result, we now attempt to determine analogous effective diffusion terms for the two-dimensional upwind differencing scheme (2.5-2).

Taylor series expansions for the various terms in (2.5-2) may be written in the forms

$$\begin{aligned}
A^{n+1}_{j,k} &= A^n_{j,k} + \Delta t\left(\frac{\partial A}{\partial t}\right)^n_{j,k} + \frac{(\Delta t)^2}{2!}\left(\frac{\partial^2 A}{\partial t^2}\right)^n_{j,k} + \cdots \\
A^n_{j+1,k} &= A^n_{j,k} + \Delta x\left(\frac{\partial A}{\partial x}\right)^n_{j,k} + \frac{(\Delta x)^2}{2!}\left(\frac{\partial^2 A}{\partial x^2}\right)^n_{j,k} + \cdots \\
A^n_{j-1,k} &= A^n_{j,k} - \Delta x\left(\frac{\partial A}{\partial x}\right)^n_{j,k} + \frac{(\Delta x)^2}{2!}\left(\frac{\partial^2 A}{\partial x^2}\right)^n_{j,k} - + \cdots
\end{aligned} \tag{2.5-7}$$

with similar expressions for $A^n_{j,k+1}$ and $A^n_{j,k-1}$. Retaining second order terms in these series and substituting the resulting expressions in (2.5-2)

yields the differential equation

$$\frac{\partial A}{\partial t} + \frac{1}{2}\Delta t \frac{\partial^2 A}{\partial t^2} = - u\left[\frac{\partial A}{\partial x} - (sgn\ u)\frac{1}{2}\Delta x \frac{\partial^2 A}{\partial x^2}\right] - v\left[\frac{\partial A}{\partial y} - (sgn\ v)\frac{1}{2}\Delta y \frac{\partial^2 A}{\partial y^2}\right] \tag{2.5-8}$$

where we define the function $sgn\ x$ to be -1 for $x \leq 0$ and +1 for $x > 0$. The second derivative with respect to time appearing in equation (2.5-8) may be replaced by spatial derivatives through application of equation (2.5-1). Differentiation of (2.5-1) with respect to time gives

$$\frac{\partial^2 A}{\partial t^2} = \left(- u \frac{\partial}{\partial x} - v \frac{\partial}{\partial y}\right)\frac{\partial A}{\partial t}\ , \tag{2.5-9}$$

where we assume both u and v to be constant. Using (2.5-1) once again and substituting for $\partial A/\partial t$ in (2.5-9), we obtain

$$\frac{\partial^2 A}{\partial t^2} = u^2 \frac{\partial^2 A}{\partial x^2} + 2uv \frac{\partial^2 A}{\partial x \partial y} + v^2 \frac{\partial^2 A}{\partial y^2}\ , \tag{2.5-10}$$

where $\partial^2 A/\partial x \partial y$ and $\partial^2 A/\partial y \partial x$ have been assumed equal. By means of (2.5-10) equation (2.5-8) can now be written as

$$\frac{\partial A}{\partial t} = - u \frac{\partial A}{\partial x} - v \frac{\partial A}{\partial y} + u\,(sgn\ u)\frac{1}{2}\Delta x \frac{\partial^2 A}{\partial x^2} + v\,(sgn\ v)\frac{1}{2}\Delta y \frac{\partial^2 A}{\partial y^2} - \frac{1}{2}\Delta t\left(u^2 \frac{\partial^2 A}{\partial x^2} + 2uv \frac{\partial^2 A}{\partial x \partial y} + v^2 \frac{\partial^2 A}{\partial y^2}\right) \tag{2.5-11}$$

or

$$\frac{\partial A}{\partial t} = - u \frac{\partial A}{\partial x} - v \frac{\partial A}{\partial y} + \frac{1}{2}|u|\left(1 - \left|\frac{u\Delta t}{\Delta x}\right|\right)\Delta x \frac{\partial^2 A}{\partial x^2} + \frac{1}{2}|v|\left(1 - \left|\frac{v\Delta t}{\Delta y}\right|\right)\Delta y \frac{\partial^2 A}{\partial y^2} - \Delta t\, uv \frac{\partial^2 A}{\partial x \partial y}\ . \tag{2.5-12}$$

It is seen that (2.5-12) contains those terms appearing in the advection equation (2.5-1), two diffusion-type terms, and a term involving a mixed partial derivative of A.

Since there is no clear interpretation of the effect of the mixed derivative term, we attemnt to eliminate this term through a suitable rotation of the coordinate axes. Letting $\xi = \xi(x,y)$ and $\eta = \eta(x,y)$ with $A(\xi,\eta)$ replacing $A(x,y)$, (2.5-12) transforms to

$$\begin{aligned}\frac{\partial A}{\partial t} = {} & (\alpha\xi_x^2 + \beta\xi_x\xi_y + \gamma\xi_y^2)\frac{\partial^2 A}{\partial \xi^2} + [2\alpha\xi_x\eta_x + \beta(\xi_x\eta_y + \xi_y\eta_x) \\ & + 2\gamma\xi_y\eta_y]\frac{\partial^2 A}{\partial \xi \partial \eta} + (\alpha\eta_x^2 + \beta\eta_x\eta_y + \gamma\eta_y^2)\frac{\partial^2 A}{\partial \eta^2} \\ & + f(A_\xi, A_\eta, \xi, \eta, \ldots)\end{aligned} \tag{2.5-13}$$

where

$$\begin{aligned}f(A_\xi, A_\eta, \xi, \eta, \ldots) = {} & \alpha(\xi_{xx}\frac{\partial A}{\partial \xi} + \eta_{xx}\frac{\partial A}{\partial \eta}) + \beta(\xi_{yx}\frac{\partial A}{\partial \xi} + \eta_{yx}\frac{\partial A}{\partial \eta}) \\ & + \gamma(\xi_{yy}\frac{\partial A}{\partial \xi} + \eta_{yy}\frac{\partial A}{\partial \eta}) + \delta(\xi_x\frac{\partial A}{\partial \xi} + \eta_x\frac{\partial A}{\partial \eta}) \\ & + \varepsilon(\xi_y\frac{\partial A}{\partial \xi} + \eta_y\frac{\partial A}{\partial \eta})\end{aligned} \tag{2.5-14}$$

and

$$\begin{aligned}\alpha &= \tfrac{1}{2}|u|\left(1 - \left|\frac{u\Delta t}{\Delta x}\right|\right)\Delta x, \qquad \beta = -uv\Delta t, \\ \gamma &= \tfrac{1}{2}|v|\left(1 - \left|\frac{v\Delta t}{\Delta y}\right|\right)\Delta y, \qquad \delta = -u, \\ \varepsilon &= -v.\end{aligned} \tag{2.5-15}$$

Since we require that the transformation be a rotation of the x,y-plane about the origin, ξ and η must be of the form

$$\xi = x\cos\phi + y\sin\phi \tag{2.5-16}$$

and

$$\eta = -x \sin\phi + y \cos\phi \tag{2.5-17}$$

for some angle ϕ. Then since $\xi_x = \eta_y = \cos\phi$ and $\xi_y = -\eta_x = \sin\phi$, the coefficient of the mixed derivative term in the transformed equation (2.5-13) will vanish provided that

$$-\alpha(2\sin\phi\cos\phi) + \beta(\cos^2\phi - \sin^2\phi) + \gamma(2\sin\phi\cos\phi) = 0 \tag{2.5-18}$$

or

$$(\gamma - \alpha)\sin 2\phi + \beta\cos 2\phi = 0 \ . \tag{2.5-19}$$

It follows from equations (2.5-18) and (2.5-19) that a suitable angle of rotation is given by the relation

$$\phi = \frac{1}{2}\tan^{-1}\left(\frac{\beta}{\alpha - \gamma}\right) \ . \tag{2.5-20}$$

Under such a rotation of coordinate axes, the advection equation takes the form

$$\frac{\partial A}{\partial t} = (\delta\cos\phi + \varepsilon\sin\phi)\frac{\partial A}{\partial \xi} + (-\delta\sin\phi + \varepsilon\cos\phi)\frac{\partial A}{\partial \eta} + K_1\frac{\partial^2 A}{\partial \xi^2} + K_2\frac{\partial^2 A}{\partial \eta^2} \tag{2.5-21}$$

where K_1 and K_2 are given by the formulas

$$K_1 = \alpha\cos^2\phi + \beta\sin\phi\cos\phi + \gamma\sin^2\phi \tag{2.5-22}$$

and

$$K_2 = \alpha\sin^2\phi - \beta\sin\phi\cos\phi + \gamma\cos^2\phi \ . \tag{2.5-23}$$

In order that K_1 and K_2 may be interpreted as diffusion coefficients, both quantities must be positive. To find conditions under which this is the case, we note that since the discriminant is invariant under a rotation of the axes about the origin, we have

$$4\alpha\gamma - \beta^2 = 4K_1K_2 \quad . \tag{2.5-24}$$

Now in terms of u and v,

$$4\alpha\gamma - \beta^2 = |u|\,|v| \left(1 - \left|\frac{u\Delta t}{\Delta x}\right| - \left|\frac{v\Delta t}{\Delta y}\right|\right) \Delta x\Delta y \quad . \tag{2.5-25}$$

From (2.5-24) and (2.5-25), it follows that if K_1, $K_2 > 0$, then

$$\left|\frac{u\Delta t}{\Delta x}\right| + \left|\frac{v\Delta t}{\Delta y}\right| < 1 \quad . \tag{2.5-26}$$

Conversely, suppose inequality (2.5-26) holds so that $|u\Delta t/\Delta x|$, $|v\Delta t/\Delta v| < 1$. Noting from (2.5-22) and (2.5-23) that $K_1 + K_2 = \gamma + \alpha$, or

$$K_1 + K_2 = \frac{1}{2}\left[|u| \left(1 - \left|\frac{u\Delta t}{\Delta x}\right|\right) \Delta x + |v| \left(1 - \left|\frac{v\Delta t}{\Delta y}\right|\right) \Delta y\right] , \tag{2.5-27}$$

we have that $K_1 + K_2 > 0$. But then either K_1 or K_2 must be greater than 0 ; and since (2.5-26) requires their product to be greater than 0, both K_1 and K_2 must be greater than 0. Thus, equation (2.5-26) is a necessary and sufficient condition that both K_1 and K_2 be positive. With condition (2.5-26) satisfied, the effective diffusion can be calculated by means of (2.5-20), (2.5-22) and (2.5-23). Since

$$K_1 = \frac{1}{2}\left[(\alpha + \gamma) + (\alpha - \gamma)\cos 2\phi + \beta \sin 2\phi\right] \tag{2.5-28}$$

and

$$K_2 = \frac{1}{2}\left[(\alpha + \gamma) - (\alpha - \gamma)\cos 2\phi - \beta \sin 2\phi\right] , \tag{2.5-29}$$

the diffusive effect will be greater in the ξ-direction than in the η-direction (i.e. $K_1 > K_2$) if and only if

$$\beta \sin 2\phi > (\gamma - \alpha)\cos 2\phi \quad . \tag{2.5-30}$$

2.5.2 The stability criterion for the two-dimensional upwind differencing scheme

Just as for the one-dimensional case in which inequality (2.5-6) turned out to be the von Neumann stability criterion for the upwind difference scheme, now for the two-dimensional case the inequality (2.5-26) is the stability criterion for the generalized scheme (2.5-2) (Forsythe and Wasow [1964]). To show this, we first assume that $A^n_{j,k}$ can be written in the form

$$A^n_{j,k} = \sum_{m,\ell} a_{m,\ell} \exp(im j\Delta x + i\ell k\Delta y)[\zeta(m,\ell)]^n \quad . \tag{2.5-31}$$

Substitution of this expansion in (2.5-2) and application of the orthogonality relations yield for u, $v > 0$

$$\zeta = 1 - \frac{u\Delta t}{\Delta x}(1 - e^{-im\Delta x}) - \frac{v\Delta t}{\Delta y}(1 - e^{-i\ell\Delta y}) \quad , \tag{2.5-32}$$

so that

$$|\zeta|^2 = \left[1 - \left|\frac{u\Delta t}{\Delta x}\right|(1 - \cos m\Delta x) - \left|\frac{v\Delta t}{\Delta y}\right|(1 - \cos \ell\Delta y)\right]^2 + \left[\left|\frac{u\Delta t}{\Delta x}\right| \sin m\Delta x + \left|\frac{v\Delta t}{\Delta y}\right| \sin \ell\Delta y\right]^2 \quad . \tag{2.5-33}$$

After some manipulation, (2.5-33) may be written in the form

$$|\zeta|^2 = 1 - 2\left[\left|\frac{u\Delta t}{\Delta x}\right|(1 - \cos m\Delta x) + \left|\frac{v\Delta t}{\Delta y}\right|(1 - \cos \ell\Delta y)\right] \cdot \left[1 - \left|\frac{u\Delta t}{\Delta x}\right| - \left|\frac{v\Delta t}{\Delta y}\right|\right] - 2\left|\frac{u\Delta t}{\Delta x}\right|\left|\frac{v\Delta t}{\Delta y}\right|[1 - \cos(\ell\Delta y - m\Delta x)] \quad . \tag{2.5-34}$$

In practice, the necessary and sufficient condition for stability is that

$$\max_{m,\ell} |\zeta(m,\ell)| \leq 1 \tag{2.5-35}$$

(e.g. see Richtmyer and Morton [1967]).

Case a) $1 - |u\Delta t/\Delta x| - |v\Delta t/\Delta y| \geq 0$. For this case the right hand side of (3-30) is clearly ≤ 1 for all possible values of m,ℓ . Hence $\max_{m,\ell}|\zeta(m,\ell)| \leq 1$.

Case b) $1 - |u\Delta t/\Delta x| - |v\Delta t/\Delta y| < 0$. Since in practice Δx and Δy can be prescribed only to a finite number of decimal places, we may assume that both Δx and Δy are rational numbers. Then we can choose ℓ and m such that $\ell/m = \Delta x/\Delta y$ (so that $1 - \cos(\ell\Delta y - m\Delta x) = 0$); moreover, $m\Delta x$ $(= \ell\Delta y)$ is rational and hence not an integral multiple of 2π (so that $1 - \cos m\Delta x > 0$). For such ℓ and m , $|\zeta|^2 = 1 - a$ where $a < 0$ so that $\max_{m,\ell}|\zeta|^2 \geq 1 - a > 1$.

Thus we have found that condition (2.5-35) is satisfied if, and only if,

$$\left|\frac{u\Delta t}{\Delta x}\right| + \left|\frac{v\Delta t}{\Delta y}\right| \leq 1 \ . \qquad (2.5\text{-}36)$$

Had we allowed either K_1 or K_2 to be zero in the discussion in Section 2.5.1, an equality sign would have been included in (2.5-26) making the inequalities (2.5-26) and (2.5-36) identical. For the cases in which u and v are allowed to be negative or zero, the above argument needs only minor modifications.

It is of some interest to note that the stability criterion derived by Richtmyer [1963] for the Lax-Wendroff scheme applied to the two-dimensional advection equation implies the criterion (2.5-36). For $\Delta x = \Delta y$, Richtmyer's criterion

$$(u^2 + v^2)^{\frac{1}{2}} \frac{\Delta t}{\Delta x} < \frac{1}{\sqrt{2}} \qquad (2.5\text{-}37)$$

implies that

$$2(u^2 + v^2)\left(\frac{\Delta t}{\Delta x}\right)^2 < 1 \qquad (2.5\text{-}38)$$

or

$$[(|u| + |v|)^2 + (|u| - |v|)^2]\left(\frac{\Delta t}{\Delta x}\right)^2 < 1 \qquad (2.5\text{-}39)$$

from which (2.5-36) follows directly.

2.6 Some Details of Practical Interest

A horizontal array of $M \times N$ (of order of magnitude 10×10) equidistant grid points is used with the grid interval specified for each simulation. At each grid point, there are up to 30 height levels to define the vertical profile for each of the dependent variables. Above the top level of the modelled layer there are prespecified pressure, temperature, humidity, and cloud levels that are used in radiation computations. The integration of the basic equation has used a 4.8 minute time step. Internally calculated time steps are used for the calculation of horizontal advection.

The upper boundary values of temperature and humidity are specified initially and held constant throughout the integration period. On the other hand, the geostrophic wind (i.e., the horizontal pressure gradient) is specified at key time steps at the upper boundary and a linear interpolation is used to obtain values at each time step. For the case of an air-water interface, the lower boundary values of temperature and salinity are specified like their counterparts at the upper boundary. The geostrophic current is specified at the interface for each time step in the same fashion as above. For an air-soil interface, lower boundary values of temperature are prescribed initially and held constant throughout the prediction period. Density and specific heat are time independent and are specified in the soil layer. Thermal conductivity-diffusivity is also independent of time and initially prescribed for each soil layer.

The vertical velocity is required to remain 0 at the interface and is calculated at both the upper and lower boundaries of the model.

The present computer is an IBM 360/65 at the University of Connecticut. The storage required is 132K bytes with additional intermediate storage on disks. The time required for 600 time steps at each grid point in the horizontal array is approximately one minute.

3.0 EXPERIMENTAL RESULTS WITH THE SINGLE STATION (z-t) MODEL

3.1 The Single Station Model

The development of the boundary layer model during the past eight years, described in Section 1.0, started with the model being applied to one station. It was only during the last couple of years the the model has been made three dimensional and applied at more than one station, and, specifically, applied at a horizontal array of grid points (as described in Section 2.0). The equations for the single station model are the same as the equations for the three-dimensional model with only two exceptions. The first is that vertical velocities are zero at all time. The second is that horizontal gradients are used at all times and are not internally recomputed. In the experiments described in this section, the gradients were input as zero.

There are several practical advantages for continuing to use the single station program. The first is the savings in time used on a computer and the computer space required. Thus, experimental results are available more rapidly and economically. A second advantage is that new programming techniques and additions to the model which are concerned solely with the vertical transfer processes can be readily tested. For example, the new features added to the previous three-dimensional and single station models during the present contract were the addition of pollutants as dependent variables and the optional subsurface of land or water. New radiation routines developed previously by Atwater [1970] were incorporated into the model which reduced the required computer time by 75 percent. These tests and additions would have been much more difficult and expensive to test if they had been added to the three-dimensional model first. Another advantage is that simpler experiments can be conducted with fewer variables, e.g. the internal computations of gradients can be neglected in these experiments.

Thus, advantages are apparent to having both a single station program and a three-dimensional model in which the subroutines are nearly identical. While the present contract did not explicitly require results for a single station, experiments were performed with minimum effort to obtain results illustrating several features of the urban boundary layer. Three experiments were performed using the single station program. The first was an estimation of the effects on interface temperature and vertical stability of variation in the surface parameters. The second examined the effects of varying elevation of pollution sources to note consistency with what might be expected from simpler models. The third experiment examined the modification of the thermal structure by nontransparent pollutants and the feedback effects on the pollution concentration.

3.2 An Experiment Illustrating the Effects of Variation of Surface Physical Parameters

3.2.1 The data

A realistic simulation of the boundary layer requires the correct specification of the physical parameters that describe the surface. These parameters include the solar albedo, the soil heat conductivity, the soil heat capacity, the roughness height, and the amount of heat released by combustion. The spatial variations in these parameters account for a large part of the horizontal variations in surface temperature and low level stability on the mesoscale, e.g., the differences observed between the urban and rural areas.

The specification of these parameters over a given modelled region is difficult in view of the large spatial variations. For example, when one grid point in a horizontal array in a city includes both parks and commercial regions, which have large differences in the parameters, the proper grid point

value to be chosen for each of the parameters is difficult to specify. Therefore, an experiment was made to examine the effects of various values for each of the parameters on the interface temperatures and the low level stability.

Representative values for an urban and rural area were adopted with slight modification from Myrup [1969]. These values, in addition to those for water, are given in Table 2. A series of seven simulations was made with various values of the surface parameters, as indicated in Table 3.

TABLE 2

Interface parameters for urban, rural, and land simulations

Parameter	Urban	Rural	Water
Albedo	.20	.20	*
Soil heat conductivity (cal/cm/sec/°K)	.011	.0026	*
Soil heat capacity (cal/cm^3/°K)	.55	.52	.935
Roughness Height (cm)	100	1	*
Moisture parameter	.20	.90	1.0
Artificial heat source (mly/sec)	2.17	0	0

* computed

TABLE 3

Rural/urban surface values used in each of the simulations

Parameter \ Simulation	1	2	3	4	5	6	7
Soil conductivity/ heat capacity	R	U	R	R	R	U	U
Moisture parameter	R	R	U	R	R	U	U
Artificial heat source	R	R	R	U	R	U	U
Roughness	R	R	R	R	U	U	U
Lower boundary temperature	R	R	R	R	R	R	U

In addition to the parameters specified in Table 2, a lower boundary (soil) temperature is assumed equal to 273.2 in the rural areas and 277.2 is assumed in the urban areas. The initial atmospheric data is given in Table 4, based on Atwater [1971]. The winds are assumed to be southerly, and the soil temperatures are linearly interpolated from the interface value to the lower boundary temperature. The upper and lower boundary values are assumed constant for all simulations.

TABLE 4

Data for the winter simulations (from Atwater [1971])

	Height m	Pressure (mb)	Temperature °K	Specific Humidity g/kg	Wind Velocity cm/sec
Initial Data	0	1018	278.20	2.30	0
	24.0	1015	277.80	2.40	40
	64.2	1010	277.60	2.50	100
	104.5	1005	277.40	2.50	130
	145.0	1000	277.20	2.50	180
	185.7	995	276.95	2.47	240
	226.5	990	276.70	2.45	290
	267.5	985	276.45	2.37	340
	308.7	980	276.20	2.35	380
	391.6	970	275.70	2.30	420
	475.1	960	275.20	2.25	460
	559.4	950	274.70	2.20	480
	773.5	925	273.45	2.10	500
Upper Level Data (constant for the duration of the simulation)		900	272.20	2.00	
		850	270.00	1.80	
		800	267.20	1.60	
		750	264.40	1.20	
		700	261.80	1.00	
		650	258.00	.80	
		600	255.20	.40	
		500	252.40	.10	
		400	237.00	.02	
		300	225.00	.004	
		200	218.00	.008	

In order to compare the stability in a summer simulation, two simulations were run in the summer that used the same surface parameters as used in Simulations 1 and 6. The atmosphere data is given in Table 5. The lower boundary temperature was held constant at 295.5 for the summer runs. Advection effects are ommited in all simulations.

TABLE 5

Data for the summer simulations (from Atwater [1971])

	Height m	Pressure (mb)	Temperature °K	Specific Humidity g/kg	Wind Velocity cm/sec
Initial Data	0	1010	299.5	9.0	0
	6	1009	298.8	9.0	20
	25	1007	298.1	9.3	40
	75	1001	296.7	9.4	110
	150	993	295.8	9.2	180
	300	976	293.9	8.9	380
	500	953	292.0	8.5	470
	750	926	290.0	7.7	500
	1000	899	287.4	7.0	530
	1500	847	284.4	6.0	550
	2000	797	281.1	4.6	555
Upper Level Data		700	277.9	3.75	
		600	270.6	2.35	
		500	261.3	1.25	
		400	250.8	.55	
		300	236.4	.17	
		200	222.1	.03	

3.2.2 The interface temperature

One of the necessary features for a realistic simulation of the boundary layer is a realistic simulation of the interface temperature. This experiment is designed to show changes in the interface temperature that result from changes in the surface parameters. The simulated interface temperature as

a function of time is shown in Fig. 3.2-1. The maximum and minimum temperature and diurnal variation are shown in Table 6.

TABLE 6

Summary of maximum and minimum temperatures for various simulations

Urban Parameter Used / Run*	1	2	3	4	5	6	7
Maximum Interface Temperature	282.4	279.9	284.9	285.6	279.4	28.10	281.7
Minimum Interface Temperature	264,3	269.8	264.2	273.5	264.6	273.1	276.3
Amplitude of Diurnal Wave	18.1	10.1	20.7	12.1	14.8	7.9	1 5.4

* 1 Rural
2 Soil
3 Moisture
4 Heat
5 Roughness
6 All Urban
7 All Urban and Temperature, -20 cm

It is seen that the urban values of the soil properties and the artificial heating increase the minimum temperature. The urban value of the moisture parameter and the artificial heat source increase the maximum temperature, while the urban value for soil and roughness decrease the maximum temperature. An increase in the lower boundary temperature increases both the maximum and minimum temperature.

In summary, each of the parameters tested had a noticeable effect on the interface temperature.

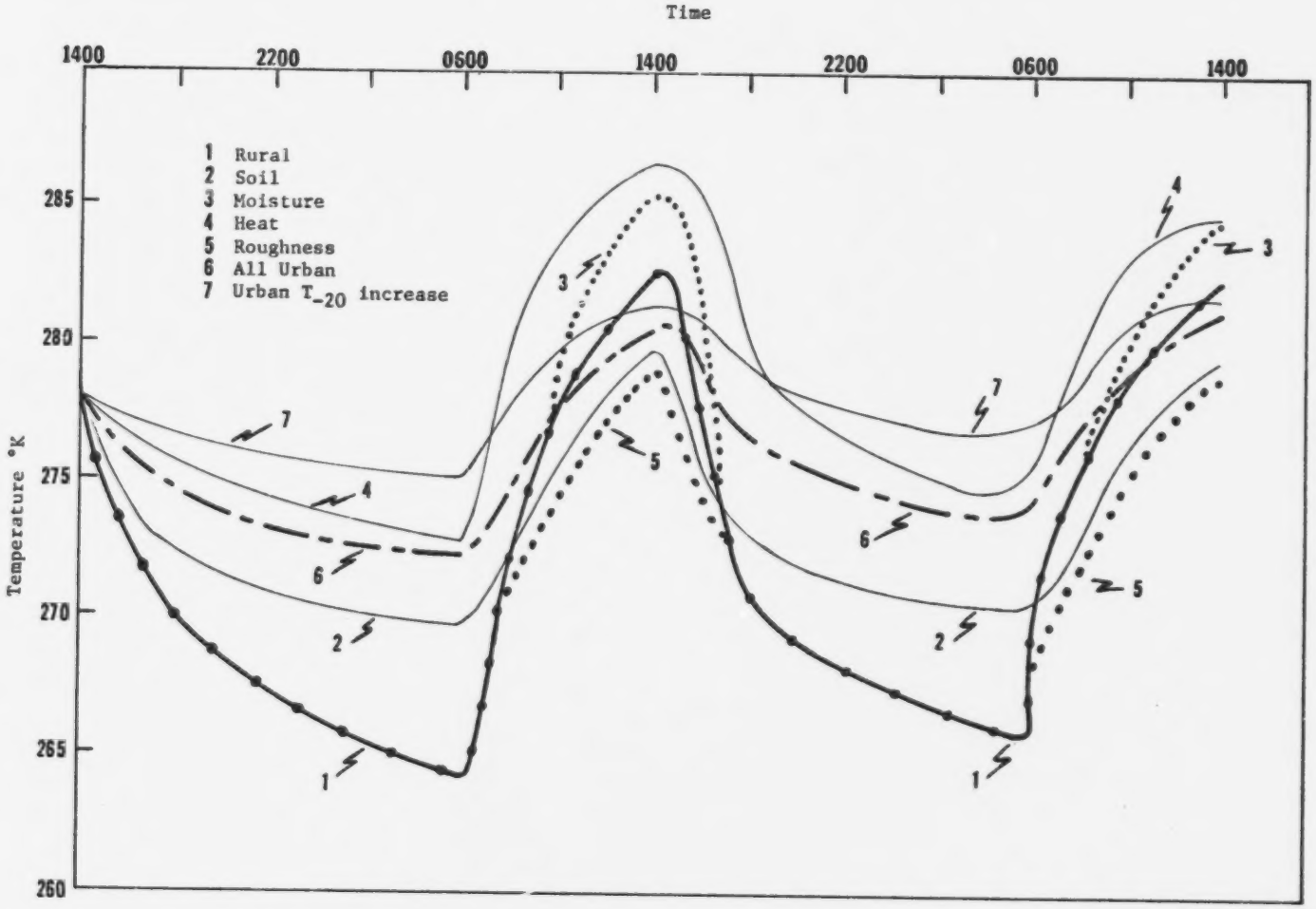

Figure 3.2-1. The interface temperature as a function of time and rural-urban parameters. Rural parameters used except as indicated .

3.2.3 Vertical stability and mixing depth

Until recently there have been few studies of the thermal structure over urban areas. Much of the early data gathered was restricted to the lower levels and showed that fewer inversions were present. Recently, observations have been made from helicopters in New York (Davidson [1967]), Cincinnati (Clarke [1969]), and Montreal (Oke and East [1971]). The results of these observational studies showed that weak, elevated inversions of temperature occur frequently during the early morning hours. These inversions inhibit the escape of pollutants from layers below the inversions.

Observations of the thermal structure in the afternoon are fewer than in the morning. Thus, the top of the mixing layer, important in many pollution prediction models, is relatively undocumented.

The results from these simulations can be used to show the depth of the mixing layer obtained in each of the simulations during the day or night and the strength of the nocturnal inversion. The two simulations for summer conditions, urban and rural, have been added here. The top of the inversion was 104 m in winter and 86 m in summer

TABLE 7

Depth (m) of the mixing layer and strength of the nocturnal inversion (°K)

Run	1	2	3	4	5	6	7	Summer Rural	Summer Urban
Day	433	350	517	660	288	350	600	1250	1250
Night	15	15	15	15	15	15	84	50	50
Temperature at top of nocturnal inversion	276	276	277	278	275	277	278	293	293
Temperature increase	11.9	7.2	12.8	4.9	10.3	3.7	1.3	5.2	.2

Comparisons of Table 7 with Table 6 show that the height of the mixing depth is strongly correlated to the maximum interface temperature.

3.3 The Sensitivity to the Effective Height of Pollution Sources

3.3.1 The data

An experiment was made to examine the resultant vertical profiles of pollution concentration from various elevations of the pollution source emissions. The initial atmospheric data and physical values are given in Table 8. The upper air profiles are the same above 750 mb as shown in Table 4. Southerly geostrophic wind is assumed with a speed of 500 cm/sec. All initial winds are assumed southerly. The lower boundary temperature is 277.2°K.

TABLE 8

Initial atmospheric data and physical surface values

Height (m)	Pressure (mb)	Temperature (°K)	Specific Humidity (g/kg)	Wind Velocity (cm/sec)
0	1018.0	278.2	2.40	0
6	1017.2	278.0	2.40	20
25	1014.9	277.8	2.45	40
50	1011.8	277.7	2.45	76
100	1005.6	277.4	2.50	130
150	999.4	277.2	2.50	180
200	993.2	276.8	2.46	260
300	981.0	276.2	2.35	380
500	957.0	275.0	2.23	467
750	927.1	273.5	2.11	595
1000	899.2	272.0	2.00	505
1500	849.1	269.0	1.80	510
2000	791.9	266.0	1.60	515

Albedo = .2, Soil heat capacity = .55 cal/cm^3/°K , Moisture = .2, Soil diffusivity = .2 cm^2/sec, Roughness = 100 cm, Artificial heat source = 0.

The strength of the pollutant emission is obtained from source inventories for the modelled regions. A typical set of emission values for sulfur dioxide and particulates obtained from the Connecticut source inventory (Hilst et al. [1967]) is given in Table 9 for an area near Hartford. The basic grid used in this case was 5000 ft (1.524 km). Dominant sources on the grid include a power plant in southeast Hartford at the point with coordinates 59,54 and a large number of apartments in southwest Hartford at point 58,55. Source strengths show large variations in relatively short distances. The source strength in this experiment was assumed to equal .001 $\mu gm/m^2/sec$.

TABLE 9

Source emissions of sulfur dioxide $\left(lbs/day/(1524)^2m^2\right)$ and particulates $\left(lbs/day/(1524)^2m^2\right)$ for January *

	50	51	52	53	54	55	56	57	58	59	60
60	.60	2.99	3.58	.35	8.43	46.5	44.4	45.4	168	287	130
	.53	2.65	3.18	.78	18.6	78.4	97.9	95.0	.426	94.6	66.9
59	2.98	.60	5.97	1.75	9.81	39.7	98.1	57.6	356	155	90.1
	2.64	.53	5.29	3.88	21.7	50.8	207	659	99.1	83.8	25.5
58	.74	.74	5.98	3.49	33.5	51.4	80	401	170	439	225
	1.22	1.22	9.79	7.76	32.3	106	168	235	79.1	.123	165
57	14.3	0	14.9	10.5	25.8	30.1	124	5116	98.4	179	103
	6.77	0	24.5	17.1	43.8	68.7	143	519	52.3	89.2	65.2
56	2.23	17.1	24.4	39.3	29.9	55.8	223	1292	81.1	53.7	677
	3.67	28.1	40.1	982	48.9	69.5	179	3200	35.2	30.9	281
55	5.20	33.1	33.3	21.7	8.0	20.5	81.1	75.2	2535	71.4	87.4
	8.55	43.2	54.8	20.2	11.6	17.6	259	64.5	4740	69.3	68.9
54	5.93	.74	.74	11.5	30.3	21.7	40.8	224	47.1	127400	85.7
	8.79	1.22	1.22	6.94	13.9	8.69	32.5	108	30.0	3300	103
53	15.0	5.22	29.5	97.9	37.6	38.2	67.8	82.9	29.2	12.6	117
	12.5	7.13	12.6	40.6	19.4	25.1	45.2	60.4	29.3	11.4	24
52	13.1	13.0	56.7	3076	12.2	64.6	31.3	21.1	5.99	4.15	51
	18.0	17.8	30.0	3960	57.8	38.7	21.3	21.0	6.81	3.88	43.7
51	39.8	197	2611	1696	199	83.7	15.5	16.8	4.14	4.14	32.8
	40.0	1130	106	253	75	33.6	12.4	19.5	3.88	3.88	30.4
50	8.84	7.07	19.3	66.9	790	362	70.4	21.6	0	.42	18.2
	18.1	14.3	12.0	24.8	63.5	1040	1550	27.9	200	.32	21.9

* Multiply by 1.858×10^{-3} to convert to $\mu gm/m^2/sec$.

The present source inventory does not show the effective heights, i.e. heights of chimney plus plume rise, at which the pollutants are introduced into the atmosphere. From structural considerations, rural and suburban sources may have an effective height of 6-15 m, while the urban residential sources should lie in the height range of 15-75 m in Connecticut. Power plant sources have been assumed to have an effective height in the range of 150 m. Oke and East [1971] have used an effective height of 200 m for Montreal.

Six simulations were made with the data described above with different effective heights for each simulation. The effective heights were assumed to be 0, 6, 25, 50, 100, and 150 m. All simulations started with an atmosphere without any pollutants. The duration for each of the simulations was two days.

3.3.2 The simulated profiles of pollution concentration

The vertical profiles for each of the simulations are shown in Fig. 3.3-1 for 0200 and 1400 local time. The profiles show little variation in daytime from the surface to 800 m. These daytime profiles are quite insensitive to source height. At night, the peak concentration is near the height assumed for the elevated source, and the profile is similar in shape to a Gaussian profile. Above 600 m, the simulated profiles are nearly identical. The strength of the nocturnal surface concentration is correlated with the height of the source and varies by a factor of 4.

An example of the time variation of vertical profiles of pollutant concentration for a time-constant surface source is shown in Fig. 3.3-2. It is seen that the pollution concentration at the surface varies with a range of a factor of about 6, with the maximum concentration near sunrise and the minimum concentration in the afternoon. Above 300 m there is little variation in the concentration.

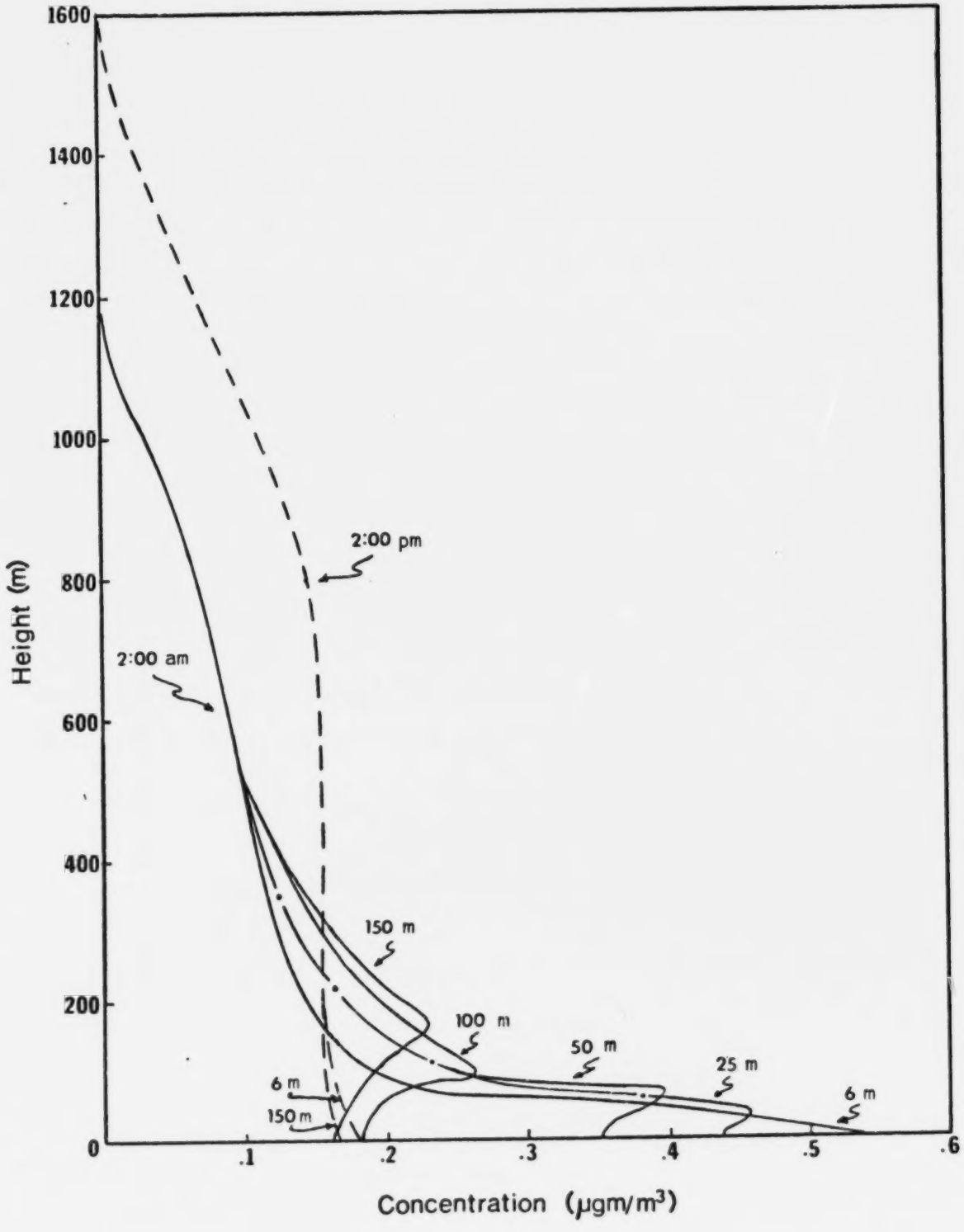

Figure 3.3-1. Concentration profiles for night and day with various effective source heights.

Figure 3.3-2. Simulated pollutant concentration ($\mu gm/m^3$) as a function of height and time.

3.3.3 Implications of experimental results for the design of simpler models

One of the uses the urban boundary layer model is to provide a standard for judging the validity of simpler, less sophisticated models. If the use of the simpler models is indicated, it provides data for determining the values and conditions of the parameters of the simpler models.

Most regional models emphasize the horizontal resolution of ground-level pollution concentrations, and limit the vertical resolution to save computational time and input data requirements. It is of interest to examine the vertical profiles of concentration generated by the present model to determine the most suitable simplified representation as a function of source location and the turbulence distribution.

The simulations for this experiment, representing winter urban conditions with homogeneity over a significant horizontal extent, is characterized by a wide range of stability over a diurnal cycle. For the cases discussed here, the Pasquill stability class would vary from "F" late in the night to "B" in the afternoon with roughly five hours in each class.

The "K-theory" analyses in two dimensions generally scale the thickness of a layer by a characteristic Gaussian length scale σ_z, which is related to the eddy coefficient by

$$\sigma_z^2 = 2K_e (t - t_0) \qquad (3.3\text{-}1)$$

or

$$\sigma_z^2 = 2K_e \frac{X}{V_X} \qquad (3.3\text{-}2)$$

where X is a distance downwind from the source, and V_X is the wind velocity in the direction of X.

For a simplified analysis, the simulations of concentration need to be

scaled by a Gaussian length scale. Since these simulations are applied for a single grid point, no horizontal scale is included. However, it is implied that the horizontal scales are large because of the assumption of horizontal homogeneity. The relationship for σ_z as a function of K_e is tabulated for several X's varying about one kilometer in Table 10. The Pasquill stability class is indicated beside each entry, where appropriate. Several examples below will show the probable values of X needed for these simulations that are comparable to the values of X used in other "K-theory" models, e.g. the CEM regional pollution model (Hilst et al. [1967]).

TABLE 10

Turbulence scale (σ_z) in m.

X(km)	K_e/V_x (m)				
	10^2	10^3	10^4	10^5	10^6
0.5	21(D)	70(A,B)	210(A)	700	2100
1.0	30(D)	100(B)	300(A)	1000(A)	3000
2.0	42(D,E)	140(C)	420(A,B)	1400(A)	4200(A+)
4.0	60(D,E)	200(C)	600(B)	2000(A,B)	6000(A)

Clear night conditions with a 10 m wind speed of about 20 cm/sec has a Pasquill stability class of "F", which are met in the simulation from sundown to sunrise. The eddy diffusivity at 10 m height for this same period is of the order of 2000 cm^2/sec. The K_e/V_x value of 100 cm is, from Table 10, consistent with "F" class stability at an X some longer than 4 km. A median value of eddy diffusivity at 10 m is about 5×10^4 cm^2/sec. During daytime, with a wind of about 3 m/sec, the stability class would be "B". A "B" stability class is consistent with $K \approx 5 \times 10^4$ cm^2/sec at an X somewhat

more than .5 km, which is not extremely consistent with the nighttime result. For comparison, the CEM regional pollution model is on a 1.54 km grid and used a length scale of 2 grid lengths or 3.1 km. The present results suggest the use of variable scale lengths may be useful. This discussion also confirms that the diurnal cycle used covers a range of stability cases of interest.

From the simulated daytime profiles, it appears that an appropriate value of the Gaussian length scale would be near 70 m and that a one layer model would be adequate during this period. The lower nocturnal eddy diffusivities are reflected in the maximum pollutant concentration at the effective height of the pollutant source. The surface concentration, as stated in Section 3.3.2, is dependent on the effective height of the source and is similar to a Gaussian profile for an elevated source. It is during this period that a simpler K-theory model, like the CEM Connecticut model, may have difficulty in defining the surface concentration adequately. However, it is possible that the present model can be used to define the parameters necessary to improve the accuracy of the simpler models.

3.4 Experiment for Radiatively Non-transparent Pollutants

3.4.1 The data

This experiment was performed to determine the possible modification of the thermal structure by non-transparent pollutants. A major motivation for conducting this experiment resulted from the adoption of more efficient radiation computation routines from Atwater [1970] which included the capability of examining the effects of non-transparent pollutants. Because the programming for the simulation of pollutant concentration was not complete, the pollution concentration during the first simulations was held constant.

Further, these simulations allow the modification of the thermal structure by non-transparent pollutants to be examined.

The two simulations described here, rural and urban, are based on the same data as run 1 and 6 described in Section 3.2 and Table 3.

The major problem in these experiments is to specify realistic absorption and scattering characteristics of the polluted layer. For this preliminary illustrative example, pollutants are assumed to be particulates. Gaseous pollutants are not considered, due to the relative weakness of their radiative effects on temperature compared to those of particles (Atwater [1970]). The absorption and scattering coefficients of particles are dependent on the complex refractive index and the size-frequency distribution of the particles. However, the heating and cooling rates are nearly proportional to the absorption and scattering coefficients assumed for realistic particle layers (Atwater [1971]). Therefore, relatively high values of the coefficients were assumed for these experiments (Atwater [1971]).

The simulations assume a uniform layer slightly above the surface. The infrared absorption coefficient is assumed to be .4 km^{-1} and the solar absorption and scattering coefficients are .2 km^{-1}. The reduction in solar energy with these coefficients is 10-15 percent.

3.4.2 An experiment with constant and specified pollutant concentration profiles

The interface temperatures in the presence of pollutants are compared to those calculated for the pollution-free atmosphere in Fig. 3.4-1 for urban and rural simulations. Since the only difference between the simulations is the presence of pollutants, it may be concluded that the presence of pollutants modified the interface temperature. The minimum surface temperature is .5 to 1°K higher in those simulations in which polluted conditions are speci-

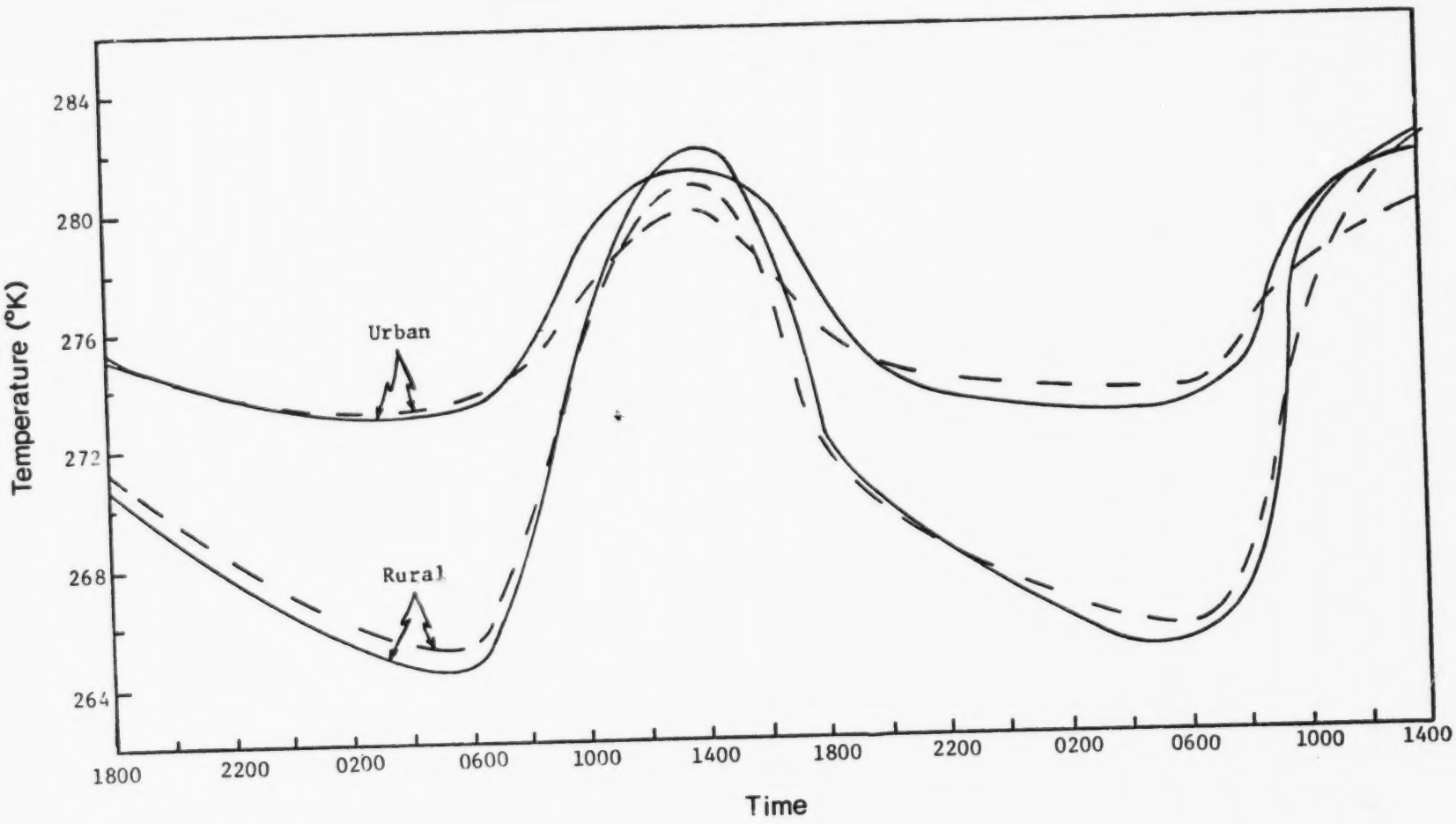

Figure 3.4-1. The simulated surface temperature as a function of time (solid lines are nonpolluted simulation, dashed lines are polluted simulation).

fied, and the maximum temperature is reduced by approximately 1°K. It should be noted that the changes here are small compared to changes due to the presence of soil characteristics typical of urban areas as seen in the results for run 2, in Section 3.2.

When the aerosol layer extends to the surface, the simulations do not differ significantly from those obtained with the elevated pollution layer.

The vertical profiles of temperature, at a time near sunrise, are shown in Fig. 3.4-2. It is seen there that the presence of pollutants reduces the temperature at the peak of the inversion by 2 to 3°K at this time for both the urban and rural simulations.

A more detailed presentation of the time-dependent modification is shown in Fig. 3.4-3 for the rural simulation and Fig. 3.4-4 for the urban simulation. These figures show the temperature as simulated without pollutants minus the temperature as simulated with pollutants. The modifications of the thermal structure are similar in both the urban and the rural cases. The maximum cooling occurs in the early morning, with minimum changes induced by pollutants seen in the afternoon. The maximum changes occur within the polluted layer and the modification gradually extends to layers above the polluted layer as time progresses.

A major factor responsible for the modification of thermal structure is the change in the atmospheric stability reflected in the diffusivity coefficient. Figure 3.4-5 shows the diffusivity coefficient for the non-polluted urban simulation and Fig. 3.4-6 shows the coefficients for the polluted simulation (time step 0 is 1400 and 50 time steps are equivalent to 4 hours). The computed stability above 100 m is unchanged at night by pollutants and reduced by pollutants during the day. These changes of stability in the polluted

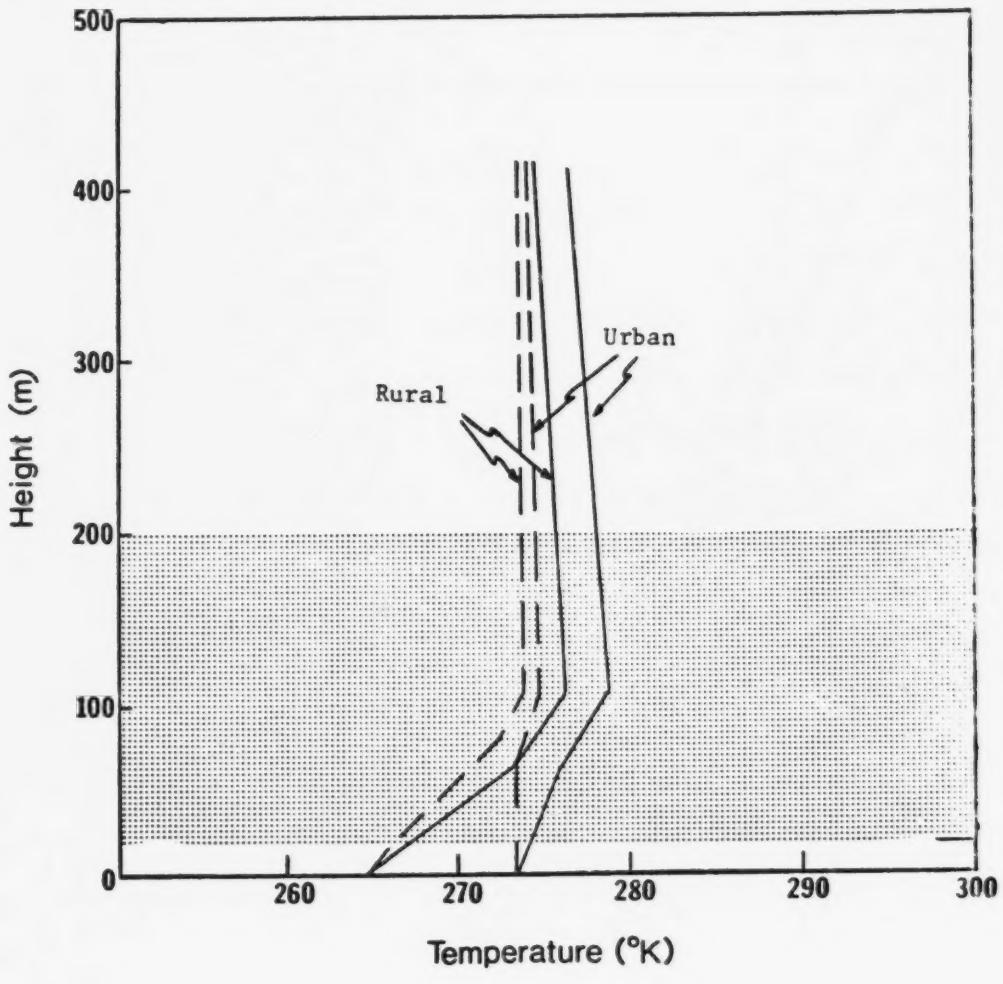

Figure 3.4-2. The simulated vertical profile of temperature at 0600.

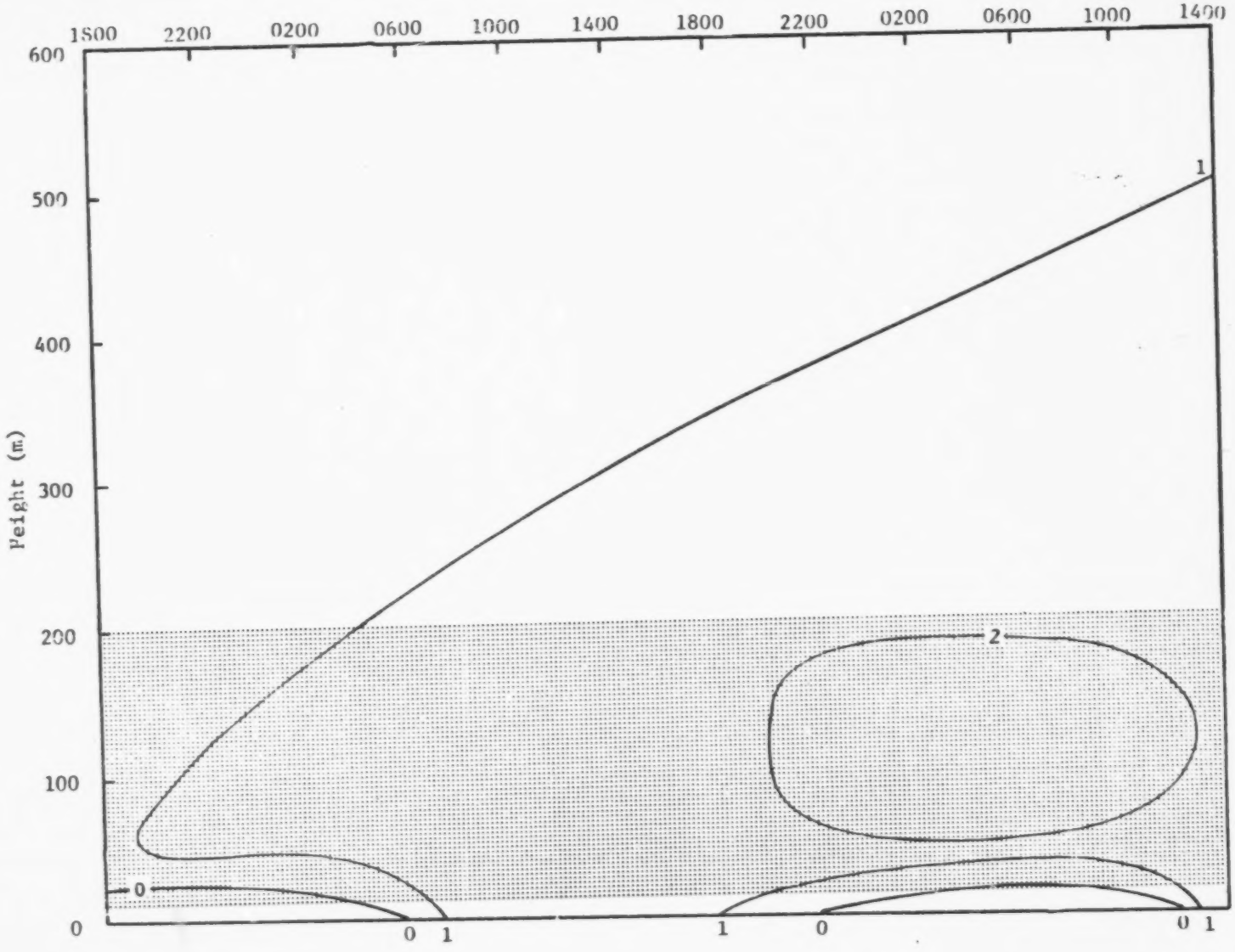

Figure 3.4-3. The temperature change (temperature without pollutants minus temperature with pollutants) induced by pollutants for the rural simulation.

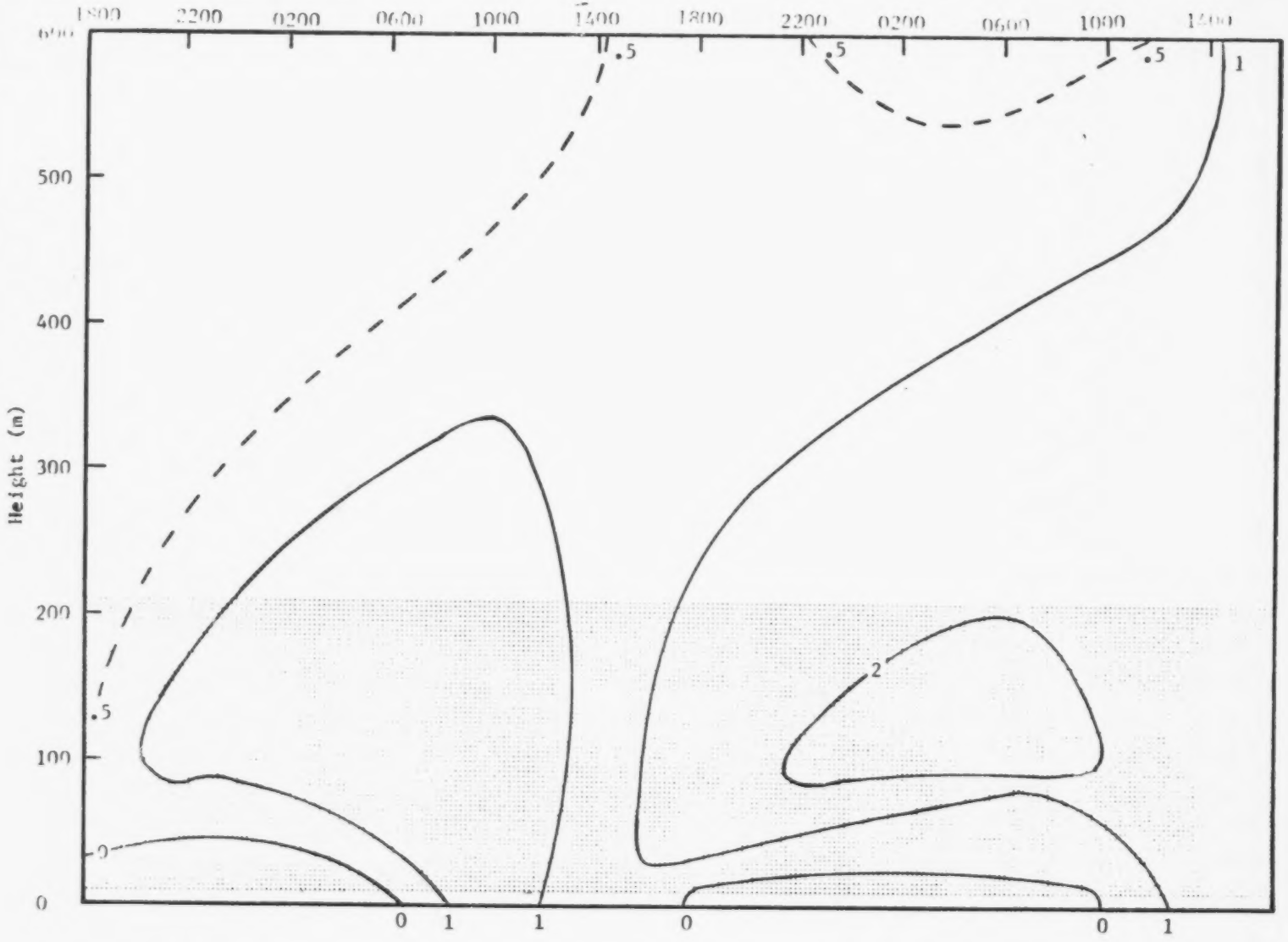

Figure 3.4-4. The temperature change (temperature without pollutants minus temperature with pollutants) induced by pollutants for the urban simulation.

EDDY CONDUCTIVITY-DIFFUSIVITY IN CM**2/SEC TIME STEP 4.[illegible] MINUTES

HEIGHT IN METERS	TIME STEP 0	TIME STEP 50	TIME STEP 100	TIME STEP 150	TIME STEP 200	TIME STEP 250	TIME STEP 300	TIME STEP 350	TIME STEP 400	TIME STEP [illegible]	TIME STEP 500	TIME STEP 550	TIME STEP 600
666.45	10000.	10000.	10000.	10000.	10000.	10000.	10000.	10000.	10000.	10000.	10000.	10000.	10000.
517.25	10000.	10000.	10000.	10000.	10000.	10000.	2953716.	10000.	10000.	10000.	10000.	10000.	3192320.
433.35	10000.	10000.	10000.	10000.	10000.	10000.	2894271.	10000.	10000.	10000.	10000.	10000.	3022005.
350.15	10000.	10000.	10000.	10000.	10000.	10000.	2484280.	10000.	10000.	10000.	10000.	10000.	2556865.
288.10	10000.	10000.	10000.	10000.	10000.	10000.	2063219.	10000.	10000.	10000.	10000.	10000.	2112334.
247.00	10000.	10000.	10000.	10000.	10000.	10000.	1749743.	10000.	10000.	10000.	10000.	10000.	1787579.
206.10	10000.	10000.	10000.	10000.	10000.	32898.	1422718.	10000.	10000.	10000.	10000.	10000.	1451252.
165.35	10000.	10000.	10000.	10000.	10000.	10000.	1093602.	10000.	10000.	10000.	10000.	93721.	1114105.
124.75	10000.	10000.	10000.	10000.	10000.	291611.	771897.	10000.	10000.	10000.	10000.	46878.	785503.
84.35	100.	100.	1141.	679.	100.	363038.	469273.	100.	1781.	546.	100.	327074.	477088.
44.10	100.	700.	2872.	2001.	4284.	192724.	201840.	354.	2790.	1177.	2813.	189161.	205051.
15.00	14260.	1658.	3904.	3158.	5180.	50197.	48448.	1326.	3201.	2186.	3971.	50037.	49207.
3.00	598.	1922.	2323.	2037.	2317.	3783.	5005.	1848.	2307.	1833.	2152.	3765.	5260.
-0.02	0.	0.	0.	0.	0.	0.	0.	0.	0.	0.	0.	0.	0.
-0.07	0.	0.	0.	0.	0.	0.	0.	0.	0.	0.	0.	0.	0.
-0.15	0.	0.	0.	0.	0.	0.	0.	0.	0.	0.	0.	0.	0.

Figure 3.4-5. The eddy diffusivity coefficients (cm^2/sec) for the nonpolluted urban simulation. (Time step 0 is 1400 LST and 50 time steps = 4 hours).

NOT REPRODUCIBLE

EDDY CONDUCTIVITY-DIFFUSIVITY IN CM**2/SEC TIME STEP 5. MINUTES

HEIGHT IN METERS	TIME STEP 0	TIME STEP 50	TIME STEP 100	TIME STEP 150	TIME STEP 200	TIME STEP 250	TIME STEP 300	TIME STEP 350	TIME STEP 400	TIME STEP 450	TIME STEP 500	TIME STEP 550	TIME STEP 600
666.45	10000.	10000.	10000.	10000.	10000.	10000.	10000.	10000.	10000.	10000.	10000.	10000.	10000.
517.25	10000.	10000.	10000.	10000.	10000.	10000.	3191456.	10000.	10000.	10000.	10000.	10000.	2174934.
433.35	10000.	10000.	10000.	10000.	10000.	10000.	2371893.	10000.	10000.	10000.	10000.	10000.	2459127.
350.15	10000.	10000.	10000.	10000.	10000.	10000.	2045953.	10000.	10000.	10000.	10000.	10000.	2251575.
266.10	10000.	10000.	10000.	10000.	10000.	10000.	1755408.	10000.	10000.	10000.	10000.	10000.	1967396.
247.00	10000.	10000.	10000.	10000.	10000.	10000.	1516013.	10000.	10000.	10000.	10000.	64581.	1632091.
208.10	10000.	10000.	10000.	10000.	10000.	439513.	1262774.	10000.	10000.	10000.	10000.	680081.	1344429.
165.35	10000.	10000.	10000.	10000.	10000.	592654.	1002586.	10000.	10000.	10000.	10000.	1006249.	1055147.
124.75	10000.	10000.	10000.	10000.	10000.	696896.	729082.	10000.	10000.	10000.	10000.	700248.	760139.
84.35	100.	100.	2525.	2010.	996.	460242.	453360.	362.	5045.	2433.	672.	479382.	469507.
44.10	100.	2345.	4723.	4009.	4601.	211199.	198410.	1874.	6763.	4056.	5796.	221022.	204547.
15.00	14260.	3122.	5055.	4650.	5884.	52847.	47927.	2593.	5848.	4416.	6568.	54876.	49340.
3.00	598.	2263.	2486.	2219.	2276.	3960.	4935.	2137.	2749.	2163.	2280.	4097.	5193.
-0.02	0.	0.	0.	0.	0.	0.	0.	0.	0.	0.	0.	0.	0.
-0.07	0.	0.	0.	0.	0.	0.	0.	0.	0.	0.	0.	0.	0.
-0.15	0.	0.	0.	0.	0.	0.	0.	0.	0.	0.	0.	0.	0.

Figure 3.4-6. The eddy diffusivity coefficients (cm^2/sec) for the polluted urban simulation. (Time step 0 is 1400 LST and 50 time steps = 4 hours).

simulation during the day are mainly due to the absorption of about 15 percent of the incident solar energy in the polluted layer. This results in less intense mixing below the top of the polluted layer. During the night, there is more intense mixing in this lower layer due to the increased surface temperature produced by the presence of pollutants.

3.4.3 An experiment with the simulated pollution concentration profiles being affected by mixing

When the capability of the model was extended to simulate time changes in pollution concentrations, the simulations of Section 3.4.2 were repeated. The major difficulty encountered was to specify the radiative absorption and scattering coefficients so as to produce realistic results. A trial and error method was used to achieve a reduction in solar energy in polluted conditions that is 10-20 percent. Recent work by Volz [1971] promises to allow a more systematic approach to the specification of the absorption and scattering coefficients.

The data for the urban area described in the previous section was used with an initially clear atmosphere. A constant pollution source strength of 1 $\mu gm/m^2/sec$ with effective source heights of 0 and 100 m was used. The effects of the variable non-transparent pollutant concentrations are qualitatively consistent with the results of the previous section. Therefore, they will not be repeated here.

Observations (e.g., Bornstein [1968], Oke and East [1971]) show that the temperatures at levels between 200 and 600 m are cooler over the urban region than they are over the surrounding rural atmosphere at the same height. Below these levels, the urban region is warmer. This feature in the temperature structure has been called the "cross over effect". The observations in Montreal (Oke and East [1971]) indicate a less frequent occurrence of the cross over

effect, and its occurrence at higher levels than observed in New York (Bornstein [1968]). The temperature difference between the simulation with and without pollutants at sunrise are shown in Fig. 3.4-7. In these simulations, it is seen that the maximum atmospheric cooling is at levels above 125 m. The magnitude of the cooling is the same as that observed in the cross over effect. Thus, the presence of non-transparent pollutants could serve as a possible cause of the cross over effect. Future simulations in which effective pollution source heights are varied are necessary to examine this hypothesis more closely.

The changes in stability caused by the thermal modification of non-transparent pollutants produce detectable changes in the pollutant concentration profiles. When the source is assumed at the surface, the surface concentration is reduced up to 25 percent at night and unchanged during the day. The concentrations at levels above 100 m were slightly greater than the values obtained in the simulation with transparent pollutants. These changes result from the stability changes induced by changes in the interface temperature and by pollutant induced cooling in the atmosphere.

When the effective source height is at 100 m, the concentration at this level at sunrise is reduced by 20 percent and the surface concentration is increased 25 percent when the thermal structure is modified by the presence of non-transparent pollutants. Vertical profiles of the concentration at sunrise are compared in Fig. 3.4-7 for the simulations with transparent and non-transparent pollutants.

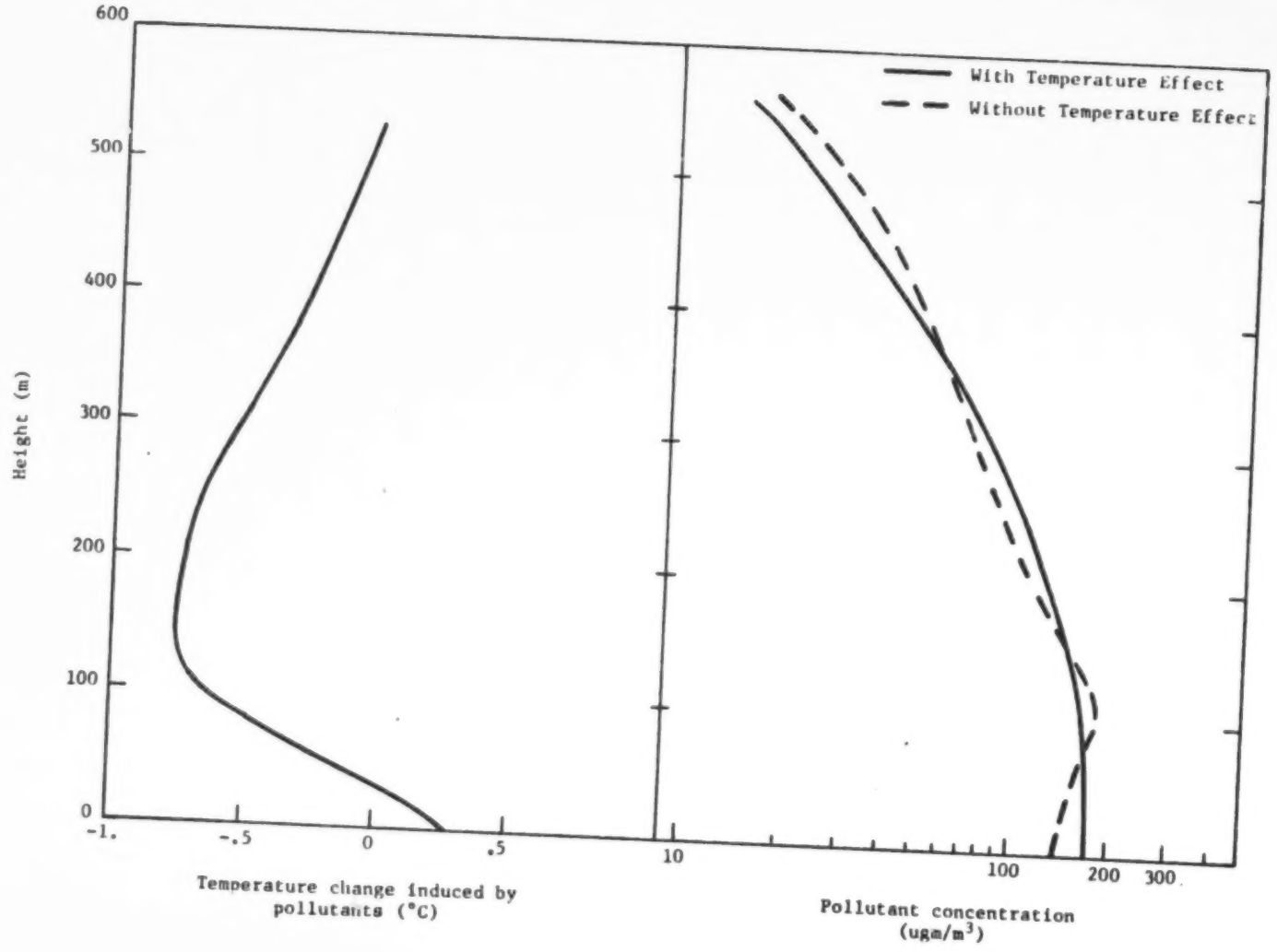

Figure 3.4-7. The change in temperature and concentration when the pollutant is changed from a transparent pollutant to an opaque pollutant.

4.0 EXPERIMENTS USING THE THREE-DIMENSIONAL BOUNDARY LAYER

Much of the effort expended during this contract has been spent in the seemingly endless and unrewarding task of programming and checkout. Minor, but irr tating, programming problems have continually slowed the work. While many minor errors probably remain, the initial simulations have produced results that indicate that the basic approach is feasible.

4.1 The Connecticut Experiment

The initial simulation experiment is based on data taken from Connecticut. The state was divided into a 6 × 4 grid with a horizontal grid interval of 24.32 km. Four of the grid squares were over Long Island Sound and were treated as containing an air-water interface. Grid squares in southwestern Connecticut, New Haven, and Hartford were assumed to have purely urban characteristics. The other grid squares were assumed to be rural. It is probable that a more realistic simulation may result from using weighted averages of urban and rural data to describe a single grid square. Pollution source data was obtained from the Connecticut source inventory (Hilst et al. [1967]). The grid is shown in Fig. 4.1-1 and the source emissions of sulfur dioxide are shown in Table 11. After the simulation was made, it was discovered that the source emissions should be multiplied by 23.667 to obtain the indicated units.

The initial data is based on the winter data of Atwater [1971], assuming an initial time of 1500 LST and a time step of 4.8 minutes. The advective time step, which is internally computed, is approximately 48 minutes. The pollutants were assumed to be transparent and a southerly geostrophic wind at the upper boundary was specified. All initial horizontal gradients were specified as zero. The duration of the simulation is 12 hours.

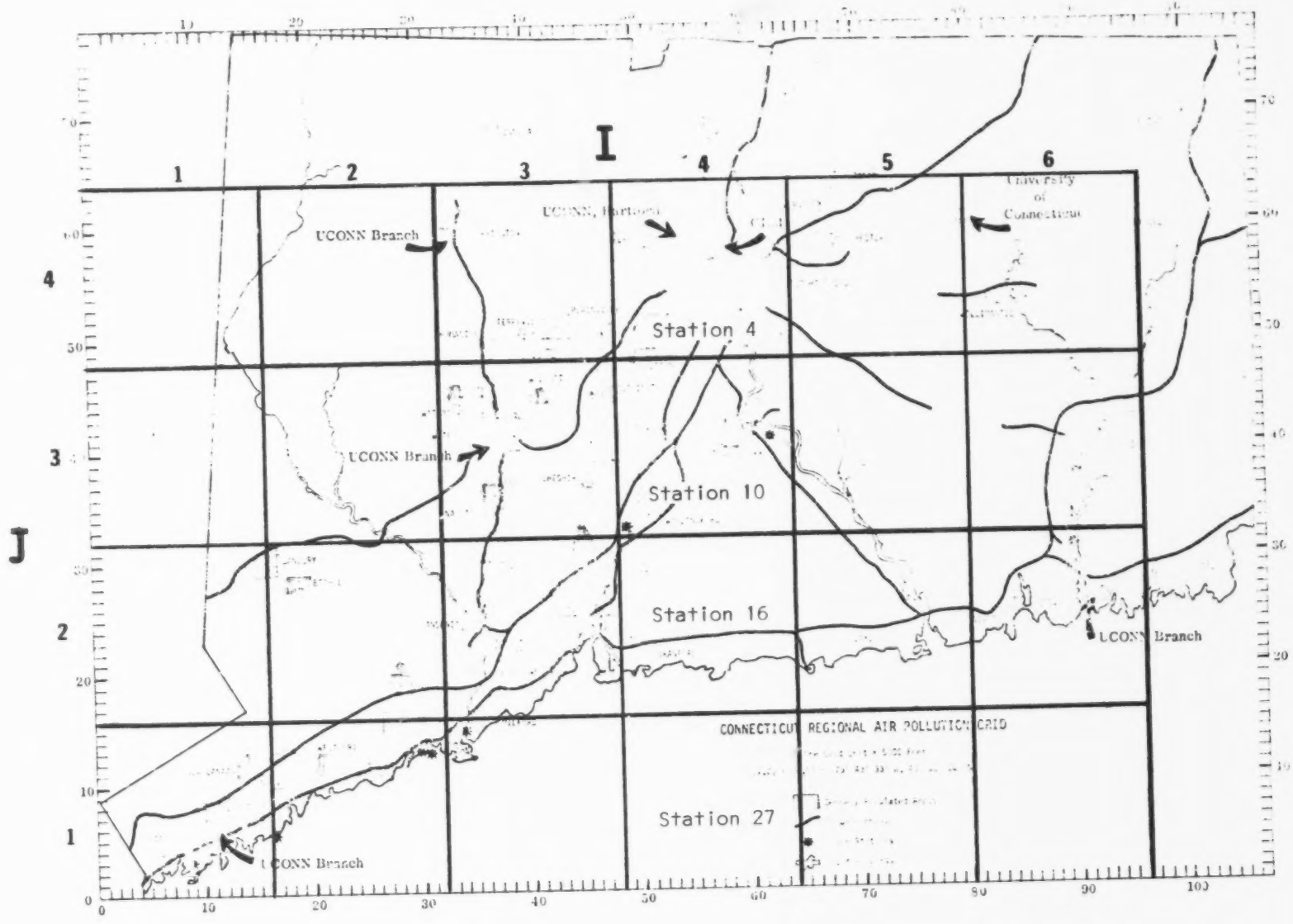

Figure 4.1-1 The grid squares used for the Connecticut experiment.

TABLE 11

Source emissions of SO_2 ($\mu gm/m^2/sec$) urban, rural, or water characteristics of the underlying surface from Table 2 and roughness heights in cm.

J \ I	1	2	3	4	5	6
4	0* R 100	.002 R 100	.014 R 1	.131 U 100	.017 R 1	.005 R 100
3	.003 R 100	.004 R 100	.023 R 1	.223 R 1	.004 R 1	.023 R 100
2	.007 R 100	.015 R 100	.103 U 100	.005 R 1	.002 R 1	.059 R 100
1	.109 U 1	.133 U 1	.103 W 1	0 W 1	0 W 1	0 W 1

* Source emission of SO_2 ($\mu gm/m^2/sec$). Type of underlying surface and roughness height (cm).

4.2 Simulated Temperatures and Winds

It is clear from the results of the previous sections that the interface temperature is one of the more important solution parameters that influence the course of simulation. The interface temperature field at 0300 LST is shown in Fig. 4.2-1. It is apparent that the water and the urban areas are the warmest. The 1000 m temperatures, also shown in Fig. 4.2-1, show the warmest temperatures generally to the north of the urban regions and over eastern Long Island Sound. An x-z cross section of temperature, which extends on a north-south line from Hartford to Long Island Sound, is shown in Fig. 4.2-2. It is seen that in this cross section the warmest surface temperatures are over the Sound, and over Hartford. Above 75 m there is a warm tongue extending from Long Island Sound northward.

CONS (4) WATER STATIONS CONNECTICUT LAND-WATER-POLLUTION MODEL JUNE 5'71

X-Y PLOT FOR VARIABLE T
TIME STEP = 150 DT = 4.80 REAL TIME = 12.00 HOURS--HEIGHT = 0.0

	1	2	3	4	5	6
4	267.045	267.113	266.282	271.437	266.277	267.224
3	267.041	266.641	265.939	266.351	266.997	267.417
2	266.814	266.549	272.007	267.719	267.584	267.739
1	271.595	271.631	273.144	273.149	273.152	273.148

NOT REPRODUCIBLE

TIME STEP = 150 DT = 4.80 REAL TIME = 12.00 HOURS--HEIGHT = 1000.0

	1	2	3	4	5	6
4	270.821	270.703	270.960	271.319	271.097	270.831
3	270.946	271.102	270.977	270.718	270.854	270.944
2	270.953	271.088	270.939	270.636	270.792	270.940
1	270.857	270.962	270.920	270.817	270.873	270.915

Figure 4.2-1 The simulated temperature (°K) at the indicated horizontal grid points for the Connecticut experiment at 0 m and 1000 m at 0300 LST.

CONS (4) WATER STATIONS CONNECTICUT LAND-WATER-POLLUTION MODEL JUNE 1971

Z-X PLOT FOR VARIABLE T
TIME STEP = 150 DT = 4.80 REAL TIME = 12.00 HOURS

HEIGHT STATIONS NOT REPRODUCIBLE

	4	10	16	22
2000.0	265.600	265.600	265.600	265.600
1500.0	268.374	267.667	267.545	267.787
1000.0	271.319	270.718	270.636	270.817
750.0	272.899	272.406	272.371	272.517
500.0	274.372	273.935	273.946	274.077
300.0	275.311	274.961	275.014	275.136
150.0	275.642	275.448	275.552	275.737
75.0	275.844	275.493	275.741	276.085
25.0	271.982	270.066	271.296	274.203
6.0	271.633	267.687	269.601	274.139
0.0	271.437	266.351	267.719	273.149
0.0	271.437	266.351	267.719	273.149
-0.5	274.284	274.599	274.633	274.175
-1.0	274.218	274.214	274.214	274.182
-2.0	273.281	273.221	273.221	273.192
-3.0	273.200	273.200	273.200	273.200

Figure 4.2-2 The simulated temperature (°K) at 0300 LST for a north-south cross section through Hartford ("Station 4") to Long Island Sound ("Station 22").

The u and v wind components at 6 m and at 500 m at 0300 LST are shown in Figs. 4.2-3 and 4.2-4 respectively. The development of a pattern of low level winds is observed in these figures. Closer inspection shows that the location of urban, rural, and water surfaces play an important part in determining the wind circulation. It should be remembered that, in this experiment, the urban characteristics were assigned to the entire grid square containing the urban center. As the urban centers are much smaller in area than a simulation grid square, these simulations should be expected to be somewhat unrealistic in detail. However, an examination of the figures, in conjunction with the vertical velocity patterns in the following figures, shows that the winds appear to be a result of thermally and frictionally induced circulations. One cause of the circulation can be assumed to lie in the differing urban and rural thermal characteristics. Ascending motions over the warmer urban and water grid squares and descending motions over the cooler rural regions are consistent with the simulated horizontal wind patterns, particularly at the lower levels.

The vertical velocity at 0300 LST is shown in Fig. 4.2-5. Here it is seen that the ascending motions do, indeed, lie in the warmer northeast-southwest urban corridor and south-eastern water regions. The remainder of the region has descending motions. It may be inferred that the urban-rural-water contrasts are partly responsible for these features, although further extensive investigation of the effects of the finite-difference schemes are required.

4.3 Experimental Pollution Concentration

The computed pollutant concentrations at 0, 25, 300, and 500 m are shown in Figs. 4.3-1 and 4.3-2. A north-south cross section through Hartford is

COMS (4) WATER STATIONS CONNECTICUT LAND-WATER-POLLUTION MODEL JUNE 1971

X-Y PLOT FOR VARIABLE U
TIME STEP = 150 DT = 4.80 REAL TIME = 12.00 HOURS--HEIGHT = 6.0

	1	2	3	4	5	6
4	-57.595	-31.042	-40.474	-46.796	-175.748	-65.289
3	-48.119	-34.223	-46.792	-120.185	-176.501	-59.115
2	-34.074	-37.149	-20.904	-80.104	-97.603	-42.820
1	-67.862	-65.752	-87.849	-89.499	-105.592	-119.861

NOT REPRODUCIBLE

X-Y PLOT FOR VARIABLE V
TIME STEP = 150 DT = 4.80 REAL TIME = 12.00 HOURS--HEIGHT = 6.0

	1	2	3	4	5	6
4	41.791	25.715	75.080	56.324	97.056	44.280
3	30.301	-14.190	63.040	151.527	173.511	35.090
2	19.077	-0.512	90.430	234.166	198.477	41.843
1	154.179	156.502	395.656	406.806	409.482	403.770

Figure 4.2-3 The simulated horizontal wind components (cm/sec) at 0300 LST at a height of 6 m for the Connecticut experiment.

COAS (4) WATER STATIONS CONNECTICUT LAND-WATER-P ELUTION MODEL JULY 1971

X-Y PLOT FOR VARIABLE U
TIME STEP = 150 DT = 4.80 REAL TIME = 12.00 HOURS--HEIGHT = 500.0

	1	2	3	4	5	6
4	130.106	177.813	244.585	132.949	74.425	120.441
3	137.783	140.176	260.040	164.113	56.827	94.639
2	164.496	158.270	161.742	157.478	138.570	132.093
1	166.005	156.812	154.386	153.045	145.397	140.563

NOT REPRODUCIBLE

X-Y PLOT FOR VARIABLE V
TIME STEP = 150 DT = 4.80 REAL TIME = 12.00 HOURS--HEIGHT = 500.0

	1	2	3	4	5	6
4	725.930	738.314	715.536	624.822	646.216	690.724
3	707.077	663.052	684.517	714.254	724.385	691.132
2	687.186	659.495	698.569	747.389	741.306	691.426
1	691.323	694.084	705.193	702.476	711.249	695.837

Figure 4.2-4 The simulated horizontal wind components (cm/sec) at 0300 LST at a height of 500 m for the Connecticut experiment.

CCMS (4) WATER STATIONS CONNECTICUT LAND-WATER-POLLUTION MODEL [illegible]

X-Y PLOT FOR VARIABLE VVEL
TIME STEP = 150 DT = 4.80 REAL TIME = 12.00 HOURS--HEIGHT = 150.0

	1	2	3	4	5	6
4	-0.121	-0.297	-0.101	0.456	0.231	-0.073
3	-0.298	-0.759	-0.216	1.303	0.624	-0.154
2	-0.095	-0.154	0.084	0.448	0.289	0.126
1	0.014	-0.020	0.124	0.054	0.118	0.159

NOT REPRODUCIBLE

X-Y PLOT FOR VARIABLE VVEL
TIME STEP = 150 DT = 4.80 REAL TIME = 12.00 HOURS--HEIGHT = 500.0

	1	2	3	4	5	6
4	-0.343	-1.118	-0.124	1.331	0.536	-0.252
3	-0.951	-2.600	-0.314	3.970	1.880	-0.525
2	-0.334	-0.441	0.131	1.271	0.714	0.070
1	0.066	0.153	0.124	-0.024	0.094	0.194

Figure 4.2-5 The simulated vertical velocity (cm/sec) at 0300 LST at heights of 150 and 500 m for the Connecticut experiment.

UCRS (4) WATER STATIONS CONNECTICUT EXPT--WATER--MULTIPLE SOURCE PPI

X-Y PLOT FOR VARIABLE PPI
TIME STEP = 150 DT = 4.80 REAL TIME = 12.00 HOURS--HEIGHT = [illegible]

	1	2	3	4	5	6
4	15.370	19.496	27.927	31.748	14.150	9.625
3	22.985	23.371	38.803	63.947	10.350	16.130
2	33.477	29.568	21.460	2.432	6.235	14.550
1	49.456	44.680	33.702	0.053	0.003	0.000

NOT REPRODUCIBLE

X-Y PLOT FOR VARIABLE PPI
TIME STEP = 150 DT = 4.80 REAL TIME = 12.00 HOURS--HEIGHT = 25.0

	1	2	3	4	5	6
4	16.210	19.136	19.379	23.243	9.731	9.628
3	23.455	22.318	19.352	26.656	9.470	13.711
2	33.103	26.208	18.075	2.658	5.356	13.005
1	40.642	37.576	26.560	0.081	0.005	0.000

Figure 4.3-1 The simulated pollutant concentrations ($\mu gm/m^3$) at 0300 LST at heights of 6 and 25 m for the Connecticut experiment.

CONS (4) WATER STATIONS CONNECTICUT LAKE-WATER-POLLUTION MODEL JUNE 3'71

X-Y PLOT FOR VARIABLE PP1
TIME STEP = 150 DT = 4.80 REAL TIME = 12.00 HOURS--HEIGHT = 300.0

	1	2	3	4	5	6
4	2.714	2.292	1.171	0.316	0.105	0.126
3	2.673	1.814	1.345	0.489	0.045	0.045
2	2.845	2.053	1.420	0.462	0.050	0.014
1	3.054	2.311	1.421	0.398	0.045	0.003

TIME STEP = 150 DT = 4.80 REAL TIME = 12.00 HOURS--HEIGHT = 500.0

	1	2	3	4	5	6
4	0.535	0.469	0.180	0.029	0.008	0.016
3	0.441	0.209	0.194	0.091	0.006	0.004
2	0.462	0.263	0.206	0.083	0.007	0.001
1	0.526	0.352	0.213	0.059	0.006	0.000

Figure 4.3-2 The simulated pollutant concentrations ($\mu gm/m^3$) at 0300 LST at heights of 300 and 500 m from the Connecticut experiment.

shown in Fig. 4.3-3. A feature that is apparent is the presence of a small negative value of pollutant concentration at an upper level. This probably can be eliminated when the numerical finite-difference routines are chosen more judiciously.

Other features of the pollutant patterns show that relatively high concentrations over the strong sources occur at the lower levels as would be expected. At higher levels, the maximum pollution concentrations shift toward the northwest of the urban regions, which is consistent with the prevalent flow during most of the simulation period.

When the pollutant concentration is examined at a fixed point in the strong emission region as a function of time, the concentration increases rapidly early in the simulation period and then decreased. However, in northwestern Connecticut, where no strong sources are located, the pollutant concentration gradually increased with time over the entire period.

CONS (4) WATER STATIONS CONNECTICUT LAND-WATER-POLLUTION MODEL JUNE 3'72

Z-X PLOT FOR VARIABLE PP1
TIME STEP = 150 DT = 4.80 REAL TIME = 12.00 HOURS

HEIGHT	STATIONS			
	4	10	16	22
2000.0	0.0	0.0	0.0	0.0
1500.0	0.000	0.000	0.000	0.000
1000.0	0.000	0.001	0.001	0.000
750.0	0.002	0.012	0.011	0.006
500.0	0.029	0.091	0.083	0.059
300.0	0.316	0.489	0.462	0.398
150.0	1.478	1.535	1.348	1.185
75.0	2.974	3.176	1.867	1.428
25.0	23.243	26.666	2.658	0.081
6.0	31.788	83.947	3.492	0.053
0.0	31.788	83.947	3.492	0.053

Figure 4.3-3 The simulated pollutant concentrations (ugm/m^3) at 0300 LST for a north-south cross section through Hartford ("Station 4") to Long Island Sound ("Station 22").

5.0 SUMMARY AND RECOMMENDATIONS FOR FUTURE WORK

The results described in Sections 3.0 and 4.0 in conjunction with the computer time and storage requirements described in Section 2.0, demonstrate that the type of model described in the statement of work is feasible. Feasibility here means the ability to simulate meteorological and pollutant variables at a horizontal array of grid points within practical limits on a computer.

In Section 3.0, it has been demonstrated that the models are capable of generating urban-rural low-level temperature differences in winter that are qualitatively realistic, with slight differences in daytime maxima, and with rural nocturnal minimum temperatures of the order of 10°K lower than urban minimum temperatures. A series of analytical experiments shows that the elevation of the urban nocturnal temperatures can be attributed in large part to artificial heating and, to a lesser extent, to the conductivity and specific heat characteristics of the underlying surface. It is also shown in Section 3.0 that the depth of the mixing layer is strongly and directly correlated to the maximum interface temperature , through the stability, as would be expected. Daytime mixing depths range from about 300 to more than 1600 meters, depending on the particular combination of physical surface characteristics input to a given simulation, while nighttime mixing depths range from about 15 meters to about 85 meters. Diurnal variations of the mixing depth yield variations in atmospheric pollutant concentrations at low levels of about a factor of 5, with minimum concentrations occurring in the afternoon, again as would be expected for steady source emissions.

The daytime vertical profiles of pollutant appear to be consistent with a simple one-layer model picture, with vertically uniform concentrations in the mixed layer. The nighttime profiles are more difficult to characterize

in this fashion, and show strong peaks of concentration near the source height. However, these profiles are not unlike Gaussian profiles for an elevated source.

When particulate effects on the meteorology are allowed, significant changes are detectable in the simulation results for all pollutants. The vertical profiles of pollutant concentration were fixed, and unaffected by changes in the thermal structure of the atmospheric boundary layer in a first series of simulation experiments. In these results, the presence of an elevated aerosol layer reduced the amplitude of the diurnal temperature wave at the interface by about 2°K; and decreased the air temperature within the aerosol layer by about 2°K after about 2 simulation days. To our knowledge, these are the first computations of the aerosol effect of pollutant on the interface temperature and agrees with the results of Atwater [1971] for the change in atmospheric temperatures due to radiation. In a second series of simulation experiments, the aerosol layer was allowed to react to these temperature changes and to the consequent changes in diffusivity. These results showed atmospheric aerosol concentrations changing by something like 25 percent.

Three-dimensional fields of meteorological variables and pollutant were obtained and are described in Section 4.0. Here it is seen that horizontal patterns of urban-rural-water interface characteristics, grossly describing the nontopographic features of the state of Connecticut, yield systematic patterns of convergence over urban areas, with upward vertical velocities and deeper polluted layers resulting in these areas. In rural areas, lower nocturnal temperatures are evident, with subsiding vertical motions.

Refinement of the finite-difference schemes for horizontal and vertical advection appears to be required in order to eliminate an undesirable feature

of the simulated pollution patterns, namely, the occurrence of small negative pollutant concentrations in regions distant from strong sources. Other minor corrections in the input numerical values of various parameters must be made prior to further experiments. Modification of the model to take into account topographic effects is straightforward in concept, and should be carried out in the near future. A set of three-dimensional simulations incorporating topographic effects, pollutant effects on the meteorology, seasonal variations, and finer horizontal grids nested within the coarse grids used until now, should be conducted. Tests should be made of more accurate advective finite-difference schemes, and of explicit inclusion of the horizontal diffusion process in the model.

6.0 ACKNOWLEDGEMENTS

During the course of this contract, several persons have provided support to the authors. The formidable computer programming task was successfully carried out by Mr. Joseph A. Sekorski. The mathematical analysis in Section 2.5 is based on work by Mr. Philip S. Brown, Jr., The heavily demanding technical typing and figure drafting has been capably handled by Miss Margaret G. Atticks. Additional support has been provided by Mr. Clifford A. Jacobs, Mr. Frank Perry, and Mrs. Phyllis A. Shechtman.

All of the computations were performed at the University Computer Center of the University of Connecticut.

7.0 REFERENCES

Atwater, M.A., 1966: Comparison of numerical methods for computing radiative temperature changes in the atmospheric boundary layer. *J. Appl. Meteor.*, *5*, 824-831.

_____, 1970: *Investigation of the Radiation Balance for Polluted Layers of the Urban Environment.* Ph.D. Thesis, New York University, New York, 116 pp (available from University Microfilm, Ann Arbor, Mich.).

_____, 1971: The radiation budget for polluted layers of the urban environment. *J. Appl. Meteor.*, *10*, 205-214.

Beeton, A.M., 1962: Variations in radiant energy and related ocean temperatures. *Proc. Fifth Conf. on Great Lakes Res., 1962*, pp. 68-78, Univ. of Michigan, Great Lakes Res. Div., Ann Arbor, Michigan.

Bornstein, R.D., 1968: Observations of the urban heat island effect in New York City. *J. Appl. Meteor.*, *7*, 575-582.

Boudreau, R.D., 1968: *A Solution to the Integral Equations for Radiative Transfer of Heat in the Atmosphere.* Research and Development Report ECOM-6034, U.S. Army Electronics Command, Fort Huachuca, Arizone, Rpt. No. AD672473, 87 pp.

Calder, K.L., 1969: *Numerical Solution of Atmospheric Diffusion Equations by Finite-Difference Methods.* Tech. Memo. 138, U.S. Army Biological Labs, Fort Detrick, Md.

Clark, J.F., 1969: Nocturnal urban boundary layer over Cincinnati, Ohio. *Mo. Wea. Rev.*, *97*, 582-589.

Cooley, D.S., J.P. Pandolfo, and M.A. Atwater, 1968: *The Development of a Multi-Station Physical Model for the Simulation of Subsynoptic Scale Meteorological Processes.* Vol. 1, The Travelers Research Center, Inc., Hartford, Conn., 7475-303a, 155 pp.

Cox, R.A., M.J. McCartney, and F. Culkin, 1970: The specific gravity/salinity/temperature relationship in natural sea water. *Deep-Sea Res.*, *17*, 679-689.

Crowley, W.P., 1968: Numerical advection experiments. *Mo. Wea. Rev.*, *96*, 1-11.

Davidson, B., 1967: A summary of the New York urban air pollution dynamics research program. *J. Air Poll. Contr. Assoc.*, *17*, 154-158.

Deirmendjian, 1969: *Electromagnetic Scattering on Spherical Polydispersions*, American Elsevier Publ. Co., Inc., New York, 290 pp.

Elsasser, W.M., 1942: Heat transfer by infrared radiation in the atmosphere. *Harvard Meteorol. Studies*, *6*, 107 pp.

_____, and M. Culbertson, 1960: Atmospheric radiation tables. *Meteor. Monogr.*, *4*, 43 pp.

Forsythe, G.E. and W.R. Wasow, 1964: *Finite-Difference Methods for Partial Differential Equations*, John Wiley and Sons, N. Y., 444 pp.

Fritz, S., 1951: Solar radiant energy and its modification by the earth and its atmosphere. *Compendium of Meteor., Amer. Meteorol. Soc.*, Boston, Mass., 13-33.

Goody, R.M., 1964: *Atmospheric Radiation*, Oxford at the Clarendon Press, London, 436 pp.

Halstead, M.H., R. Richman, W. Covey, and J. Merrman, 1957: A preliminary report on the design of a computer for micrometeorology. *J. Meteor., 14*, 308-325.

Hess, S.L., 1959: *Introduction to Theoretical Meteorology*, H. Holt & Co., N. Y., 362 pp.

Hilst, G.R., J.E. Yocum, and N.E.Bowne, 1967: *The Development of a Simulation Model for Air Pollution over Connecticut.* Vol. 1, Summary Rpt. 7233-279a, The Travelers Research Center, Hartford. Conn.

Kitaigorodsky, S.A., 1961: On the possibility of theoretical calculation of vertical temperature profile in upper layer of the sea. *Bull. (Izvestia) Acad. Sci., USSR, Geophys. Ser., 3*, 313-314.

Kondrat'yev, K., 1969: Radiation in the atmosphere. *Int'l Geophys. Ser. 12*, Academic Press, New York.

Kunn, P.M., 1963: Radiometersonde observations of infrared flux emissivity of water vapor. *J. Appl. Meteor., 2*, 368-378.

McDonald, J.E., 1960: Direct absorption of solar radiation by atmospheric water vapor. *J. Meteor., 17*, 319-328.

Molenkamp, C.R., 1968: Accuracy of finite-difference methods applied to the advection equation. *J. Appl. Meteor., 7*, 160-167.

Myrup, J.O., 1969: A numerical model of the urban heat island. *J. Appl. Meteor., 8*, 908-918.

Oke, T.R. and C. East, 1971: The urban boundary layer in Montreal. *Bound. Layer Meteor., 11*, 27-53.

Orville, H.D., 1968: Comments on "Accuracy of Finite Difference Methods Applied to the Advection Equation". *J. Appl. Meteor., 7*, p. 938.

Pandolfo, J.P., 1966: Wind and temperature profiles for constant-flux boundary layers in lapse conditions with a variable eddy conductivity to eddy viscosity ratio. *J. Atmos. Sci., 23*, 495-502.

_____, 1969: Motions with inertial and diurnal period in a numerical model of the navifacial boundary layer. *J. Mar. Res., 27,* 301-317.

_____, and P.S. Brown, 1970: *Simulation Experiments with a Numerical Sea-Air Planetary Boundary Layer Model and Its Extension to Three Space Dimensions.* Vol. I, TRC Rpt. No. 7499-386a, The Travelers Research Corporation, Hartford, Conn., 95 pp.

Pierson, W.J., 1964: The interpretation of wave spectra in terms of the wind profile instead of the wind measured at a constant height. *J. Geophys. Res., 69,* 5191-5204.

Randerson, D., 1970: A numerical experiment in simulating the transport of sulfur dioxide through the atmosphere. *Atmos. Environ., 4,* 615-632.

Richtmyer, R.D., 1963: *A Survey of Difference Methods for Non-Steady Fluid Dynamics,* NCAR Tech. Notes, No. 63-2, 25 pp.

_____, and K.W. Morton, 1967: *Difference Methods for Initial-Value Problems,* Interscience Publ., N. Y., 405 pp.

Sklarew, R.C., 1970: *Preliminary Report of the S^3 Urban Air Pollution Model Simulation of Carbon Monoxide in Los Angeles.* Systems Science and Software, Environmental Sciences Group, 26 pp.

Sverdrup, H.U., M.W. Johnson, and R.H. Fleming, 1942: *The Oceans,* Prentice-Hall, Inc., New York, 1087 pp.

Volz, F.E., 1971: *Aerosol Substance in Infrared Spectroscopy - Some New Aspects in Air Chemistry.* Paper at Conf. on Air Pollution Meteor., April 1971.

APPENDICES

APPENDIX A: **Specification for a Program of the Atmosphere-Ocean-Land Planetary Boundary Layer with Pollutants**

by Marshall A. Atwater

1. INTRODUCTION

The purpose of the program is to solve a set of finite difference equations which are the analogues of simplified forms of the prognostic differential equations for various scalar properties in the planetary boundary layer of the atmosphere, ocean, and soil system. The scalar properties include wind and current components, temperature, specific humidity, salinity, and pollutants. Much of these specifications is based on the specifications and modifications in the Appendices to Pandolfo and Brown [1970].

The upper and lower boundary values required for the numerical solutions of the equations are to be input or computed from input. The equations are to be solved on a specified, arbitrarily spaced, vertical mesh, which is also input.

2. INPUT

The input is specified either for the entire grid, for one location in the grid, or for each station of the grid.

2.1 General Parameters

1. N,n number of grid levels
2. I number of grid levels to interface
3. I_{max} number of stations in x direction
4. J_{max} number of stations in y direction
5. Δt length of time step (sec)
6. N_t total number of time steps
7. Δ horizontal grid length

Preceding page blank

8. δ solar declination (deg)

9. $\Delta\delta$ daily declination change (deg)

10. ϕ_b latitude of southern grid border (deg)

11. h_w hour angle at western grid border (deg)

12. ϵ_s infrared emissivity of surface

13. z_w height of vertical grid level used in computation of wave dimensions (cm)

14. R_e length of time step for radiation computations (min)

15. σ_{sa} solar absorption coefficient (km^{-1})

16. σ_{ss} solar scattering coefficient (km^{-1})

17. σ_{ia} infrared absorption coefficient (km^{-1})

18. z_g heights of input gradients (cm)

19. $(\partial T/\partial x),(\partial T/\partial y)$ at z_g horizontal temperature gradients at z_g initially and upwind of lateral boundaries (K°/cm)

20. $(\partial q/\partial x),(\partial q/\partial y)$ at z_g initial and upwind humidity gradients at z_g (g/kg/cm)

21. $(\partial s/\partial x),(\partial s/\partial y)$ at z_g initial and upwind salinity gradients at z_g (g/kg/cm)

22. $(\partial u/\partial x),(\partial u/\partial y)$ $(\partial v/\partial x),(\partial v/\partial y)$ at z_g initial and upwind velocity component gradients at z_g (cm/sec)

23. $(\partial P_1/\partial x),(\partial P_1/\partial y)$ $(\partial P_2/\partial x),(\partial P_2/\partial y)$ at z_g initial and upwind pollutant 1 and pollutant 2 gradients at z_g ($g/m^3/cm$)

24. N_u number of sounding levels above the boundary layer

25. $p(z_j,t)$; $z_{N+1} < z_j$ values of pressure (mb)

26. $T(z_j,t)$; $z_{N+1} < z_j$ values of temperature (°K)

27. $q(z_j,t)$; $z_{N+1} < z_j$ values of specific humidity (g/kg)

28. α conversion factor to determine temperature effect for pollutants; set to 0 whenever transparent pollutants are used

29. n_p number of time steps between each printout time step

2.2 General Grid Location

1. I_i, J_i input location for vertical profile
2. $T(z_j,0);\ z_1 \leq z_j \leq z_n$ initial values for temperature (°K)
3. $u(z_j,0);\ z_1 \leq z_j \leq z_n$ initial values of eastward wind components (cm/sec)
4. $v(z_j,0);\ z_1 \leq z_j \leq z_n$ initial values of northward wind components (cm/sec)
5. $q(z_j,0);\ z_I < z_j \leq z_n$ initial values of specific humidity (g/kg)
6. $s(z_j,0);\ z_1 \leq z_j \leq z_I$ initial values of salinity (g/kg)
7. $P_1(z_j,0);\ z_I < z_j \leq z_n$ initial values of pollutant 1 (g/100 g)
8. $P_2(z_j,0);\ z_I < z_j \leq z_n$ initial values of pollutant 2 (g/100 g)

2.2 Input at Each Station

1. n_c number of cloud layers
2. n_g number of geostrophic wind and current input values
3. LW land or water subsurface
4. $P(0,t)$ surface pressure (mb)
5. δ the steepness of the characteristic turbulent wave; for land, set to zero
6. λ the wavelength of the characteristic turbulent wave (cm); the roughness height if $\delta = 0$
7. $U_g(z_n,t)$, $V_g(z_n,t)$ eastward and northward components of the geostrophic wind at the upper boundary (cm/sec)
8. $U_g(0,t)$, $V_g(0,t)$ eastward and northward components of the geostrophic wind at the interface (cm/sec)
9. $\varepsilon_{c\ell}(z);\ z_H < z$ cloud amount (hundredths)
10. T_{yc} cloud type
11. P_r rainfall rate (cm/sec)
12. $S_1(t)$, $S_2(t)$ pollutant source strength at the station ($\mu gm/m$)
13. h_{1i}, h_{2i} fractional strength of emission at each height level

The following items are defined for land subsurface only.

14. r_s albedo

15. ρ_s density of soil (gm/cm^3)

16. c_s specific heat of soil ($cal/°K/cm^3$)

17. M_q Halstead moisture parameter

18. K(z) soil thermal conductivity for each soil layer (cm^2/sec)

19. R_x artificial heat source due to man ($\ell y/sec$)

3.0 COMPUTATIONS

3.1 Program Constants

$g = 980$

$c_p = .239$

$c_w = .935$

$f = 14.585 \sin\phi \times 10^{-5}$

$\pi = 3.1416$

$\Gamma = .98 \times 10^{-4}$

$\rho_A = 10^{-3}$

$\rho_w = 1$

$\alpha = -3$

$k_1 = .4$

$k_2 = .14$

$R_c = -1/7\ \alpha$

$c = 3(R_c)^{1/3}\ (1 + R_c)^2$

$h = k_1^2\ (3/c)^{3/2}$

$\beta_v = 10$

$\beta_T = 10/3$

$n_v = 1/2$

$n_T = 3/2$

$\sigma = 1.354 \times 10^{-12}$

$R = 2.87 \times 10^{6}$

$k = .86933 \times 10^{-6}$

3.2 Parameters Constant over Entire Grid

The height grid parameters are to be computed according to the notation

$$\hat{z}_j = \frac{z_j + z_{j+1}}{2} \qquad 0 < z_{j+1} \leq z_N$$

$$\hat{z}_j = \left|\frac{z_j + z_{j+1}}{2}\right| \qquad z_1 \leq z_j < 0 \ ,$$

so that, since $z_I = 0$,

$$\hat{z}_I = \frac{z_{I+1}}{2}$$

$$\hat{z}_{I-1} = \left|\frac{z_{I-1}}{2}\right| \ ,$$

$$\Delta z_j = z_{j+1} - z_j \ ; \qquad z_1 \leq z_j \leq z_{N-1} \ .$$

Note that

$$\Delta z_{I+1} = z_{I+1} \ ; \qquad \Delta z_{I-1} = |z_{I-1}| \ .$$

Also compute

z_{w-1} = the vertical grid level immediately below z_w

$$A_1 = \frac{\ln 1950/z_{w-1}}{\ln z_w/z_{w-1}}$$

$$A_2 = \frac{\ln z_w/1950}{\ln z_w/z_{w-1}} \ .$$

The input horizontal gradients

$$\frac{\partial T}{\partial x}(z_j) \; ; \; \frac{\partial T}{\partial y}(z_j) \qquad z_1 \le z_j \le z_N$$

$$\frac{\partial q}{\partial x}(z_j) \; ; \; \frac{\partial q}{\partial y}(z_j) \qquad z_{I+1} \le z_j \le z_N$$

$$\frac{\partial s}{\partial x}(z_j) \; ; \; \frac{\partial s}{\partial y}(z_j) \qquad z_1 \le z_j \le z_I$$

$$\frac{\partial u}{\partial x}(z_j) \; ; \; \frac{\partial u}{\partial z}(z_j) \qquad z_1 \le z_j \le z_N$$

$$\frac{\partial v}{\partial x}(z_j) \; ; \; \frac{\partial v}{\partial y}(z_j) \qquad z_1 \le z_j \le z_N$$

$$\frac{\partial P_1}{\partial x}(z_j) \; ; \; \frac{\partial P_1}{\partial y}(z_j) \qquad z_{I+1} \le z_j \le z_N$$

$$\frac{\partial P_2}{\partial x}(z_j) \; ; \; \frac{\partial P_1}{\partial y}(z_j) \qquad z_{I+1} \le z_j \le z_N$$

are to be computed by linear interpolation from the input values at z_g for the boundary layer if more than one gradient is input. If only one value is input, this value is to be applied at all grid levels. If the gradient changes at the interface, the input value is given at z_I for both the subsurface and the air. These gradients will be used at the horizontal grid boundary, whenever necessary.

3.3 Initial Profiles

The initial profile of the variables u , v , T , q , s , P_1 , P_2 are computed from the input vertical profile at grid location I_i , J_i . The initial profile of $X(z,0)$ at i,j is computed from

$$X(z,0) = X_i(z,0) - \frac{\partial X(z)}{\partial y}(J_i - j)\Delta - \frac{\partial X(z)}{\partial x}(I_i - i)\Delta$$

where the gradients are the input gradients. For u, v, and T, the added restriction

$$X_{I+1} = X_I$$

is used.

3.4 Eddy Exchange Coefficient

The eddy exchange coefficients are computed at each time step for each station. The subscripts u, v are used to indicate coefficients used with wind. Other computed K, generally with subscript T, are used with other variables. Lack of a subscript generally refer to the subscript T, unless used with wind. If the subsurface is water, compute the wave property s_w given by

$$s_w(\hat{z}_j) = g^{1/2}\,\delta\left(\frac{\lambda}{2\pi}\right)^{-1/2} e^{-\hat{z}_j \cdot 2\pi/\lambda} \qquad \hat{z}_1 \le \hat{z}_j \le \hat{z}_{N-1} .$$

If the subsurface is land, $s_w(\hat{z}_j) = 0$.

Compute the coefficients $\lambda \neq 0$

$$K_0(z_j) = k_1^2(\hat{z}_j + \frac{\delta\lambda}{2}) \qquad z_I \le z_j \le z_{N-1}$$

$$K_0(z_j) = k_1^2(\hat{z}_j + \frac{\delta\lambda}{2}) \qquad z_1 \le z_j \le z_{I-1} .$$

Whenever $\lambda = 0$ on input (the subsurface is water), δ is set = .055. Compute

$$W(z_{w,t}) = [u^2(z_w, t) + v^2(z_w, t)]^{\frac{1}{2}}$$

$$W(z_{w-1},t) = [u^2(z_{w-1}, t) + v^2(z_{w-1}, t)]^{\frac{1}{2}}$$

$$W_{1950}(t) = W(z_w, t)\cdot A_1 + W(z_{w-1}, t)\cdot A_2$$

$$\bar{H}(t) = 1.54165 \times 10^{-4}\cdot[W_{1950}(t)]^2$$

$$s_w(\hat{z}_j, t) = g^{\frac{1}{2}}\,\delta\left[\frac{\bar{H}}{\delta\cdot\pi}\right]^{-\frac{1}{2}} e^{-z_j\cdot 2\pi\cdot\delta/\bar{H}} \quad ; \quad \hat{z}_1 \le \hat{z}_j \le \hat{z}_{N-1} \;,\; \bar{H} > 0$$

$$= 0 \quad ; \qquad\qquad\qquad\qquad\qquad\qquad\qquad\qquad\quad ,\; H = 0$$

$$K_0(\hat{z}_j, t) = k_1^2\left[\hat{z}_j + \frac{\bar{H}}{2}\right]^2 \quad ; \qquad \hat{z}_I \le \hat{z}_j \le \hat{z}_{N-1}$$

$$K_0(\hat{z}_j, t) = k_2^2\left[\hat{z}_j + \frac{\bar{H}}{2}\right]^2 \quad ; \qquad \hat{z}_1 \le \hat{z}_j \le \hat{z}_{I-1} \;.$$

In both cases, compute

$$K_{u,v}(\hat{z}_I, t) = K_{T,q}(\hat{z}_I, t) = K_0(\hat{z}_I, t)\cdot s_w(\hat{z}_I, t)$$

$$K_{u,v}(\hat{z}_{I-1}, t) = K_{T,s}(\hat{z}_{I-1}, t) = K_0(\hat{z}_{I-1}, t)\cdot s_w(\hat{z}_{I-1}, t) \;.$$

For printout use

$$H_{1/3}(t) = .8727 \times 1.5989\, H(t).$$

3.4.1 For the atmospheric layer $z_{I+1} \le z_j \le z_{N-1}$

Note that the computed quantities S, L, $\bar{T}$, Ri, $K_{u,v}$, $K_{T,q}$ are understood to be dimensioned variables with the coordinates $(\hat{z}_j, t)$.

$$S = \left\{\left[\frac{u(z_{j+1}, t) - u(z_j, t)}{\Delta z_j}\right]^2 + \left[\frac{v(z_{j+1}, t) - v(z_j, t)}{\Delta z_j}\right]^2\right\}^{\frac{1}{2}}$$

$$L = \left[\frac{T(z_{j+1}) - T(z_j)}{\Delta z_j}\right] + \Gamma + .0061\,\bar{T}\left(\frac{q_{j+1} - q_j}{\Delta z_j}\right)$$

$$\bar{T} = \left[\frac{T(z_{j+1}) + T(z_j)}{2}\right]$$

$$Ri = \frac{gL}{\bar{T}[S + S_w(z_j)]^2} \quad , \quad Ri \le \left|\frac{1}{\alpha}\right| \quad .$$

If $Ri \geq 0$, proceed as in 3.4.1.1.

If $-R_c < Ri < 0$, proceed as in 3.4.1.2.

If $Ri \leq -R_c$, proceed as in 3.4.1.3.

3.4.1.1 If $Ri \geq 0$

$$K_{u,v} = K_0(\hat{z}_j)[S + S_w(\hat{z}_j)][1 + \alpha Ri]^2$$

$$K_{T,q} = K_{u,v}$$

and proceed to 3.4.1.4.

3.4.1.2 If $-R_c < Ri < 0$

$$K_{u,v} = K_0(\hat{z}_j)[S + S_w(\hat{z}_u)][1 - \alpha Ri]^{-2}$$

$$K_{T,q} = \frac{K_{u,v}}{(1 - Ri)}$$

and proceed to 3.4.1.4.

3.4.1.3 If $-R_c \geq Ri$

$$K_{T,q} = \frac{k}{k_1^2} K_0(\hat{z}_j) \cdot \left|\frac{gL}{\bar{T}}\right|^{\frac{1}{2}}$$

$$K_{u,v} = K_{T,q} \cdot \left[\frac{3}{c}\right]^{-\frac{1}{2}} \cdot |Ri|^{-1/6}$$

and proceed to 3.4.1.4.

3.4.1.4 Apply the limits

$$10^4 \leq K \leq 10^7 , \qquad \hat{z}_j \geq 10^4$$

$$10^2 \leq K \leq 10 , \qquad \hat{z}_{I+1} \leq \hat{z}_j \leq 10^4$$

3.4.2 For the oceanic layer $\hat{z}_1 \leq \hat{z}_j \leq \hat{z}_{I-2}$

Note that the computed quantities S , L , Ri , $\bar{s}$, $\bar{T}$, $\partial\sigma_T/\partial T$, $\partial\sigma_T/\partial s$, are understood to have the coordinates $(\hat{z}_j, t)$.

$$S = \left\{ \left[\frac{u(z_{j+1}) - u(z_j)}{\Delta z_j} \right]^2 + \left[\frac{v(z_{j+1}) - v(z_j)}{\Delta z_j} \right]^2 \right\}^{\frac{1}{2}}$$

$$\bar{s} = \frac{s(z_{j+1}) + s(z_j)}{2}$$

$$\bar{T} = \frac{T(z_{j+1}) + T(z_j)}{2}$$

Compute

$$\frac{\partial \sigma_T}{\partial T} = .05819402 - 2(.00811465413)\,\bar{T} + 3(.476600414 \times 10^{-4})\,\bar{T}^2 + 2(.389187483 \times 10^{-4})\,\bar{T}\,\bar{s} - .25310441 \times 10^{-2}\,\bar{s} + .28797153 \times 10^{-5}\,\bar{s}^2$$

and

$$\frac{\partial \sigma_T}{\partial s} = .79701864 - .25310441 \times 10^{-2}\,\bar{T} + 2(.131710842 \times 10^{-3})\,\bar{s} + .389187483 \times 10^{-4}\,\bar{T}^2 + 2(.28797153 \times 10^{-5})\,\bar{s}\,\bar{T} - 3(.611831499 \times 10^{-7})\,\bar{s}^2$$

$$L = -10^{-3} \left\{ \frac{\partial \sigma_T}{\partial T} \left[\frac{T(z_{j+1}) - T(z_j)}{\Delta z_j} \right] + \frac{\partial \sigma_T}{\partial s} \left[\frac{s(z_{j+1}) - s(z_j)}{\Delta z_j} \right] \right\}$$

If $S + S_w \neq 0$, check L; if $L < 0$, go to 3.4.2.3

$$Ri = -\frac{gL}{[S + S_w(\hat{z}_j)]^2}$$

If $L > 0$, set $Ri = Ri_{max}$, $1/\alpha$ atmospheric, 10^{16} ocean.

If $Ri \geq 0$, proceed as in 3.4.2.1.

If $-R_c < Ri < 0$, proceed as in 3.4.2.2.

If $Ri < -R_c$, proceed as in 3.4.2.3.

3.4.2.1 If $Ri \geq 0$

$$K_{u,v} = K_0[S + S_w(\hat{z}_j)][1 + \beta_v Ri]^{-n_v}$$

$$K_{T,s} = K_0[S + S_w(\hat{z}_j)][1 + \beta_T Ri]^{-n_T}$$

and proceed to Section 3.5.

3.4.2.2 If $-R_c < Ri < 0$

$$K_{u,v} = K_0[S + S_w(\hat{z}_j)][1 - \alpha Ri]^{-2}$$

$$K_{T,s} = K_{u,v} \Big/ [1 - \alpha Ri]$$

and proceed to Section 3.5.

3.4.2.3 If $Ri \leq -R_c$

$$K_{T,s} = h \cdot \frac{k^2}{k_i^2} \cdot \left[z_j + \frac{\lambda\delta}{2}\right]^2 \cdot |gL|^{\frac{1}{2}}$$

$$K_{u,v} = K_{s,T} \cdot \left[\frac{3}{c}\right]^{-\frac{1}{2}} \cdot |Ri|^{-1/6} \quad , \quad \text{if } S + S_w > 0$$

$$K_{u,v} = 0 \quad , \quad \text{if } S + S_w \leq 0$$

3.4.3 The soil layer

When the subsurface is soil, K_T is input.

3.5 Infrared Computations

3.5.1 Hydrostatic pressure

The pressure at each level must be computed at each time step using the temperature and surface pressure. The formula is

$$p_{i+1} = p_i \exp\left\{\frac{-2g(z_{i+1} - z_i)}{R(T_i + T_{i+1})}\right\} ,$$

where p is in millibars, T is in °A, and z is in centimeters. $R = 2.87 \times 10^6$ erg mole^{-1} °A^{-1} and $g = 980$ cm sec^{-2} .

3.5.2 Absorber path length and emissivity

The path length increment for water vapor Δu_w is computed for each layer from the surface to the top of the atmosphere by

$$\Delta u_{w_i} = \frac{(P_i - P_{i+1})(q_{i+1} + q_i)}{2g} .$$

The path length increment for carbon dioxide for each layer Δu_c is

$$\Delta u_c = .4148239\ (P_i - P_{i+1}) .$$

The path length for aerosols is computed from

$$\Delta u_a = \sigma_{ia}\ \alpha_p\ P_{1i}\ \Delta z_i \times 10^{-5}$$

where α_p is a conversion factor having units $1/P_{1i}$.

At each prediction level, an absorber path length in cm is computed to each other height level, including levels above the boundary layer. From this path length, an emissivity matrix is computed. The emissivity is based on the total path length to the level from the reference level 2 computed by

$$u = \sum_{i=2}^{z} \Delta u_i$$

for above the layer and

$$u = \sum_{i=z}^{i} \Delta u_i$$

for below the layer.

The emissivity for water vapor and carbon dioxide is computed from the formulas in Table 1.

TABLE 1

Infrared Diffuse Transmission Functions

Water Vapor

Functions derived from data of Kuhn (1963) for path length (u in precipitation - cm.)

	Log u
$\varepsilon = 0.11288 \log (1 + 12.63\ u)$ *	≤ -4
$\varepsilon = 0.104 \log (u) + .440$	≤ -3
$\varepsilon = 0.121 \log (u) + .491$	≤ -1.5
$\varepsilon = 0.146 \log (u) + .527$	≤ -1
$\varepsilon = 0.161 \log (u) + .542$	≤ 0
$\varepsilon = 0.136 \log (u) + .542$	> 0

Carbon Dioxide

Presented by Shekhter and revised by Kondrat'yev (1969) (u in atm/cm).

$$\varepsilon = .185 \{1 - exp\ (- .3919u^{.4})\}$$

$$\tau = 1 - \varepsilon$$

* Presented by Zdunkowski and Johnson (1965).

The total infrared gaseous emissivity at each layer is computed from

$$\varepsilon g_i = \varepsilon w_i + \varepsilon c_i \ .$$

When $\alpha \neq 0$, the total infrared transmission is given by

$$\tau_i = (1 - \varepsilon_{g_i})\ \tau_{p_i}$$

where τ_{p_i} is the transmission due to aerosols, which is computed from

$$\tau_{p_i} = exp\ (1.66\ u_{p_i}) \ .$$

When $\alpha = 0$, $\tau_p = 1$ (i.e., $\tau_i = 1 - \varepsilon_{g_i}$).

The emissivity at each level is given by

$$\varepsilon_i = 1 - \tau_i \ .$$

These emissivity values for each level will be stored for each reference level and recomputed at each advective time step or each 10^{th} radiative time step, whichever is smaller.

3.5.3 Infrared radiative flux

The total downward flux at the surface is computed at each time step. Otherwise the downward and upward fluxes are computed at each radiative time step R_e , or the advective time step, if it is smaller.

The downward flux is computed from

$$R_{d_a}(LR) = \sum_{i=LR}^{top-1} (\sigma T_{i+1} + \sigma T_i^4).5\ (\varepsilon_{i+1} - \varepsilon_i) * P_c$$

where $P_c = 1$ below any clouds. Above the base of the clouds

$$P_c = 1 - \varepsilon_{c\ell}$$

where $\varepsilon_{c\ell}$ is the fractional cloud cover. If clouds are present, additional radiation is computed from n layers of clouds by

$$R_{c_i}(LR) = \sum_{i=1}^{n} (\varepsilon_{c\ell_i} - \varepsilon_{c\ell_{i-1}})\, \sigma T_{c\ell}^4\, (1 - \varepsilon_z)$$

where $T_{c\ell}$ is the temperature at the cloud base and ε_z is the emissivity between the prediction level and the cloud level.

The total downward flux is

$$R_d(LR) = R_{d_a}(LR) + R_{c_i}(LR) \quad .$$

The upward flux is computed from

$$R_u(LR) = \sum_{i=1}^{LR-1} .5\sigma\, (T_{i+1} + T_i)(\varepsilon_i - \varepsilon_{i+1}) + \sigma T_g^4\, (1 - \varepsilon_1)$$

where ε_1 is the emissivity from the reference level to the surface.

3.5.4 Radiative cooling rates

The infrared cooling at each layer, above the first atmospheric layer, is computed from

$$\left(\frac{\partial \hat{T}}{\partial t}\right)_i = \frac{g}{c_p} \times 10^{-3} \left[\frac{R_u(i) - R_d(i) - R_u(i+1) + R_d(i+1)}{P_{i+1} - P_i}\right] \quad .$$

The cooling at the first atmospheric level is assumed equal to the cooling computed in the second atmospheric layer. The cooling at all higher levels is computed from

$$\left[\left(\frac{\partial T}{\partial t}\right)_{ir}\right]_{i+1} = \left(\frac{\partial \hat{T}}{\partial t}\right)_i + \left(\frac{P_{i+1} - P_i}{P_{i+2} - P_i}\right) \left[\left(\frac{\partial \hat{T}}{\partial t}\right)_{i+1} - \left(\frac{\partial \hat{T}}{\partial t}\right)_i\right] \quad ,$$

for $i = I+2$ to $N - 2$. No cooling rates are computed at the top boundary.

3.6 Solar Radiation

Solar radiation is computed at each time step. The cosine of the zenith angle is computed from

$$\cos Z = \sin\phi \sin\delta + \cos\phi \cos\delta \cos H$$

where H is the hour angle. The hour angle is recomputed at each step by

$$H_{t+1} = H_t + \frac{\Delta t}{86400} 2\pi .$$

Whenever $\cos Z \leq 0$, the solar radiation $R_s = 0$, and all solar heating rates $(\partial T/\partial t)_{sol} = 0$.

3.6.1 Solar radiation flux in the atmosphere

When $\cos Z > 0$, the total path length of water is computed according to the equations in Section 3.5.2. If aerosol scattering occurs within a layer, compute

$$Bs_i = \alpha\sigma_{ss} P_{1i} \Delta z_i \times 10^{-5}$$

where P_i is the pollutant concentration at level i. Similarly if aerosol absorption occurs within a layer, compute

$$Ba_i = \alpha\sigma_{sa} P_{1i} \Delta z_i \times 10^{-5} .$$

The method is based on equations given by Kondrat'yev [1969] and by Atwater [1970].

Initially, the downcoming flux at the top of the prediction level is computed from the following equations

$$\tau_1 = \left(1.041 - 0.16 \sqrt{\frac{.00949P + 0.051}{\cos Z}}\right)$$

$$a_2 = .007 \left(\frac{U_T}{\cos Z}\right)^{.3}$$

where P is the pressure at the top prediction level, U_T is the total path length of water vapor above the boundary layer, and Z is the zenith angle.

To account for forward scattering, compute

$$P_3 = .5(1 - \tau_1) \quad .$$

The downward solar flux R_s' at the top of the boundary layer is given by

$$R_s' = I_0 \cos Z \, (\tau_1 + P_3 - a_2) \, V$$

where I_0 is .0325 ly/sec , and V is computed from

$$V = 1 \qquad \cos Z \geq .17365$$

$$V = \cos Z/.17365 \qquad \cos Z < .17365$$

If clouds are present, compute

$$M = \sec Z$$

and compute from cloud transmission a revised downward flux from

$$R_s = [1 - N_1(1 - \psi_1)][1 - N_2(1 - \psi_2)] \ldots R_s'$$

where N_1 , N_2 , ... N_m are the fractional cloud amount for the cloud layer and ψ_i are the transmission, as given in Table 2.

The transmission ψ is given as a function of cloud type and air mass. When interpolation is necessary above, the transmission should be checked to insure values between 0 and 1 . If there are no cloud amounts,

$$R_s = R_s' \quad .$$

Table 2

Transmission equations for clouds

Cloud type	Equation
1. Fog	* ψ = 16.26 + 0.54 M
2. St	ψ = 26.84 - 1.01 M
3. Sc	ψ = 36.58 - 1.49 M
4. Cu	ψ = 36.58 - 1.49 M
5. Cb	ψ = 23.63 + 1.45 M
6. As	ψ = 41.30 - 0.14 M
7. Ac	ψ = 54.56 - 2.36 M
8. Ci	ψ = 87.17 - 1.79 M
9. Cs	ψ = 90.55 - 6.38 M

* ψ is in percent.

For heating and radiative changes within the boundary layer, the following equations are used:

$$\Delta I_z = V \frac{I_0 \; 2.4674 \times 10^{-5}}{\sqrt{\frac{.00949P + 0.051}{\cos Z}}}$$

$$\Delta I_w = V \; 7.55 \times 10^{-4} \left(\frac{U_t}{\cos Z}\right)^{-.7} \Delta u$$

where U_T is the path length above the midpoint of the layer and Δu is the path length within the layer. Also set $I_n = R_s$.

If scattering occurs within the layer, compute for each layer

$$\Delta I_s = V \; I_n \; B_{s_i} \; e^{-B_{si}/\cos Z}$$

and if absorption occurs within the layer, compute

$$\Delta I_a = V \; I_n \; B_{a_i} \; e^{-B_{ai}/\cos Z} \quad .$$

The heating at the layer is computed from

$$\left(\frac{d\hat{T}}{dt}\right)_{sol} = \frac{980}{239} \frac{\Delta I_w + \Delta I_a}{\Delta P}$$

where P is in mb. The new downwind flux at the top of the next layer I_{n-1} (or on the ground) is computed from

$$I_{n-1} = I_n - (\Delta I_z + \Delta I_w + \Delta I_a + \Delta I_s) \quad .$$

The additional flux out of the top of the boundary layer I_u is

$$I_u = I_u + \Delta I_z + \Delta I_s \quad .$$

This is repeated for each layer. After the last layer, $I_{n-1} = I_{I+1}$ is the incoming flux at the ground. The reflected solar radiation is added to the upward flux, or

$$I_u = I_u + a(I_{n_{I+1}}) \quad .$$

The solar heating at each level $(\partial T/\partial t)_{sol}$ is computed by linear interpolation in the pressure coordinate from $(\partial \hat{T}/\partial t)_{sol}$.

3.6.2 Solar absorption in the ocean

Solar radiation is also absorbed by the ocean. The amount of energy available for heating the ocean is given by

$$I_0 = I_{n_{I+1}} (1 - r_s)$$

where r_s is the albedo computed from

$$r_s = -1.39 + 4.67 \tan Z$$

with a minimum value of 3. This equation is based on results of Sverdrup et al. [1942].

The transmission at any level z is given by

$$I_z = I_0 \exp(- k_w |z| \sec Z)$$

where k_w is computed from Table 3 below.

Table 3

Extinction Coefficients in the Ocean

Depth	K
< 2 m	$k = 1.034 - .5698 \ell nz$
2 m	.6370
5 m	.3510
10 m	.2350
20 m	.1650
50 m	.1160
100 m	.0977

Now the change of radiation in each level will be calculated. In the uppermost layer,

$$R_H = I_o - I_1$$

and in the layer m (the bottom layer)

$$\Delta I_m = I_m - 0 = I_m .$$

The remaining layers are computed similarly from

$$\Delta I_i = I_{i-1} - I_i .$$

The heating rate at levels i (i goes from 1 to m) are computed from

$$\left[\frac{dT}{dt}\right]_i = \frac{\rho}{c_p} \frac{\Delta I_i}{\Delta z_{i+1}} ,$$

where ρ is the water density (= 1), c_p is the specific heat of water (= 1), ΔI_i is as computed above and Δz_{i+1} is the thickness of the layer in cm.

A diagram for the calculations with m equal to 3 is shown in Fig. 1.

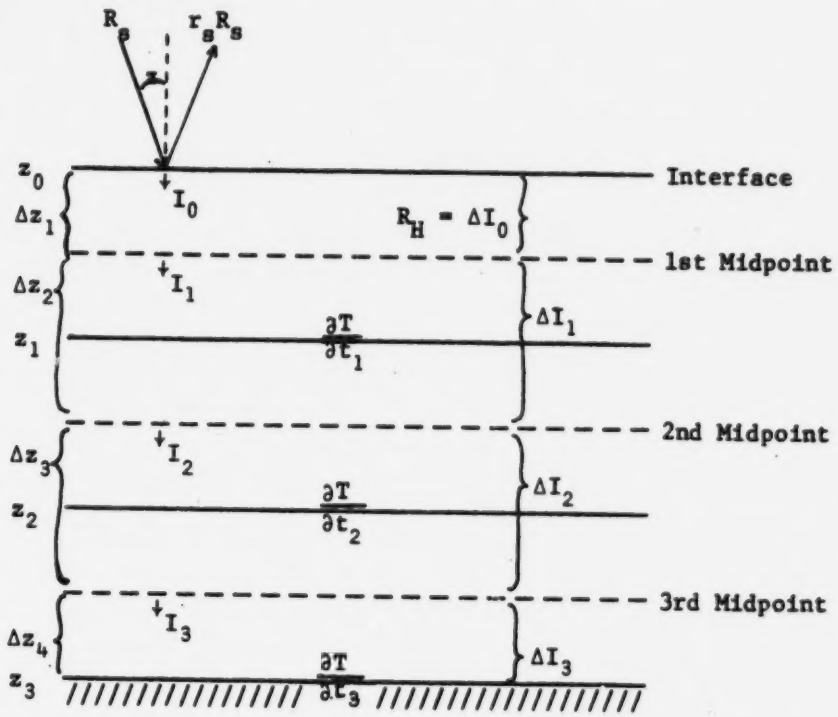

Fig. 1 Diagram for radiation computations in the ocean with m = 3 .

The dT/dt will then be added to the temperature at the same levels and at the same time as the atmospheric radiative temperature changes are included.

3.7 Geostrophic Wind (Current) at Each Level at Each Time Step

In the following two sections (3.71, 3.72), $U_g(z_N)$, $V_g(z_N)$, $U_g(z_I)$, $V_g(z_I)$ are computed by linear interpolation from the input values of $U_g(z_{n,t})$, $V_g(z_{n,t})$, $U_g(0,t)$, and $V_g(0,t)$. For a land subsurface, $U_g(0,t)$ and $V_g(0,t)$ are zero.

3.7.1 For the atmospheric layer j = I+1, ... N

$$U_g(z_j, t) = \frac{U_g(z_N)\cdot T(z_j, t)}{T(z_N)} + \frac{g\cdot T(z_j, t)}{f} \sum_{i=j+1}^{N} \frac{\Delta z_{i-1}}{T^2(z_i, t)} \cdot \frac{\partial T}{\partial y}(z_i)$$

$$V_g(z_j, t) = \frac{V_g(z_N)\cdot T(z_j, t)}{T(z_N)} - \frac{g\cdot T(z_j, t)}{f} \sum_{i=j+1}^{N} \frac{\Delta z_{i-1}}{T^2(z_i, t)} \cdot \frac{\partial T}{\partial x}(z_i)$$

3.7.2 For the water subsurface j = 1, ... I-1

$$\frac{\partial \rho}{\partial y}(z_i, t) = 10^{-3}\left[\frac{\partial \sigma_T}{\partial t}(\hat{z}_{i-1}, t)\frac{\partial T_w}{\partial y}(z_i) + \frac{\partial \sigma_T}{\partial s}(\hat{z}_{i-1}, t)\frac{\partial s}{\partial y}(z_i)\right]$$

$$\frac{\partial \rho}{\partial x}(z_i, t) = 10^{-3}\left[\frac{\partial \sigma_T}{\partial t}(\hat{z}_{i-1}, t)\frac{\partial T_w}{\partial x}(z_i) + \frac{\partial \sigma_T}{\partial s}(\hat{z}_{i-1}, t)\frac{\partial s}{\partial x}(z_i)\right]$$

$$U_g(z_j, t) = U_g(z_1) - \frac{g}{f} \sum_{i=1}^{j+1} \frac{\Delta z_i}{\rho_w} \frac{\partial \rho}{\partial y}(z_{i+1}, t)$$

$$V_g(z_j, t) = V_g(z_1) + \frac{g}{f} \sum_{i=1}^{j+1} \frac{\Delta z_i}{\rho_w} \frac{\partial \rho}{\partial x}(z_{i+1}, t)$$

No subsurface computations are performed for a soil subsurface.

3.8 Interface Values

The boundary and interface values are computed for each station at each time step.

3.8.1 Humidity

The saturated humidity at the interface is computed from

$$q_s(0,t) = \frac{3.7943}{1013.2}\ 10\ exp\left\{3 + 7.5\ \frac{T(0,t) - 273.16}{T(0,t) - 35.66}\right\}$$

The interface humidity is computed from

$$q(0,t) = M_q\, q_s(0,t) + (1 - M_q)\, q(z_1,t)$$

where $q(z_1,t)$ is the humidity at the first atmospheric level above the interface. M_q is input for a soil subsurface and equals 1 for a water subsurface.

3.8.2 Winds, currents, and salinity

Whenever $\delta \neq 0$, always a water subsurface, the computations proceeds for the interface value for u, v, and salinity as follows:

$$u(z_I) = \frac{[\rho_A K_{u,v}(\hat{z}_I)\cdot u(z_{I+1})/\Delta z_I] + [\rho_w K_{u,v}(\hat{z}_{I-1})\cdot u(z_{I-1})/\Delta z_{I-1}]}{[\rho_A K_{u,v}(\hat{z}_I)/\Delta z_I] + [\rho_w K(\hat{z}_{I-1})/\Delta z_{I-1}]}$$

$$v(z_I) = \frac{[\rho_A K(\hat{z}_I)\cdot v(z_{I+1})/\Delta z_I] + [\rho_w K(\hat{z}_{I-1})\cdot v(z_{I-1})/\Delta z_{I-1}]}{[\rho_A K(\hat{z}_I)/\Delta z_I] + [\rho_w K(\hat{z}_{I-1})/\Delta z_{I-1}]}$$

$$E = -10^{-3} \cdot \rho_A K(\hat{z}_I)\left[\frac{q(z_{I+1}) - q(z_I)}{z_{I+1}}\right]$$

$$F = \frac{s(z_{I-1})\,(E - P_r)}{1 - s}$$

$$s(z_I) = -\frac{F}{\rho_w K(\hat{z}_{I-1})} \cdot \Delta z_{I-1} + s(z_{I-1})$$

Then proceed with Section 3.8.3.

When $\delta = 0$ and the subsurface is water, the interface value of u, v, and s is computed as follows. Compute the value

$$B_1 = \frac{1}{k_1}\, \ell n\, \frac{z_{I+1}}{\lambda}$$

$$B_2 = \frac{1}{k_1}\, \ell n\, \left|\frac{z_{I-1}}{\lambda}\right|$$

Then compute

$$w(z_{I+1}) = [u^2(z_{I+1}) + v^2(z_{I+1})]^{\frac{1}{2}}$$

$$w(z_{I-1}) = [u^2(z_{I-1}) + v^2(z_{I-1})]^{\frac{1}{2}}$$

If $\lambda < 0$, compute

$$u^* = \frac{w(z_{I+1})}{B_1}$$

and

$$w(z_I) = w(z_{I-1}) + u^* B_2 \sqrt{\rho_A/\rho_w}$$

and proceed with computations from the computation $u(z_I)$ below.

If $\lambda > 0$, compute

$$u^* = [w(z_{I+1}) - w(z_{I-1})][B_1 + \sqrt{\rho_A/\rho_w}\ B_2]^{-1}$$

$$w(z_I) = w(0) = w(z_{I+1}) - u^* B_1$$

The computation proceeds with the computation of $u(z_I)$ and other variables as follows:

$$u(z_I) = u(z_{I+1}) - \left[\frac{u(z_{I+1}) - u(z_{I-1})}{w(z_{I+1}) - w(z_{I-1})}\right] [w(z_{I+1}) - w(z_I)]$$

$$v(z_I) = v(z_{I+1}) - \left[\frac{v(z_{I+1}) - v(z_{I-1})}{w(z_{I+1}) - w(z_{I-1})}\right] [w(z_{I+1}) - w(z_I)]$$

$$q^* = [q(z_{I+1}) - q(z_I)] \cdot B_1^{-1} \; ; \quad K_{u,v}(z_I) = |u^*|\ k_1\ \hat{z}_I$$

$$E = -10^{-3} \cdot \rho_A \cdot |u^*| \cdot q^* \; ; \quad K_{T,q}(\hat{z}_I) = K_{u,v}(\hat{z}_I)$$

$$F = s(z_{I-1}) \cdot \frac{E}{1 - s} \; ; \quad K_{u,v}(z_{I-1}) = \sqrt{\frac{\rho_1}{\rho_2}}\ k_1 \cdot |u^*| \cdot \hat{z}_{I-1}$$

$$s^* = \frac{F}{\sqrt{\rho_A \rho_w} \cdot |u^*|} \quad ; \qquad K_{T,s}(\hat{z}_{I-1}) = K_{u,v}(\hat{z}_{I-1})$$

$$s(z_I) = s(z_{I-1}) + s^* \cdot B_2$$

When the subsurface is land, $\delta = 0$ and $\lambda < 0$ (i.e., $\lambda = -z_0$).

The computations follow the previous section for the water subsurface, except the following equation is used for

$$w(z_I) = 0 \ .$$

All values of u and v at heights below the interface are zero. This results in

$$u(z_I) = v(z_I) = 0 \ .$$

Similarly,

$$s(z_I) = 0 \ .$$

The remaining equations are unchanged.

3.8.3 Temperature

The incoming radiation, both solar and infrared, is computed according to Sections 3.6. The solar energy at the surface is given by

$$R_H = I_{n_{I+1}} (1 - r_s)$$

for a soil layer and is

$$R_H = \Delta I_1$$

for the water layer, when ΔI_1 is the amount of solar energy absorbed in the first half layer.

The heat of vaporization, L, is calculated from

$$L = 597.3 - 0.57\,(T_g - 273.16) = 753.0 - 0.57\,T_g$$

for $T_g \geq 273.16$. If $T_g < 273.16$, then $L > 677.0$.

The value E is computed from

$$E = -10^{-3}\,\rho_A\,K(\hat{z}_I)_T\left[\frac{q(z_{I+1}) - q(z_I)}{z_{I+1}}\right] .$$

The air heat flux is calculated from

$$A = H_A = -\rho_A\,c_p\,K(\hat{z}_I)_T\left[\frac{T(z_{I+1}) - T(z_I)}{\Delta z_I}\right] + \Gamma ,$$

and the surface flux is calculated from

$$S = H_w = \rho\,c_w\,K(\hat{z}_{I-1})_T\left[\frac{T(z_I) - T(z_{I-1})}{\Delta z_{I-1}}\right] .$$

Compute

$$P_t = c_w\,\rho_w\,P_r\,(T_r - T_I)$$

where P_r is the precipitation ratio and T_r is the rainfall temperature, assumed to equal the average wet bulb temperature near the sea surface.

The quartic heat balance equation is solved to give a new value of T_g from

$$(T_g)_{t+1} = \left[\frac{1}{\varepsilon\sigma}\,(R_H + R_a + R_x + P_t - A - S - LE)\right]^{\frac{1}{4}} \qquad (1)$$

where all parameters have been previously defined using $(T_g)_t$. However, instabilities in the computation of the effective interface temperature T_g require an iteration procedure at each time step.

On the iterative procedure, R_H, R_a, and L will remain constant. The values of A, S, and E will be recomputed using the iterative value of T_g in the previous iteration.

The procedure will be to compute T_g from equation (1) for each new iteration n. Then

$$\Delta_n = T_g(n+1) - T_g(n)$$

is computed. When $n = 1$, $T_g(n)$ is the value of T_g in the previous time step, and if $|\Delta_n| \leq 0.00015\ \Delta t$ and the value $(T_g)_t = T_g(n)$, the computations will continue using this as the effective temperature.

The value of T_g computed in equation (1) will be set for the first iteration

$$T_g(1) = (T_g)_{t+1} ,$$

and $\Delta_1 = T_g(1) - (T_g)_t$ and the iteration continues using $T_g(1)$. If $|\Delta_1| \leq c_t$, where $c_t = 0.00015\ \Delta t$, then the value $T_g(1)$ will be the value of $(T_g)_{t+1}$ and no iteration will be required.

If the initial value of $T_g(1)$ is negative, a new iteration value of $T_g(1)$ will be

$$T_g(1) = (T_g)_t \Big/ 2 ,$$

and the iteration continues.

Now for the following iterations,

$$\delta n = T_g(N) - T_g(N-1) .$$

If $\delta n \leq c_t$, then

$$(T_g)_{t+1} = \frac{T_g(N) + T_g(N-1)}{2} ,$$

and the iteration is terminated. However, when $\delta n > c_t$, the sign of Δ_{n+1} and Δ_n are compared. If the signs are the same, $\Delta n = \Delta(n-1)/2$, and

$$T_g(N) = T_g(N-1) + \Delta n \ ,$$

continuing the iteration with $T_g(N)$, let $\Delta n = \delta n$, and continue the iteration.

Briefly, the temperature which is desired will be found between $(T_g)_t$ and $T_g(1)$. When the first $|\Delta_1| > c_t$, there must be one instance which δn is opposite in sign to Δn . When the conditions on Δn or δn are met, the final $(T_g)_{t+1}$ will be calculated and the computations of cooling and diffusion will continue. There may be up to 25 iterations.

In the iterations, it may be more easy to use the following equations

$$S(n+1) = S(n)\left[\frac{T_g(n+1) - T(z_{I-1})}{T_g(n) - T(z_{I-1})}\right]$$

$$A(n+1) = A(n)\left[\frac{T(z_{I+1}) - T_g(n+1)}{T(z_{I+1}) - T_g(n)}\right]$$

and

$$E(n+1) = E(n)\left[\frac{q(z_{I+1}) - q_g(n+1)}{q(z_{I+1}) - q_g(n)}\right]$$

where $q_g(n+1)$ is calculated from the saturated specific humidity for $T_g(n+1)$.

At each time step after all iterations have been complete, a time sum of each of the components of the heat balance is computed from

$$X_t = \Sigma x \, \Delta t$$

where X is R_H , R_a , A , S , LE , P_T , R_x , and σT_g^4 .

3.8.4 Air pollutants

If pollutants are present, the value of the pollutant concentration is computed as follows:

Compute the source emission S_{1t} as a function of time by linear interpolation from the input values of $S_1(t)$. Then the interface value for the first pollutant is computed from

$$P_1(0,t) = \frac{S_{1t}\ \hat{z}_I\ h_{11}}{\rho_A\ K_T(\hat{z}_I)} + P_1(z_{I+1},\ t) .$$

Similarly for the second pollutant, if present, compute

$$P_2(0,t) = \frac{S_{2t}\ \hat{z}_I\ h_{11}}{\rho_A\ K_T(\hat{z}_I)} + P_2(z_{I+1},\ t) .$$

3.8.5 Computation of interface fluxes for printout

If $\delta \neq 0$, the computation proceeds as in 3.8.5.1. If $\delta = 0$, the computation proceeds as in 3.8.5.2.

3.8.5.1 If $\delta \neq 0$

$$\tau(0,\ t) = \rho_A \cdot K(\hat{z}_I,\ t) \cdot \left[\frac{w(z_{I+1}) - w(z_I)}{\Delta z_I}\right]$$

$$H_A = -\rho_A \cdot c_p \cdot K(\hat{z}_I) \cdot \left[\frac{T(z_{I+1}) - T(z_I)}{\Delta z_I} + \Gamma\right]$$

$$H_w = \rho \cdot c_w \cdot K(\hat{z}_{I-1}) \cdot \left[\frac{T(z_I) - T(z_{I-1})}{\Delta z_{I-1}}\right]$$

$$E = E$$

$$F = F$$

3.8.5.2 If $\delta = 0$

$$\tau(0, t) = \rho_A \cdot u^{*2}$$

$$E(0, t) = E$$

$$F(0, t) = F$$

$$H_A(0, t) = -\rho_A \cdot c_p \cdot |u^*| \cdot [T(z_{I+1}) - T(z_I) + \Gamma \cdot \Delta z_I][B_1]^{-1}$$

$$H_s(0, t) = \rho_w \cdot c_w \cdot |u^*| \cdot [T(z_I) - T(z_{I-1})][B_2]^{-1}$$

3.9 Upper and Lower Boundary Values

3.9.1 Winds and currents

The winds and currents at the upper and lower levels at time step t+1 are based on the geostrophic winds computed in Section 3.7. The upper level winds are computed from

$$u(z_n, t+1) = u(z_n,t) + \Delta t \cdot f\,[v(z_n,t) - V_g(z_n,t)]$$

$$v(z_n, t+1) = v(z_n,t) + \Delta t \cdot f\,[U_g(z_n,t) - u(z_n,t)] \quad .$$

The lower current values, if the subsurface is water, are computed from

$$u(z_1, t+1) = u(z_1,t) + \Delta t \cdot f\,[v(z_1,t) - V_g(z_1,t)]$$

$$v(z_1, t+1) = v(z_1,t) + \Delta t \cdot f\,[U_g(z_1,t) - u(z_1,t)] \quad .$$

3.9.2 Temperature, humidity, salinity, and pollutants

The upper and lower boundary values (i.e., z_1, z_n) are held constant for T , q , s , P_1 , and P_2 .

3.9.3 Printout of boundary fluxes

$$\tau(z_N, t) = \rho_A \cdot K_{u,v}(\hat{z}_{N-1}, t) \cdot S(\hat{z}_{N-1}, t)$$

$$\tau(z_1, t) = \rho_w \cdot K_{u,v}(\hat{z}_1, t) \cdot S(\hat{z}_1, t)$$

$$H_A(z_N, t) = -\rho_A \cdot c_p \cdot K_{T,q}(\hat{z}_{N-1}, t) \cdot \left[\frac{T(z_N) - T(z_{N-1})}{\Delta z_{N-1}} + \Gamma\right]$$

$$H_w(z_1, t) = \rho_w \cdot c_w \cdot K_{T,s}(\hat{z}_1, t) \cdot \left[\frac{T(z_2) - T(z_1)}{\Delta z_1}\right]$$

$$E(z_N, t) = -\rho_A \cdot K_{T,q}(\hat{z}_{N-1}, t) \cdot \left[\frac{q(z_N) - q(z_{N-1})}{\Delta z_{N-1}}\right]$$

$$F(z_1, t) = \rho_w \cdot K_{T,s}(\hat{z}_1, t) \cdot \left[\frac{s(z_2) - s(z_1)}{\Delta z_1}\right]$$

3.10 Solution of the Finite Difference Equation

3.10.1 T , q , and s

The finite difference equations for T , q , and s take the form

$$d_1 = b_1\chi_1 + c_1\chi_2$$

$$d_2 = a_2\chi_1 + b_2\chi_2 + c_2\chi_3$$

$$d_n = a_n\chi_{n-1} + b_n\chi_n$$

where the χ_j's denote the unknown values of T , q , and s as the case may be, and the coefficients are known quantities.

Generalized coefficient formulas are

$$a_1 = 0$$

$$a_j = -\frac{2\Delta t}{(\Delta z_{j+1} + \Delta z_j)}\left[\frac{K_j}{\Delta z_j} + 0.5\, w_{j+1}\right] \qquad j = 2, \ldots, n$$

$$c_j = -\frac{2\Delta t}{(\Delta z_{j+1} + \Delta z_j)} \left[\frac{K_{j+1}}{\Delta z_{j+1}} - 0.5\, w_{j+1} \right] \qquad j = 1, \ldots, n-1$$

$$c_n = 0$$

$$b_j = C5 + \frac{2\Delta t}{(\Delta z_{j+1} + \Delta z_j)} \cdot \left[\frac{K_a(\hat{z}_{j+1})}{\Delta z_{j+1}} + \frac{K_a(\hat{z}_j)}{\Delta z_j} \right] \qquad j=2, \ldots, n-1$$

$$d_1 = C6 \cdot X_2^t + \frac{K_a(\hat{z}_1)}{\Delta z_1} \cdot \frac{2\Delta t}{(\Delta z_2 + \Delta z_1)} \cdot X_1^t - \frac{\delta \cdot X_2^{t-1}}{2} + \Delta t \cdot A_{a_2} + w_1 \left[-\varepsilon\Gamma + \frac{\Delta t}{\Delta z_2 + \Delta z_1} X_1^t \right]$$

$$d_n = C6 \cdot X_{n+1}^t + \frac{2\Delta t}{(\Delta z_{n+1} + \Delta z_n)} \cdot \frac{K_a(\hat{z}_n)}{\Delta z_{n+1}} \cdot X_{n+2}^t - \frac{\delta \cdot X_{n+1}^{t-1}}{2} + A_{a_{n+1}} \cdot \Delta t + w_n \left[-\varepsilon\Gamma - \frac{\Delta t}{\Delta z_{n+1} + \Delta z_n} X_{n+2}^t \right]$$

$$d_j = C6 \cdot X_{j+1}^t - \frac{\delta \cdot X_{j+1}^{t-1}}{2} + \Delta t \cdot A_{a_{j+1}} - \varepsilon\Gamma \cdot w_{j+1} \qquad j = 2, \ldots, n-1$$

where $\varepsilon = 1$ for the atmospheric temperature and $\varepsilon = 0$ for all other variables. In the initial time step, the constants $C5 = 1$, $C6 = 1$, and $\delta = 0$. In all subsequent time steps, these constants are $C5 = 1.5$, $C6 = 2$, and $\delta = 1$.

Table 4 gives specific symbols in our previous notation for the undefined quantities in our generalized equations above.

Table 4

Definitions of Generalized Coefficients

Quantity \ X	$T(z_{I+1} \le z \le z_{N-1})$	$T(z_2 \le z \le z_{I-1})$	q	s
K_a	$K_{T,q}$	$K_{T,s}$	$K_{T,q}$	$K_{T,s}$
A_a	$-\left[u^n_{j+1}\frac{\partial T_A}{\partial x} + v^n_{j+1}\frac{\partial T_A}{\partial y}\right]$ $+ 2\Gamma/(\Delta z_j + \Delta z_{j-1})$ $[K(\hat{z}_j) - K(\hat{z}_{j-1})]$ $+\left[\left(\frac{\partial T}{\partial t}\right)_{ir}\right]_j + \left[\left(\frac{\partial T}{\partial t}\right)_{sol}\right]_j$	$-\left[u\frac{\partial T_w}{\partial x} + v\frac{\partial T_w}{\partial y}\right]$ $+ \left[\left(\frac{\partial T}{\partial t}\right)_{sol}\right]_j$	$-\left[u\frac{\partial q}{\partial x} + v\frac{\partial q}{\partial y}\right]$	$-\left[u\frac{\partial s}{\partial x} + v\frac{\partial s}{\partial y}\right]$
$X_1 = X_2$	T_{I+1}	T_2	q_{I+1}	s_2
$X_n = X_{n+1}$	T_{N-1}	T_{I-1}	q_{N-1}	s_{I-1}
$X_0 = X_1$	T_I	T_1	q_I	s_1
$X_{n+1} = X_{n+2}$	T_N	T_I	q_N	s_I
$\hat{z}_0 = \hat{z}_0$	$\hat{z}_I$	$\hat{z}_1$	$\hat{z}_I$	$\hat{z}_1$
$\hat{z}_n = \hat{z}_{n+1}$	$\hat{z}_{N-1}$	$\hat{z}_{I-1}$	$\hat{z}_{N-1}$	$\hat{z}_{I-1}$

Once these coefficient values are computed, the solutions to the finite difference equations can be computed recursively from the formulas

$$c_1^* = -\frac{c_1}{b_1}$$

$$d_1^* = +\frac{d_1}{b_1}$$

$$c_j^* = -\frac{c_j}{a_j c_{j-1}^* + b_j} \quad ; \qquad j = 2, \ldots, n-1$$

$$d_j^* = \frac{d_j - a_j d_{j-1}^*}{a_1 c_{j-1}^* + b_j} \quad ; \qquad j = 2, \ldots, n-1$$

$$X_n = \frac{d_n - a_n d_{n-1}^*}{a_n c_{n-1}^* + b_n}$$

$$X_j = c_j^* X_{j+1} + d_j^* \quad ; \qquad j = n-1, n-2, \ldots, 1$$

3.10.2 u and v

The finite difference equations for u and v take the form

$$A_j \bar{u}_{j-1} + B_j \bar{u}_j + C_j \bar{u}_{j+1} = \bar{f}_j$$

where the vectors are defined

$$\bar{u}_{j-1} = \begin{bmatrix} u(z_j, \overline{m+1}\ k) \\ v(z_j, \overline{m+1}\ k) \end{bmatrix}$$

$$\bar{f}_j = \begin{pmatrix} c_6 u_{j+1}^t + \Delta t \left[- fV_g(j+1) - u_{j+1}^t \left(\frac{\partial u}{\partial x}\right)_{j+1} - v_{j+1}^t \left(\frac{\partial u}{\partial y}\right)_{j+1} \right] - \frac{\delta \cdot u_{j+1}^{t-1}}{2} \\ c_6 v_{j+1}^t + \Delta t \left[fU_g(j+1) - u_{j+1}^t \left(\frac{\partial v}{\partial x}\right)_{j+1} - v_{j+1}^t \left(\frac{\partial v}{\partial y}\right)_{j+1} \right] - \frac{\delta \cdot v_{j+1}^{t-1}}{2} \end{pmatrix}$$

$$j = 2, \ldots, n-1$$

$$\bar{f}_1 = \begin{bmatrix} C6 \cdot u_2^t - \Delta t \cdot fV_g(2) - \dfrac{\delta \cdot u_2^{t-1}}{2} + \dfrac{K(\hat{z}_0)}{\Delta z_0} \dfrac{u_0^t \cdot 2\Delta t}{(\Delta z_1 + \Delta z_0)} \\ C6 \cdot v_2^t + \Delta t \cdot fU_g(2) - \dfrac{\delta \cdot v_2^{t-1}}{2} + \dfrac{K(\hat{z}_0)}{\Delta z_0} \dfrac{v_0^t \cdot 2\Delta t}{(\Delta z_1 + \Delta z_0)} \end{bmatrix}$$

$$+ w_1 \frac{\Delta t}{\Delta z_2 + \Delta z_1} \begin{bmatrix} u_1^t \\ v_1^t \end{bmatrix}$$

$$\bar{f}_n = \begin{bmatrix} C6 \cdot u_{n+1}^t - \Delta t \cdot fV_g(n+1) - \dfrac{\delta \cdot u_{n+1}^{t-1}}{2} + \dfrac{K(\hat{z}_{n+1})}{\Delta z_{n+1}} \dfrac{u_{n+2}^t \cdot 2\Delta t}{(\Delta z_n + \Delta z_{n+1})} \\ C6 \cdot v_{n+1}^t + \Delta t \cdot fU_g(n+1) - \dfrac{\delta \cdot v_{n+1}^{t-1}}{2} + \dfrac{K(\hat{z}_{n+1})}{\Delta z_{n+1}} \dfrac{v_{n+2}^t \cdot 2\Delta t}{(\Delta z_n + \Delta z_{n+1})} \end{bmatrix}$$

$$- w_n \frac{\Delta t}{\Delta z_n + \Delta z_{n+1}} \begin{bmatrix} u_{n+2}^t \\ v_{n+2}^t \end{bmatrix}$$

and the matrix elements

$$A_1 = 0$$

$$A_j = - \frac{2\Delta t}{(\Delta z_j + \Delta z_{j-1})} \cdot \frac{K(\hat{z}_1)}{\Delta z_{j-1}}$$

$$BR(j) = C5 + \frac{2\Delta t}{(\Delta z_j + \Delta z_{j-1})} \left[\frac{K(\hat{z}_{j+1})}{\Delta z_j} + \frac{K(\hat{z}_j)}{\Delta z_{j-1}} \right]$$

$$BG(j) = - f \cdot \Delta t$$

$$C_j = - \frac{2\Delta t}{(\Delta z_j + \Delta z_{j-1})} \cdot \frac{K(\hat{z}_{j+1})}{\Delta z_j}$$

$$C_n = 0 .$$

The constants C5 , C6 , and δ are defined as before. Quantities for the upper and lower atmospheric and oceanic sublayers are given in Table 5.

Table 5

Identification of quantities

Quantity \ X	$u,v(z_{I+1} \le z \le z_{N-1})$	$u,v(z_2 \le z \le z_{I-1})$
K	$K_{u,v}$	$K_{u,v}$
$\bar{u}_2$	$\bar{u}_{I+1}$	$\bar{u}_2$
$\bar{u}_0$	$\bar{u}_I$	$\bar{u}_1$
$\bar{u}_{n+1}$	$\bar{u}_{N-1}$	$\bar{u}_{I-1}$
$\bar{u}_{n+2}$	$\bar{u}_N$	$\bar{u}_I$
$\hat{z}_0$	$\hat{z}_I$	$\hat{z}_1$
Δz_0	$\Delta z_I = z_{I-1}$	Δz_1

Recursion formulas for the solution of the finite difference equations are

$$E_1 = -B_1^{-1} C_1$$

$$\bar{f}_1^* = B_1^{-1} \bar{f}_1$$

$$E_j = -(A_j - E_{j-1} + B_j)^{-1} C_j \quad ; \qquad j = 2, \ldots, N-2$$

$$\bar{f}_j^* = (A_j E_{j-1} + B_j)^{-1} (\bar{f}_j - A_j f_{j-1}^*) \quad ; \qquad j = 2, \ldots, N-1$$

$$\bar{u}_{N-1} = \bar{f}_{N-1}^*$$

$$\bar{u}_j = E_j \bar{u}_{j+1} + \bar{f}_j^* \quad ; \qquad j = N-2, N-3, \ldots, 1$$

3.10.3. Pollutants 1 and 2

The finite difference equations for P_1 and P_2 take the same form as for q, described in Section 3.10.1, with the addition of only a source term, and the substitution of the appropriate pollution term. The source term at level j is $2S_{1t}h_{1j}/[\rho_A(z_{j+1} - z_{j-1})]$ for pollutant 1, and $2S_{2t}h_{2j}/[\rho_A(z_{j+1} - z_{j-1})]$ for pollutant 2. This term is added to A_a for the pollutants.

3.11 Horizontal Advection

The horizontal array is to consist of a rectangular array of equally spaced grid points with no limitation on the number of stations in the grid. The initial horizontal gradients are also used at later selected time steps; the horizontal gradients for each of the unknown variables, u, v, T, q, s, P_1, P_2 are computed according to the scheme outlined in the model formulation of Gerrity [1965].

The number of basic time steps to elapse before recomputation of the horizontal gradients is required, is to be calculated in the following way. The entire three-dimensional array is to be scanned for the maximum absolute velocity component value, c_m. The number of basic time steps to elapse is then

$$N_u = \frac{\Delta}{(\sqrt{2} + .01)\ |c_m| \cdot \Delta t}$$

3.11.2 Horizontal advection gradients

The horizontal gradients $\delta_j \partial A/\partial X_i$ of a variable A_j in the x $(i = 1)$ and y $(i = 2)$ directions are computed at each time step for station j,k

$$\frac{\delta_i \partial A_{j,k}}{\partial x_i} = \frac{\delta_i A_{j,k}}{\Delta x}$$

where $\delta_i A^n_{j,k}$ is computed by

$$\delta_1 A^n_{j,k} = \begin{cases} A^n_{j,k} - A^n_{j-1,k} & \text{for } u_{j,k} > 0 \\ A^n_{j+1,k} - A^n_{j,k} & \text{for } u_{j,k} \leq 0 \end{cases}$$

and

$$\delta_2 A^n_{j,k} = \begin{cases} A^n_{j,k} - A^n_{j,k-1} & \text{for } v_{j,k} > 0 \\ A^n_{j,k+1} - A^n_{j,k} & \text{for } v_{j,k} \leq 0 \end{cases}$$

Whenever one of the grid points to be used in the computations above (e.g., $A_{j,0}$) falls outside of the horizontal array, the corresponding input normal gradients are used for $\delta_i \partial A/\partial x_i$.

These gradients are used whenever advection appears, particularly in Section 3.10.

3.11.2 Space centered gradients

Space centered gradients are computed for $\delta_i \partial A/\partial x_i$ from

$$\frac{\delta_i \partial A_{j,k}}{\partial x_i} = \frac{\delta_i \Delta A_{j,k}}{2\Delta x}$$

where

$$\delta_1 \Delta A_{j,k} = A_{j+1,k} - A_{j-1,k}$$

and

$$\delta_2 \Delta A_{j,k} = A_{j,k+1} - A_{j,k-1}$$

for all internal points. For all boundary points, $\delta_i \Delta A_{j,k}$ will be restricted to the boundary point and the internal point and the gradient will be computed from

$$\frac{\delta_i \partial A_{j,k}}{\partial x_i} = .5 \left[\frac{\delta_i \Delta A_{j,k}}{\Delta x} + \left(\frac{\partial A}{\partial x_i} \right)_p \right] \qquad i = 1, 2$$

where $(\partial A/\partial x_i)_p$ is the input normal gradient. These gradients are the gradients used in Section 3.7 and with the vertical velocities in Section 3.11.3.

3.11.3 Vertical velocity

The vertical velocity at each grid height z_k is then computed by summation from the interface height, $z_{IX} = z_{IX+1}$

$$w^k_{\ell,m} = -\sum_{k'=IX+1}^{k'=k} \left| \left(\frac{\partial u}{\partial x}\right)^{k'}_{\ell,m} + \left(\frac{\partial v}{\partial y}\right)^{k'}_{\ell,m} \right| \cdot \Delta z_{k'}, \qquad k \geq IX + 2$$

and

$$w^k_{\ell,m} = \sum_{k'=k}^{k'=IX} \left| \left(\frac{\partial u}{\partial x}\right)^{k'}_{\ell,m} + \left(\frac{\partial v}{\partial y}\right)^{k'}_{\ell,m} \right| \cdot \Delta z_{k'}, \qquad k \leq IX - 1$$

and

$$w^k_{\ell,m} = 0 , \qquad k = IX = IX + 1 .$$

This is to be used, like the upwind gradients, until N_u time steps have elapsed, at which time it is recalculated from computed velocity fields.

4.0 OUTPUT

The output will be written on a tape or disk for later use. For each there will be up to 11 records (all records of 600 words length) that will show the height and time variations of the following parameters:

1. u eastward wind/current component (cm/sec)
2. v northward wind/current component (cm/sec)
3. w wind/current speed (cm/sec)
4. T temperature °K
5. g humidity (g/kg) $z_j \geq z_{I+1}$
6. s salinity (g/kg) $z_j \leq z_I$

7. P_1 pollutant 1 (ugm/m^3) if present

8. P_2 pollutant 2 (ugm/m^3) if present

9. K_u eddy diffusivity (cm^2/sec)

10. ω vertical velocity (cm/sec)

11. Ri Richardson number

12. $(\partial T/\partial t)_r$ infrared and solar heating rates (°K/day)

The following parameters will also be printed out. They will all be in one 600 word record for each station:

13. h height of wave (cm)

14. r_s albedo (n.d.)

15. R_x artificial heat source (ℓy/sec)

16. M_q moisture parameter (n.d.)

17. δ steepness of characteristic wave (n.d.)

18. ρ soil/water density (cal/gm/°K)

19. λ wave length of turbulent wave (cm) if water; if negative, indicates land and is $-z_0$, the roughness height (cm)

20. $R_d(N)$ downward infrared flux at $z = z_N$ (mℓy/sec)

21. $R_u(N)$ upward infrared flux at $z = z_N$ (mℓy/sec)

22. $R_s(N)$ downward solar flux at $z = z_N$ (mℓy/sec)

23. $R_d(0)$ downward radiative flux at the surface (mℓy/sec)

24. $R_u(0)$ downward radiative flux at the surface (mℓy/sec)

25. $R_s(0)$ downward radiative flux at the surface (mℓy/sec)

26. $I_v(n)$ upward solar flux at z_N (mℓy/sec)

27. $\tau(0,t)$ The eddy stress at the interface (dynes cm^{-2})

28. $H_A(0,t)$ The eddy heat flux into the atmosphere at the interface (cal cm^{-2} sec^{-1})

29. $H_s(0,t)$ The eddy heat flux into the ocean at the interface (cal cm^{-2} sec^{-1})

30. $E(0,t)$ The eddy water-vapor flux into the atmosphere at the interface ($g\ cm^{-2}\ sec^{-1}$)

31. $F(0,t)$ The eddy salinity flux into the ocean at the interface ($g\ cm^{-2}\ sec^{-1}$)

32. $\tau(z_N,t)$
33. $H_A(z_N,t)$
34. $H_s(z_1,t)$
35. $E(z_N,t)$
36. $F(z_1,t)$
37. $\tau(z_1,t)$

} Corresponding eddy fluxes at the upper and lower boundary

The following time sums will also be printed, all in ℓy .

38. LE_t latent heat flux
39. A_t heat flux into the atmosphere
40. S_t heat flux into the subsurface
41. P_t heat flux due to precipitation
42. Rs_e solar flux used for heating interface
43. Ra_t incoming infrared flux at surface
44. Rx_t artificial heat source
45. b_t outgoing infrared flux at surface.

APPENDIX B. Specifications for Analysis of the Boundary Layer Model Results

by Marshall A. Atwater

1.0 INTRODUCTION

This specification will use the output tape or disk generated by the boundary layer model, described in Appendix A. The tape will contain all the information needed to set the indices and a minimum of input will be necessary in this program to define the printout. There will be four separate options, each having its own input and output.

2.0 TIME SERIES

2.1 Input

The input will consist of the following:

1) variable to be printed,

2) location on horizontal graid array, and

3) height level (if applicable).

2.2 Computations and Output

For each parameter defined by the input for which a time series is desired, two time series will be prepared. The abscissa is the time step in both graphs. The ordinate for both graphs consists of 51 values.

For the first graph, compute

$$X_i = \frac{2 \sum_{i=1}^{N} X}{25N} \qquad \text{(B1)}$$

and

$$R(1) = 25X_i \ . \qquad \text{(B2)}$$

Preceding page blank

For the second graph, compute

$$X_i = \frac{X_{max} - .5(X_{max} + X_{min})}{25.} \quad \text{(B3)}$$

and

$$R(1) = X_{max} . \quad \text{(B4)}$$

The remaining values of the ordinate are computed from

$$R_{n+1} = R_n - X_i \quad \text{(B5)}$$

for $1 \leq n \leq 50$.

An asterisk (*) is printed at the appropriated time step for the value of the parameter. Whenever the value of the parameter is out of the range of values of the ordinate, a zero (0) is printed.

3.0 HORIZONTAL X-Y PLOT

3.1 Input

1) Variable to be Printed.

2) Time Step.

3) Height (if applicable).

3.2 Printout

The parameter will be printed unaltered in map form with the same dimensions as the original model. An alternate will allow computer analysis of the map.

4.0 HEIGHT-SPACE (Z-X) CROSS SECTIONS

4.1 Input

The input consists of:

1) variable,

2) time step, and

3) stations in the cross section.

4.2 Printout

The printout of each variable, unaltered, will be at all heights for the stations listed. An option will allow for contouring to be performed by the computer.

5.0 HEIGHT-TIME (Z-t) CROSS SECTION

5.1 Input

The input will consist of the following:

1) variable, and

2) station.

5.2 Printout

The variable will be printed, unaltered, for each specified station with function of height as the ordinate and time as the abscissa.

APPENDIX C. Related Studies

Related work at the Center for the Environment and Man, Inc. have produced results that either have already been adopted in the form of modification of the computer programs, or will be adopted in the near future. These studies resulted in the following.

- The completion of a series of three-dimensional model simulations which generate atmospheric vertical velocity fields which are consistent with the first estimates of large scale velocity field obtained for the project BOMEX. The simulation with a one-dimensional model, of realistic time changes of near-surface meteorological conditions during the period June 22-24, 1969 for the same project. The completion of an experiment in which simulations with alternative formulations of vertical eddy flux in the planetary boundary layer were compared with each other, and with observed conditions (Pandolfo and Jacobs, NSF grant GA-18669).

- A series of simulations of near-surface meteorological conditions over the tundra within the context of a general tundra ecosystem model. The sensitivity of the atmospheric behavior to variations in subsurface soil conditions, and, in particular, the level of the permafrost boundary was estimated (Lord and Atwater, NSF grant GB-25064).

- The development of improved numerical techniques for the integration of conservation equations containing advective terms. Comparative tests of these techniques and conventional techniques (Arnason and Brown, USARO-DD grant DA-HCO-4-70-0030).

- Modelling of topographic effects on the horizontal windfield in several regions. A paper (by G.E. Anderson) describing this technique has been accepted for publication in the June 1971 issue of *The Journal of Applied Meteorology*.

- Source inventories of SO_2, NO_x, CO, hydrocarbons, and particulates that were collected for the State of Connecticut and reorganized to be presented on arbitrarily defined grids. This data is available and has been used to provide realistic input to the three-dimensional urban boundary layer model.

- An analysis of the time dependent turbulent correlation equation which has been carried out under internal funding. This has led to criteria for neutral stability and growth or decay or turbulent energy in complex flows with space gradients of all dependent variables. Common stability criteria, such as Richardson's criterion, Rayleigh's criterion, the Synge criterion, etc., are recovered for special cases of this analysis. In general, more complex criteria are obtained for

Preceding page blank

more complex, realistic flows. These criteria are functions of wavelength and the values and gradients of the mean variables.

The analysis is now being used under an NSF grant to examine the limits of predictability of atmospheric motions. The approach shows promise of providing an analytic determination of the time and space distribution of the turbulent transport coefficients when these conservation of correlation equations are solved simultaneously with the urban boundary layer's mean variable equations.

APPENDIX D: Properties of the Modified Gamma Distribution

The modified gamma distribution has been described by Deirmendjian [1969] and will briefly be described below.

The modified gamma distribution is represented by

$$n(r) = ar^{\alpha} \exp(-br^{\gamma}) , \qquad 0 \leq r < \infty \tag{D1}$$

where a , α , b , and γ are positive real constants, r is the radius, and $n(r)$ is the number density.

The total number of particles N is given by

$$N = a \int_0^{\infty} r^{\alpha} \exp(-br^{\gamma})\, dr \tag{D2}$$
$$= a\, \gamma^{-1}\, b^{-(\alpha+1)/\gamma}\, \Gamma\left(\frac{\alpha + 1}{\gamma}\right) ,$$

where Γ is the gamma function. This can be written to solve for "a" as a function of N by

$$a = \frac{N\gamma b^{(\alpha+1)/\gamma}}{\Gamma\left(\frac{\alpha+1}{\gamma}\right)} . \tag{D3}$$

Differentiation of the distribution with respect to r , which will be 0 at the radius size of the maximum frequency r_c , called the modal radius, at $r = 0$ $(\alpha \neq 1)$, and at $r = \infty$, results in

$$\frac{d}{dr}\left(\frac{n}{r}\right) = ar^{\alpha-1} (\alpha - \gamma br^{\gamma}) \exp(-br^{\gamma}) \tag{D4}$$

or

$$b = \frac{a}{\gamma r_c^{\gamma}} . \tag{D5}$$

The frequency at r_c is given by

$$n(r_c) = a r_c^{\alpha} \exp\left(-\frac{\alpha}{\gamma}\right) . \tag{D6}$$

For comparisons with power law distribution, the logarithmic derivative of $n(r)$ is useful. This is given by

$$\begin{aligned} r \frac{d}{dr} \{\ell n[n(r)]\} &= \alpha - b\gamma r^{\gamma} \\ &= \alpha \left[1 - \left(\frac{r}{r_c}\right)^{\gamma}\right] , \end{aligned} \tag{D7}$$

which represents the slope of the curve $\ell n[n(r)]$ versus $\ell n(r)$.

When the negative logarithmic slope of the distribution equals 4, or correspondingly

$$r_r \geq r_c \left(1 + \frac{4}{\alpha}\right)^{1/\gamma} , \tag{D8}$$

the size range of the modified gamma distribution can be approximated by the power law. The radius r_r is also the radius beyond which radiative factors using the modified gamma distribution converge.

A table of various constants is given in Table D-1.

Table D-1

Constants used by various authors for the modified gamma distribution.

Author and Year	Name	Representation	N cm^{-3}	r_c μ	α	γ	a	b	$n(r_c)$ $cm^{-3}\ \mu^{-1}$	$-r\frac{d}{dr}\{\ell n[n(r)]\}$ ≥ 4
Deirmendjian [1964]	Haze M	Maritime Aerosols	100	.05	1	.5	53300	8.944	360.9	1.25
Deirmendjian [1969], and Bauer [1964]	C.1	Fair Weather Cumulus Cloud	100	4	6	1	2.373	1.5	24.1	6.67
DeLuisi [1967]	C^1	Continental Aerosols	2000	.04	13	.125	n.c.*	n.c.	n.c.	n.c.
Kattawar and Plass [1968]	N	Nimbostratus	100	12	6	1	1.08×10^{-3}	1.5	8.0	20.00
Deirmendjian [1969]	Haze H	Stratospheric Aerosols	100	.10	2	1	4.000×10^5	20.000	541.4	.3
Deirmendjian [1969]	Haze L	Continental Aerosol close to Junge power distribution	100	.07	2	.5	4.9757×10^6	15.1186	446.6	.63
Deirmendjian [1969]	C.2	Corona Cloud	100	4	8	3	.01085	1/24	49.41	4.58
Deirmendjian [1969]	C.3	Mother of Pearl Cloud	100	2	8	3	5.5551	1/3	98.82	2.29
Atwater [1970]	"P"	Urban Aerosol	10^5	.005	3	.25	5.655×10^{18}	45.13	4.34×10^6	.1415

* n.c.: not computed, $a > 100^{100}$.